

Nusselt Number for Steady Periodically Developed Heat Transfer in Micro- and Mini-Channels with Arrays of Offset Strip Fins Subject to a Uniform Heat Flux

A. Vangeffelen,^{1, 2, 3, a)} G. Buckinx,^{1, 2, 3} C. De Servi,^{2, 3} M. R. Vetrano,^{1, 3} and M. Baelmans^{1, 3}

¹⁾*Department of Mechanical Engineering, KU Leuven, Celestijnenlaan 300A, 3001 Leuven, Belgium*

²⁾*VITO, Boeretang 200, 2400 Mol, Belgium*

³⁾*EnergyVille, Thor Park, 3600 Genk, Belgium*

(Dated: 28 June 2022)

In this work, the Nusselt number is examined for periodically developed heat transfer in micro- and mini-channels with arrays of offset strip fins, subject to a constant heat flux. The Nusselt number is defined on the basis of a heat transfer coefficient which represents the spatially constant macro-scale temperature difference between the fluid and solid during conjugate heat transfer. Its values are determined numerically on a single unit cell of the array for Reynolds numbers between 1 and 600 and fin height-to-length ratios below 1. Two combinations of the Prandtl number and the thermal conductivity ratio are selected, corresponding to air and water. It is shown that the Nusselt number correlations from the literature mainly apply to air in the transitional flow regime in larger conventional channels if the wall temperature remains uniform. As a result, they do not correctly capture the observed trends for the Nusselt number in micro- and mini-channels subject to a constant heat flux. Therefore, new Nusselt number correlations, obtained through a least-squares fitting of 2282 numerical simulations, are presented for air and water. The suitability of these correlations is assessed via the Bayesian approach for parameter estimation and model validation. The correlations respect the observed asymptotic trends and limits of the Nusselt number for all the geometrical parameters of the offset strip fins. In addition, they predict a linear dependence of the Nusselt number on the Reynolds number, in good agreement with the data from this work. Nevertheless, a detailed analysis reveals a more complex scaling of the Nusselt number with the Reynolds number, closely related to the underlying flow regimes, particularly the weak and strong inertia regimes. Finally, through 62 additional simulations, the influence of the material properties on the Nusselt number is illustrated and compared to the available literature.

Key words: Offset Strip Fin, Nusselt Number, Correlation, Periodically Developed Heat Transfer, Unit Cell, Bayesian Inference

^{a)}Electronic mail: arthur.vangeffelen@kuleuven.be.

I. INTRODUCTION

Heat transfer in periodic fin arrays in micro- and mini-channels has been investigated over the past twenty years due to the increasing demand for high-power-density heat transfer devices in numerous applications (Refs. 1–4). The channels of heat transfer devices are commonly categorized based on their smallest dimension. Notably, it is the practice to distinguish between micro- and mini-channels if the smallest dimension ranges from $10\text{ }\mu\text{m}$ to $200\text{ }\mu\text{m}$ or $200\text{ }\mu\text{m}$ to 3 mm , respectively (Refs. 1). Particular attention in the literature has been devoted to micro- and mini-channels with arrays of periodic offset strip fins due to their favorable thermo-hydraulic characteristics (Refs. 5–13). For example, micro-channels with an array of periodic offset strip fins have been exploited for the cooling of microelectronic systems to cope with the increased thermal management needs resulting from the continuous miniaturization of such devices (Refs. 5–7, 14, and 15). Offset strip fins in mini-channels are also adopted in various energy conversion applications where a compact design of the heat transfer device or a small temperature difference between two flows is desired. This is the case for heat recuperators of small-capacity gas turbines (Refs. 8 and 9), heat exchangers for refrigeration and liquefaction in cryogenic systems (Refs. 10 and 11), and solar air heating collectors (Refs. 12 and 13).

As highlighted in our previous work (Refs. 16), the flow regime inside micro- and mini-channels with offset strip fins is typically steady and laminar due to the small dimensions. Moreover, as the fin height-to-length ratio commonly remains below 1, the flow regime is characterized by low to moderate Reynolds numbers ranging from 10 to 500 (Refs. 5–14).

The heat transfer regime in most micro- and mini-channel applications is typically characterized by a fluid Prandtl number Pr_f which equals 0.7 or 7, for air and water, respectively (Refs. 5–9, 12–15). For cryogenic fluids such as helium, hydrogen, and nitrogen, both in the gaseous and liquid state, the Prandtl number is of the same order of magnitude as for air (Refs. 10 and 11). Furthermore, the heat transfer process in typical micro- and mini-channel applications can be accurately simulated by assuming that a steady and uniform heat flux is established on the channel wall. This so-called *H-type* boundary condition is often assumed to be representative of the heat transfer process occurring in cooling systems for electronics, as well as balanced counter-flow heat exchangers, such as gas turbine recuperators (Refs. 17–21). Similarly, a steady and uniform heat flux is commonly considered to model the heat transfer process in micro- and mini-channels of solar air heaters and heat exchangers of cryogenic systems (Refs. 11–13, and 22).

In the literature, both experimental and numerical studies have been conducted to investigate the heat transfer regime occurring in channels with an offset strip fin array (Refs. 23–29). Nonetheless, these studies are primarily limited to conventional channels with fin dimensions in the centimeter range and air as working fluid. Then, the investigated conditions are representative of applications such as automotive radiators and air-conditioning condensers and evaporators, which operate at high air flow rates. Therefore, the experimental and numerical data in the literature are mainly applicable to transitional and turbulent flows of working fluids with Prandtl numbers around 0.7, and heat transfer processes occurring under the condition of a uniform channel wall temperature. In our previous work (Refs. 16), we have characterized the friction factor for steady laminar periodically developed flow through offset strip fins arrays in micro- and mini-channels. It was found that the friction factor correlations available in the literature, which were constructed based on the data for the transitional flow regime in larger conventional channels, result in discrepancies of 20% to 80% for micro- and mini-channels. In this work, similar discrepancies are found for the Nusselt number correlations from the literature, in particular when the channel walls are subject to a constant heat flux instead of a constant temperature. Therefore, the present work aims to study the Nusselt number for offset strip fin arrays in micro- and mini-channels, subject to a constant heat flux. In contrast to previous studies, the conjugate heat transfer between the fluid and the solid fins is taken into account, as we aim to include the influence of the material properties of the solid on the Nusselt number. Besides, it is known that conjugate heat transfer can have a significant effect on the Nusselt number (Refs. 30 and 31), which may not be recognizable from the available data in the literature.

The experimental Nusselt number data reported in the literature are typically derived from temperature measurements upstream and downstream of an air-side offset strip fin array for a range of flow rates through the array. For such measurements, the channel wall temperature is mainly maintained at steady and uniform conditions using a control flow, which is a condensing steam or an evaporating water flow along the outer surface of the channel. The temperature measurements are used to evaluate the area-averaged temperature at the in- and outlet section of the array. This information allows the overall heat transfer coefficient h_0 to be estimated by applying the effectiveness-and-number-of-transfer-units (ε -NTU) method, or the logarithmic mean temperature difference (LMTD) approach (Refs. 25, 28, 32, and 33). However, both methods rely on two critical assumptions: i) the temperature distribution is assumed to be one-dimensional, and ii) the overall heat transfer coefficient is assumed to be spatially constant. Also, a simplified expression

for the fin temperature effectiveness is used with these methods.

The relation between the overall heat transfer coefficient and the flow rate is usually expressed by means of a correlation between the Stanton number $St \triangleq \frac{Nu}{ReD_h Pr_f}$ or the Colburn j-factor $j \triangleq \frac{Nu}{ReD_h Pr_f^{1/3}}$, based on the Nusselt number $Nu \triangleq h_0 D_h / k_f$, and the Reynolds number $ReD_h \triangleq \rho_f U_{\text{ref}} D_h / \mu_f$. These dimensionless numbers depend on the hydraulic diameter D_h , the conductivity k_f , the density ρ_f , and the dynamic viscosity μ_f of the fluid, as well as some reference flow speed U_{ref} . The heat transfer correlations for offset strip fin arrays reported in the literature are chronologically listed in Tables I and II. For each study, the tables include the corresponding definition of the hydraulic diameter D_h , which is derived from the geometrical parameters of the offset strip fin array. These are the fin length l , the fin height h , the lateral fin pitch s and the fin thickness t , as shown in Figure 1. Figure 1 also displays an actual offset strip fin mini-channel which has been fabricated by the additive manufacturing technique of laser powder bed fusion (Refs. 34). In addition, the considered ranges of the Reynolds number ReD_h , the fin height-to-length ratio h/l and the fluid Prandtl number Pr_f in each study are given in Tables I and II. In the study of Joshi and Webb, the reference velocity U_{ref} is defined as the average bulk velocity through the cross-section area $(s - t)h$, whereas in the study of Bhowmik and Lee, it is based on the cross-section area $(s + t)h$. In the remaining studies listed in Tables I and II, U_{ref} is defined with respect to the flow passage area sh . Next, the correlations from Tables I and II are briefly reviewed.

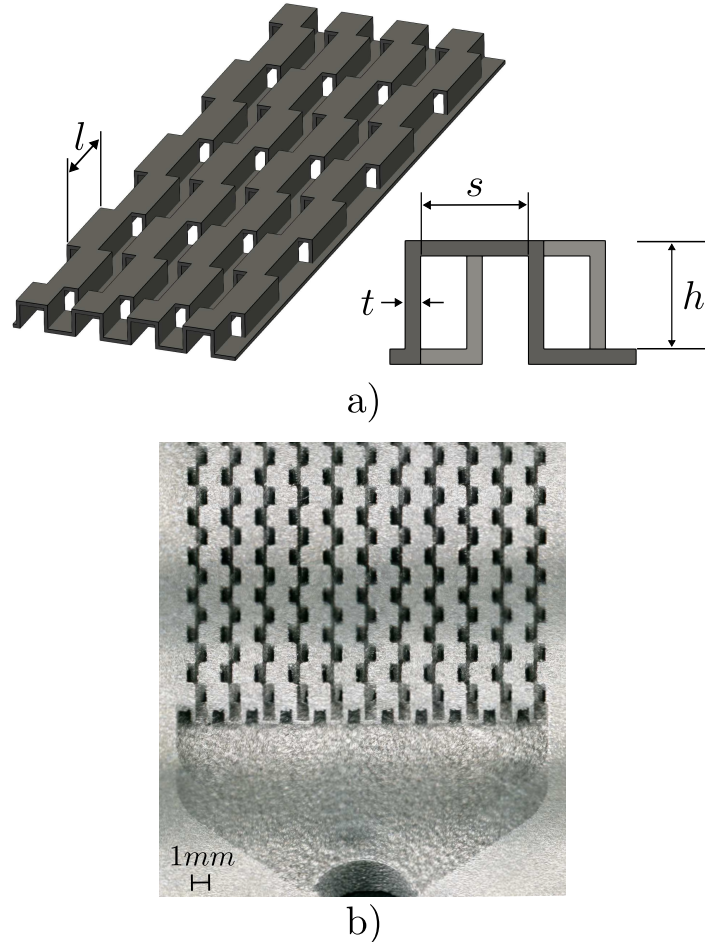


FIG. 1. (a) Geometrical parameters of an array of periodic offset strip fins, actual mini-channel with an array of periodic offset strip fins, (b) produced in-house by the laser powder bed fusion manufacturing technique

TABLE I. Chronological list of heat transfer correlations for offset strip fin channels

Researchers	Correlation	Re_{D_h}	h/l	Pr_f
Manson (1950)	$j = \begin{cases} 0.6(l/D_h)^{-0.5} Re_{D_h}^{-0.5} & \text{for } l/D_h \leq 3.5 \\ 0.6(3.5)^{-0.5} Re_{D_h}^{-0.5} & \text{for } l/D_h > 3.5 \end{cases}$ <p>where $D_h = 2sh/(s+h)$</p>	370-9020	4.8-7.9	0.7
Wieting (1975)	<p>For $Re_{D_h} \leq 1000$</p> $j = 0.483(l/D_h)^{-0.162}(s/h)^{-0.184} Re_{D_h}^{-0.536}$ <p>For $Re_{D_h} > 2000$</p> $j = 0.242(l/D_h)^{-0.322}(t/D_h)^{0.089} Re_{D_h}^{-0.368}$ <p>where $D_h = 2sh/(s+h)$</p>	120-50000	0.23-5.1	0.7
Joshi & Webb (1987)	<p>For $Re_{D_h} < Re^*$</p> $j = 0.53(l/D_h)^{-0.15}(s/h)^{-0.14} Re_{D_h}^{-0.50}$ <p>For $Re_{D_h} > Re^* + 1000$</p> $j = 0.21(l/D_h)^{-0.24}(t/D_h)^{0.02} Re_{D_h}^{-0.40}$ <p>where</p> $Re^* = 257(l/s)^{1.23}(t/l)^{0.58} D_h$ $\times \left[t + 1.328(Re_{D_h}/(lD_h))^{-0.5} \right]^{-1}$ $D_h = 2(s-t)h/((s+h)+ht/l)$	120-50000	0.23-5.1	0.7
Manglik & Bergles (1995)	$j = 0.6522(s/h)^{-0.1541}(t/l)^{0.1499}(t/s)^{-0.0678} Re_{D_h}^{-0.5403}$ $\times \left[1 + 5.269 \cdot 10^{-5} (s/h)^{0.504} (t/l)^{0.456} (t/s)^{-1.055} Re_{D_h}^{1.340} \right]^{0.1}$ <p>where $D_h = 4shl/(2(sl+hl+th)+ts)$</p>	120-10000	0.23-5.1	0.7
Dong et al. (2007)	$j = 0.101(s/h)^{-0.488}(t/l)^{-0.297}(t/s)^{0.479} Re_{D_h}^{-0.189}(L/l)^{-0.315}$ <p>where</p> <p>L is the flow length</p> <p>$D_h = 2sh/(s+h)$</p>	500-7500	0.91-2.3	0.7

TABLE II. Chronological list of heat transfer correlations for offset strip fin channels (continued)

Researchers	Correlation	Re_{D_h}	h/l	Pr_f
Guo et al. (2008)	$j = 0.8452(2(s+t)/D_h)^{-0.5476\alpha+0.2326}(h/D_h)^{0.1819\alpha-1.4207}$ $\times(l/D_h)^{0.2558\alpha-0.7685}Re_{D_h}^{-0.3958}\alpha^{0.05855}$ <p>where</p> α is the flow angle of attack $D_h = 4V_{\text{free}}/A_{\text{surface}}$ V_{free} is the free flow volume A_{surface} is the wetted surface area	20-400	1.9-2.9	>100
Bhowmik & Lee (2009)	$j = 0.489Re_{D_h}^{-0.445}$ <p>where $D_h = 2(s-t)h/(s+h+th/l)$</p>	10-3500	1	7
Kim et al. (2011)	<p>For $\beta < 0.2$</p> $j = \exp(1.96)(s/h)^{-0.098}(t/l)^{0.235}(t/s)^{-0.154}$ $\times Re_{D_h}^{0.0634\ln(Re_{D_h})-1.3} Pr_f^{0.00348}$ <p>For $0.2 \leq \beta < 0.25$</p> $j = 1.06(s/h)^{-0.1}(t/l)^{0.131}(t/s)^{-0.08}$ $\times Re_{D_h}^{0.0323\ln(Re_{D_h})-0.856} Pr_f^{0.0532}$ <p>For $0.25 \leq \beta < 0.3$</p> $j = \exp(1.3)(s/h)^{0.004}(t/l)^{0.251}(t/s)^{0.031}$ $\times Re_{D_h}^{0.0507\ln(Re_{D_h})-1.07} Pr_f^{0.051}$ <p>For $0.3 \leq \beta < 0.35$</p> $j = 0.2(s/h)^{-0.125}(t/l)^{0.21}(t/s)^{-0.069}$ $\times Re_{D_h}^{0.0005\ln(Re_{D_h})-0.338} Pr_f^{0.0549}$ <p>where</p> $\beta = ((2s+2t)(h+t) - 2sh)/((2s+2t)(h+t))$ $D_h = 4shl/(2(sl + hl + th) + ts)$	100-6000	0.046-10	0.72-50

Manson developed the first Colburn j -factor correlations from temperature measurements related to airflows over three different offset strip fin array geometries, as well as channels with other fin geometries, such as louvered fins and flat finned tubes (Refs. 23). Manson's study mainly deals with the transitional and turbulent flow regime in larger conventional channels, as apparent from the range of both Re_{D_h} and h/l reported in Table I. Moreover, it did not report under which thermal boundary condition the heat transfer was established in the offset strip fin array. Therefore, the applicability of Manson's correlations to micro- and mini-channels remains limited.

The temperature measurements of Kays and London were employed to construct multiple heat transfer correlations (Refs. 25). However, the experimental data is limited to only 50 operating points for the laminar flow regime, and the experimental study was conducted with a uniform channel wall temperature. This condition was established by circulating saturated steam on the outer surface of the air channels, the so-called control side of the setup.

Wieting (Refs. 24) presented one of the first correlations based on the data of Kays and London. One of the main limitations of Wieting's work is that it is unclear whether a consistent definition of the hydraulic diameter was used throughout the study (Refs. 27).

Wieting's correlation was adapted by Joshi and Webb (Refs. 26). They re-calibrated a Colburn j -factor correlation based on a data set which included, besides the data of Kays and London, measurements from London and Shah for one offset strip fin geometry (Refs. 35) and measurements from Walters for two other geometries (Refs. 36). Similarly to Kays and London, London and Shah used a condensing steam flow to impose a uniform channel wall temperature. The same experimental condition was achieved in the study of Walters through a large cooling water flow rate. The correlation of Joshi and Webb exhibits a discontinuity when the Reynolds number approaches a critical value $Re_{D_h}^*$ at the transition to a turbulent flow regime.

Manglik and Bergles (Refs. 27) analyzed the same data sets of Joshi and Webb. Their Colburn j -factor correlation is one of the most referenced in the literature since it features an accuracy of 20% without a discontinuous dependence on the Reynolds number over the transitional regime. Still, due to the considered experimental data sets, the correlation is only applicable to larger conventional offset strip fin channels.

In order to account for entrance effects in relatively short offset strip fin arrays, Dong et al. (Refs. 28) developed a Colburn j -factor correlation which includes a dependence on the flow length L (see Table I). This correlation was calibrated based on the experimental data for 16 offset strip fin channel geometries with a relatively large height and a flow length ranging from 5 to 14 fin lengths.

The experiments were carried out with air and Reynolds numbers characteristic of the transitional flow regime. A high flow rate of hot water was imposed on the control side to approximately achieve a uniform channel wall temperature. Given the geometries considered in the experiments, also the correlation of Dong et al. has a limited applicability to offset strip fins in micro- and mini-channels.

All the previously mentioned correlations were derived from tests carried out with air as the working fluid. Only a limited amount of studies considered other fluids. Guo et al. (Refs. 37) studied the heat transfer performance of lubrication oil with a Prandtl number above 100. They aimed to study novel designs of oil coolers containing inclined offset strip fin arrays with respect to the flow direction. The authors developed a Colburn j -factor correlation based on the experimental data for 16 different geometries with $h/l > 1$ and array inclination angles α between 0° and 90° . This data was gathered for the laminar flow regime, as it can be seen in Table II, and a uniform heat flux was imposed to the channel using an electrical film heater. Nevertheless, since the data set encompasses different Prandtl numbers and relatively large fin heights, the correlation is not accurate enough for the micro- and mini-channel applications considered in this work. Moreover, its use is also hampered by the lack of an explicit definition for the hydraulic diameter and a missing fin thickness value.

In the work of Bhowmik and Lee (Refs. 38), the working fluid is water with a Prandtl number of 7. Moreover, as it can be seen from the range of Reynolds numbers in Table II, their j -correlation covers both the laminar and turbulent flow regime. Their correlation was fitted to numerical data from simulations for a single offset strip fin geometry with $h/l = 1$. Therefore, its validity for different geometries is limited. The simulations were performed on a three-dimensional domain containing one fin row spanning 20 fin lengths in the streamwise direction under the assumption of lateral flow and temperature periodicity. All material properties were assumed constant. Furthermore, a uniform temperature was imposed as the thermal boundary condition on the top and bottom walls of the channel. As mentioned before, this boundary condition is not representative of the majority of micro- and mini-channel applications where offset strip fins are employed.

The extension of the correlations presented above to fluids with a different Prandtl number is generally obtained by assuming the Colburn j -factor to be independent of the Prandtl number (Refs. 25, 27, and 38). More specifically, if j is independent of Pr_f , this implies that the Nusselt number scales according to $Nu \sim Pr_f^{1/3}$. In the work of Kays and London (Refs. 25), it is men-

tioned that this scaling law applies to fluids with a Prandtl number between 0.5 and 15. However, they note that for viscous fluids with a high value of Pr_f , the relation $Nu \sim Pr_f^{0.4}$ is more appropriate. The influence of the Prandtl number on the Colburn j-factor for offset strip fin channels was explicitly analyzed by Kim et al. (Refs. 29). In their work, to cover a range of working fluids varying from air and water to diesel fuel, a Colburn j-factor correlation is presented for Prandtl numbers ranging from 0.72 to 50. Their correlation was fitted to heat transfer data obtained from numerical simulations on a three-dimensional fin row of 68 fin lengths in the streamwise direction, with a periodic boundary condition in the lateral direction. A wide range of values for the so-called blockage ratio β , as defined in Table II, and consequently also the relative fin height h/l , has been included in the data set by analyzing 39 different geometries. Yet, the numerical study of Kim et al. focuses on the turbulent flow regime and is based on the assumption of a uniform temperature in the entire solid domain of the channel. The accuracy of their correlation for the laminar flow regime thus remains questionable. The same consideration applies to the investigated range of Prandtl numbers, as the used numerical data are not available.

Also, other studies have examined the influence of the Prandtl number on the heat transfer in offset strip fin channels. The most notable references are the works of Tinaut et al. (Refs. 39) and Hu and Herold (Refs. 32). Tinaut et al. (Refs. 39) experimentally confirmed the independence of the Colburn j-factor with respect to the Prandtl number for $Pr_f \in (1, 100)$. Their measurements were performed for both laminar and turbulent flows on a single offset strip fin geometry, cooled by a large water flow rate on the control side. Although the authors fitted an empirical Colburn j-factor correlation to their experimental data, it has little relevance to the present study since their work reports no explicit definition of the hydraulic diameter nor a value of the fin length l and fin thickness t . Conversely, Hu and Herold (Refs. 32) tried to capture the influence of the fluid Prandtl number on the Nusselt number through an analytical model for Prandtl numbers between 0.7 and 150. The model used was based on simplified heat transfer relations for flow through rectangular channels and is therefore expected to have limited validity for offset strip fin arrays. Their results show that the correlations calibrated on experimental data for air overestimate the Colburn j-factor with a factor of two in the case of a liquid working fluid. This demonstrates the limitations of assuming j to be independent of Pr_f and therefore contradicts the conclusion from Tinaut et al. (Refs. 39).

It must be emphasized that, due to their empirical nature, the discussed correlations do not pro-

vide an explicit definition of the heat transfer coefficient in the Nusselt number. However, the heat transfer coefficients for periodic fin arrays are commonly defined on the basis of a cross-sectional averaged or bulk-temperature difference, or the one-dimensional reference temperature which appears in the $\varepsilon - NTU$ or LMTD methods (Refs. 25), similar to the theoretically derived heat transfer coefficients for straight channels without fins. As such, they are all spatially dependent along the channel in case of a periodic fin array. Nevertheless, their space dependence has been ignored in the correlations from the literature, so that the existing Nusselt number correlations are not exact and challenging to interpret from a theoretical viewpoint (Refs. 40 and 41). For that reason, in this work, we adopt the definition of the heat transfer coefficient proposed by Buckinx and Baelmans (Refs. 40 and 41). The latter is spatially constant and has a clear physical meaning in the macro-scale description of the periodically developed heat transfer regimes (Refs. 40 and 41). Its definition is also consistent with that of the interfacial heat transfer coefficient in porous media (Refs. 42–44), apart from some geometric scaling factors.

The previous literature review shows that a thorough analysis of the laminar heat transfer regime in micro- and mini-channels with offset strip fin arrays is still required. After all, it was found that only 50 temperature measurement points are available for the laminar flow regime (Refs. 16). Therefore, our study aims to investigate the Nusselt number in micro- and mini-channels for a steady laminar flow of water and air. In particular, we present the first study on the Nusselt number in the periodically developed conjugate heat transfer regime, in which the channel wall is subject to a uniform heat flux. This heat transfer regime is of interest, since it is expected to occur after a short development length from the channel inlet in the specified applications (Refs. 45 and 46), based on previous flow observations (Refs. 16). Furthermore, the boundary condition of a uniform heat flux, instead of a constant wall temperature, is more suitable for the analysis of many micro- and mini-channel applications. Finally, in contrast to the existing correlations in the literature, the Nusselt number correlations in this work are based on an exact heat transfer coefficient which is spatially constant and represents the macro-scale temperature difference between the fluid and the fins.

This paper is organized as follows. Section II presents the numerical model, from the geometry of the unit cell to the periodic temperature equations in the periodically developed regime, and the numerical procedure. Afterwards, in Section III, the influence of the Reynolds number, the Prandtl number and the geometrical parameters on the Nusselt number are discussed in detail.

The analysis covers a wide range of values for each of the geometrical parameters of the offset strip fins, as well as for the Reynolds number, which is varied between 1 and 600. Section IV presents the final Nusselt number correlation for periodically developed flow and heat transfer in micro- and mini-channels with an offset strip fin array. Some final remarks on the influence of the thermal boundary condition and the reference temperature difference are given in Section V.

II. UNIT CELL GEOMETRY AND PERIODICALLY DEVELOPED HEAT TRANSFER EQUATIONS

A. Geometry

Figure 2 illustrates the three-dimensional unit cell Ω_{unit} (Refs. 16) in which the periodically developed heat transfer regime is simulated. The unit cell consists of a fluid domain Ω_f and a solid domain Ω_s , divided by a fluid-solid interface Γ_{fs} . The top surface Γ_t and bottom surface Γ_b , which are a part of the unit cell's exterior boundary $\Gamma = \partial\Omega_{\text{unit}}$, coincide with the solid walls at the top and bottom of the channel. The unit cell is spanned by the three lattice vectors $\mathbf{l}_1 = l_1 \mathbf{e}_1 = 2l \mathbf{e}_1$, $\mathbf{l}_2 = l_2 \mathbf{e}_2 = 2(s+t) \mathbf{e}_2$ and $\mathbf{l}_3 = l_3 \mathbf{e}_3 = (h+t) \mathbf{e}_3$, with respect to the normalized Cartesian vector basis $\{\mathbf{e}_j\}_{j=1,2,3}$. Furthermore, the geometry of the unit cell is uniquely determined by the non-dimensional geometrical parameters h/l , s/l , and t/l , where the fin length l represents the reference length. From these three non-dimensional parameters, the porosity of the unit cell can be computed as

$$\epsilon = \frac{(h/l)(s/l)}{[(h/l)+(t/l)][(s/l)+(t/l)]}. \quad (1)$$

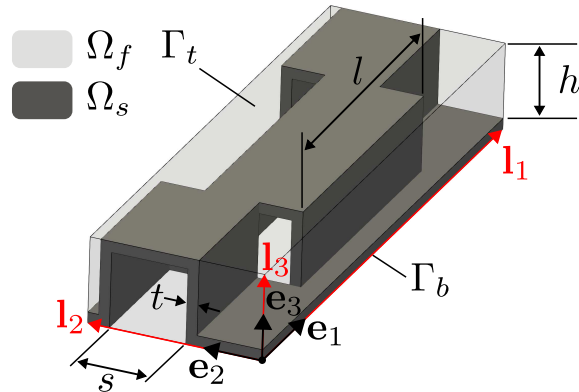


FIG. 2. Unit cell domain of an offset strip fin array

B. Periodically developed conjugate heat transfer equations

In the steady periodically developed heat transfer regime driven by an imposed uniform heat flux, the temperature field can be decomposed into a component that varies linearly with a spatially constant gradient ∇T and a spatially periodic component T^* (Refs. 44 and 47). Therefore, the periodic temperature field T^* , which equals T_f^* in Ω_f and T_s^* in Ω_s , is governed by the following energy conservation equations, if viscous dissipation is negligible, and other heat sources are absent (Refs. 41):

$$\begin{aligned} \rho_f c_f \nabla \cdot (\mathbf{u} T_f^*) &= -\rho_f c_f \mathbf{u} \cdot \nabla T + k_f \nabla^2 T_f^* && \text{in } \Omega_f, \\ 0 &= k_s \nabla^2 T_s^* && \text{in } \Omega_s. \end{aligned} \quad (2)$$

The applicable periodicity conditions and boundary conditions for the conjugate heat transfer problem are given by

$$\begin{aligned} T^*(\mathbf{x} + \mathbf{l}_j) &= T^*(\mathbf{x}) && \text{in } \Omega_f \cup \Omega_s, \\ T_f^* &= T_s^* && \text{in } \Gamma_{fs}, \\ -\mathbf{n}_{fs} \cdot k_f (\nabla T_f^* + \nabla T) &= -\mathbf{n}_{fs} \cdot k_s (\nabla T_s^* + \nabla T) && \text{in } \Gamma_{fs}, \\ -\mathbf{n} \cdot k_f (\nabla T_f^* + \nabla T) &= q_b && \text{in } \Gamma_{bf}, \\ -\mathbf{n} \cdot k_s (\nabla T_s^* + \nabla T) &= q_b && \text{in } \Gamma_{bs}, \\ \langle T^* \rangle &= \text{constant}, \end{aligned} \quad (3)$$

with $j = \{1, 2\}$. In the former equations, the thermal conductivity of the fluid and solid, k_f and k_s , as well as the densities ρ_f and ρ_s , are assumed to be constant, just like the dynamic viscosity μ_f and specific heat capacity c_f of the fluid. The temperature field T^* is spatially periodic over the unit cell along the lattice vectors \mathbf{l}_1 and \mathbf{l}_2 , similarly to the periodically developed velocity field \mathbf{u} , which follows from the periodic flow equations given in (Refs. 16). At the fluid-solid interface Γ_{fs} , the continuity of the temperature field and heat flux is required. In addition, at the bottom surface of the unit cell, which contains parts that belong to the fluid and solid ($\Gamma_b = \Gamma_{bf} \cup \Gamma_{bs}$), a uniform heat flux q_b is imposed in the form of a Neumann boundary condition. We remark that the unit normal vector \mathbf{n}_{fs} at Γ_{fs} points from the fluid domain Ω_f towards the solid domain Ω_s , while the unit normal vector \mathbf{n} at Γ points outward of the unit cell Ω_{unit} , such that the heat flux q_b is negative when directed towards Ω_{unit} . Finally, in order to have a unique solution for the periodic temperature field, its volume-averaged value over the unit cell domain $\langle T^* \rangle$ is imposed. This value depends on the development of the temperature field in the channel but does not affect the heat

transfer coefficient.

For a specified volume-averaged velocity vector $\langle \mathbf{u} \rangle$ over the unit cell, the temperature field T^* can be computed from equations (2)-(3), since the constant temperature gradient ∇T is determined by the imposed heat flux q_b (Refs. 41 and 44):

$$\nabla T = \frac{\langle q_b \delta_b \rangle}{\rho_f c_f \| \langle \mathbf{u} \rangle \|} \mathbf{e}_s. \quad (4)$$

Here, the Dirac surface indicator δ_b associated with the bottom interface Γ_b is defined such that $\langle \delta_b \rangle = 1/l_3$ represents the integral area of bottom surface per unit cell volume. In the right hand side of (4), the unit vector $\mathbf{e}_s \triangleq \langle \mathbf{u} \rangle / \| \langle \mathbf{u} \rangle \|$ indicates the direction of the volume-averaged velocity, and $\| \cdot \|$ denotes the Euclidean vector norm. Lastly, the volume-averaged value of any physical quantity ϕ is defined as

$$\langle \phi \rangle \triangleq \frac{1}{V_{\text{unit}}} \int_{\mathbf{r} \in \Omega_{\text{unit}}(\mathbf{x})} \phi(\mathbf{r}) d\Omega(\mathbf{r}), \quad (5)$$

$$V_{\text{unit}} = \mathbf{l}_1 \cdot (\mathbf{l}_2 \times \mathbf{l}_3). \quad (6)$$

The temperature field T^* in the unit cell determines the following heat transfer coefficient between the fluid and solid:

$$h_{\text{unit}} \triangleq \varepsilon_f^{-1} \frac{\langle q_b \delta_b \rangle}{\langle T^* \rangle^f - \langle T^* \rangle^s}. \quad (7)$$

This heat transfer coefficient characterizes the difference between the intrinsic volume-averaged temperatures of the fluid and solid in the unit cell, which are defined by $\langle T^* \rangle^f \triangleq \varepsilon_f^{-1} \langle T^* \gamma_f \rangle$ and $\langle T^* \rangle^s \triangleq \varepsilon_s^{-1} \langle T^* \gamma_s \rangle$, with $\varepsilon_f \triangleq \langle \gamma_f \rangle = \varepsilon$ and $\varepsilon_s \triangleq \langle \gamma_s \rangle = 1 - \varepsilon$. Here, we have used γ_f and γ_s to denote the fluid indicator and solid indicator respectively: $\gamma_f(\mathbf{x}) = 1 \leftrightarrow \mathbf{x} \in \Omega_f$, $\gamma_f(\mathbf{x}) = 0 \leftrightarrow \mathbf{x} \notin \Omega_f$ and $\gamma_s(\mathbf{x}) = 0 \leftrightarrow \mathbf{x} \in \Omega_f$, $\gamma_s(\mathbf{x}) = 1 \leftrightarrow \mathbf{x} \notin \Omega_f$. The heat transfer coefficient h_{unit} in equation (7) has been introduced in the macro-scale descriptions of periodically developed heat transfer by Buckinx and Baelmans (Refs. 40 and 41). In their macro-scale descriptions, the macro-scale variables are obtained through a double volume-averaging operation $\langle \cdot \rangle_m$ so that the interfacial heat transfer coefficient $h_{fs} \triangleq \varepsilon_{fm}^{-1} \langle q_{fs} \delta_{fs} \rangle_m / (\langle T \rangle_m^f - \langle T \rangle_m^s)$ becomes spatially constant in the periodically developed heat transfer regime, and identical to h_{unit} . Therefore, h_{unit} is the exact and physically meaningful heat transfer coefficient that relates the constant macro-scale heat transfer rate $\langle q_{fs} \delta_{fs} \rangle_m$ between the fluid and solid to the constant macro-scale temperature difference $\langle T \rangle_m^f - \langle T \rangle_m^s = \langle T^* \rangle^f - \langle T^* \rangle^s$ (Refs. 41).

The relationship between the heat transfer coefficient h_{unit} and the volume-averaged velocity $\langle \mathbf{u} \rangle$ will further be expressed as a non-dimensional relationship between the Nusselt number,

$$Nu_{\text{unit}} \triangleq \frac{h_{\text{unit}} l^2}{k_f}, \quad (8)$$

and the Reynolds number,

$$Re_l \triangleq \frac{\rho_f \|\langle \mathbf{u} \rangle\| l}{\mu_f}. \quad (9)$$

To be consistent with our previous work (Refs. 16), the fin length l is thus chosen as the reference length for the Nusselt number and the Reynolds number. Contrary to the hydraulic diameter D_h , the fin length l simplifies the interpretation of the Nusselt number and Reynolds number, as l is a single geometrical parameter instead of a combination of all the geometrical parameters. Besides, the actual definition of the hydraulic diameter implies that the latter varies in the streamwise direction along the fin, since the wetted area is different at each cross section of the channel.

When the periodically developed heat transfer regime extends over the largest part of the channel with offset strip fins, the Nusselt number Nu_{unit} will give an accurate indication of the overall temperature difference over the channel, for a constant heat flux at the channel wall. Furthermore, the volume-averaged velocity and thus the Reynolds number Re_l will correspond directly to the bulk velocity through the channel, as long as the flow retardation near the side walls of the channels does not significantly impact the total mass flow rate through the channel.

C. Numerical procedure

The periodic temperature equations (2)-(3) have been solved for periodic velocity fields at different Reynolds numbers, and for different material properties, using a finite-element discretization, in which the discretized temperature field was represented by continuous Galerkin tetrahedral elements of the second order. The same structured mesh as in (Refs. 16) was employed for the spatial discretization of the unit cell. For the finite-element formulation and the numerically parallelized solution of the discretized temperature equations, we use the software package FEniCSLab. This package was developed by G. Buckinx in the finite-elements-based computing platform FEniCS (Refs. 48).

To validate the employed numerical discretization, a mesh-independence study was performed at the two largest Reynolds numbers, for the four lowest unit cell porosities. Through the Richardson extrapolation and grid convergence index (Refs. 49 and 50), the relative discretization error on

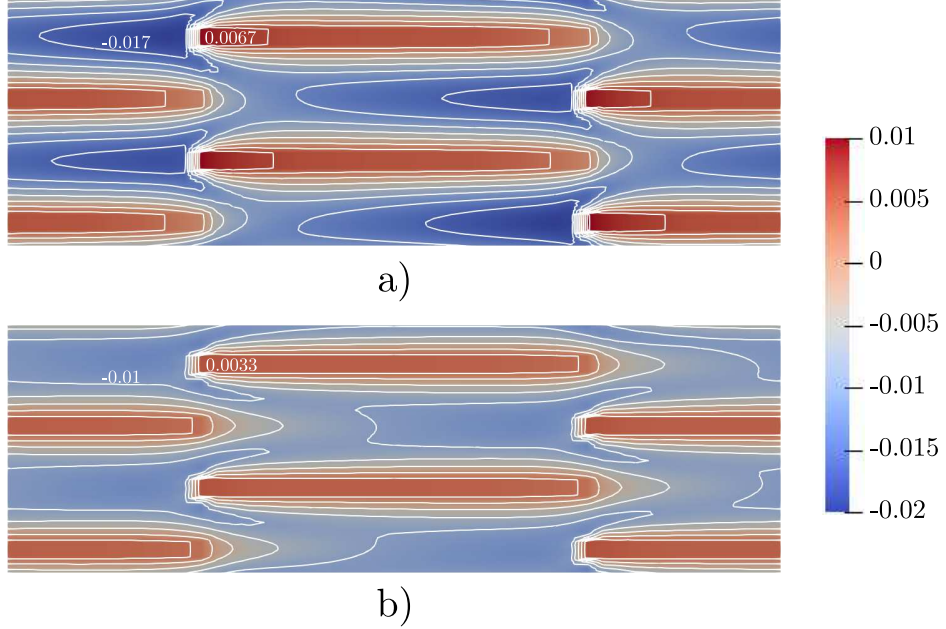


FIG. 3. The non-dimensional periodic temperature field $(T^* - \langle T^* \rangle) k_f / (q_b l)$, visualized by its iso-lines in the unit cell's mid-plane spanned by \mathbf{l}_1 and \mathbf{l}_2 for (a) $Re_l = 100$ (b) and $Re_l = 300$ when $Pr_f = 0.7$, $k_s/k_f = 10^4$, $t/l = 0.04$, $h/l = 0.48$, $s/l = 0.28$

the computed Nusselt number was estimated to remain below 1%.

In Figure 3, the non-dimensional periodic temperature field $(T^* - \langle T^* \rangle) k_f / (q_b l)$ in the mid-plane of the unit cell, spanned by \mathbf{l}_1 and \mathbf{l}_2 , is visualized through its iso-lines at a Reynolds number of 100 and 300 for a fluid Prandtl number of 0.7. From the depicted iso-line values, it can be seen that the temperature difference between the fluid and solid domain decreases when the Reynolds number Re_l is higher, which indicates an increased heat transfer coefficient.

Finally, we remark that due to the linearity of the periodic temperature equations (2)-(3) and the top-down symmetry of the fin geometry, the obtained heat transfer coefficient h_{unit} for an imposed heat flux q_b at the bottom surface of the unit cell is identical to h_{unit} when a heat flux q_b is imposed at both the top and bottom surface.

III. NUSSELT NUMBER FOR PERIODICALLY DEVELOPED HEAT TRANSFER

Considering the case where the volume-averaged velocity is aligned with the lattice vector \mathbf{e}_1 , we have determined the Nusselt number Nu_{unit} for a large set of Reynolds numbers and geometrical parameters, relevant to micro- and mini-channel applications (Refs. 5–13). The Nusselt number has been determined for two fluids, air and water, with a Prandtl number of $Pr_f = 0.7$ and $Pr_f = 7$ respectively (Ref. 51). The thermal conductivity ratio has been chosen accordingly as $k_s/k_f = 500$ and $k_s/k_f = 10^4$, since these values are representative for copper and air, and copper and water. All the geometrical parameters and material properties selected for our study are listed in Table III. The periodically developed heat transfer equations were solved for 197 different offset strip fin geometries. In total, 1168 data points for the Nusselt number were obtained for $Pr_f = 0.7$ and $k_s/k_f = 10^4$, while 1114 data points were collected for $Pr_f = 7$ and $k_s/k_f = 500$. The entire data set is tabulated in Appendix C. In the remainder of this section, the influence of the Reynolds number and the geometrical parameters on the unit cell's Nusselt number will be discussed in detail.

TABLE III. Values for the Reynolds number, the geometrical parameters, the Prandtl number, and thermal conductivity ratio, considered in the numerical study.

Re_l	1, 10, 15, 25, 35, 50, 75, 100, 150, 200, 300, 400, 600		
h/l	0.12, 0.16, 0.20, 0.24, 0.28, 0.32, 0.40, 0.48, 0.56, 0.68, 1.00		
s/l	0.12, 0.16, 0.20, 0.24, 0.28, 0.32, 0.40, 0.48		
t/l	0.01, 0.02, 0.04, 0.06	Air	Water
Pr_f		0.7	7
k_s/k_f		10^4	500

A. The influence of the Reynolds number Re_l on the Nusselt number

The dependence of the Nusselt number on the Reynolds number is illustrated in Figures 4 and 5 for various offset strip fin geometries. It can be observed that a linear relationship of the form

$$Nu_{\text{unit}} \simeq A + B Re_l, \quad (10)$$

accurately captures the data from our work. In this linear relationship, the parameters A and B are both functions of the geometrical parameters, the Prandtl number and the thermal conductivity

ratio. For all the parameters in Table III, the linear correlation (10) captures the dependence of the Nusselt number on the Reynolds number with an average and maximum relative error of 2% and 15%, respectively. A log-linear regression analysis confirmed that when the exponent of the Reynolds number equals 1, the relative error with respect to the data from this work is minimized, and the standard deviation on this exponent is 0.3. At the same time, the constant A exhibits no significant dependence on Pr_f and k_s/k_f . This can also be observed from the fitted functions in Figures 4 and 5. The influence of the Prandtl number and the thermal conductivity ratio on Nu_{unit} will be discussed in more detail in Section III F.

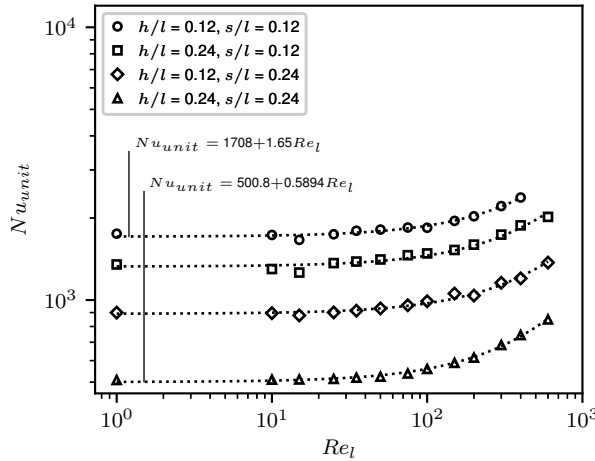


FIG. 4. Influence of the Reynolds number on the Nusselt number for steady periodically developed heat transfer, when $Pr_f = 0.7$, $k_s/k_f = 10^4$, $t/l = 0.04$

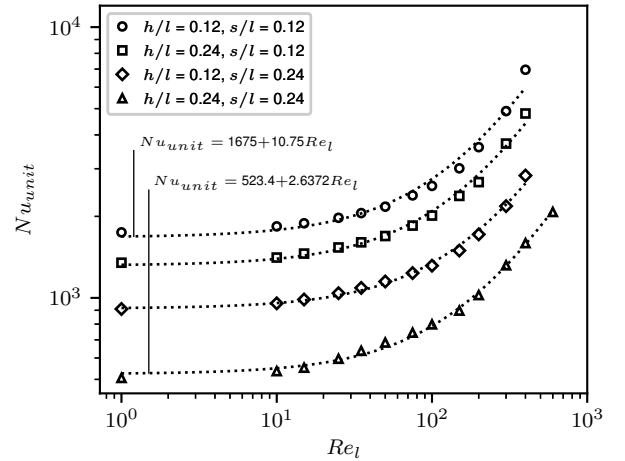


FIG. 5. Influence of the Reynolds number on the Nusselt number for steady periodically developed heat transfer, when $Pr_f = 7$, $k_s/k_f = 500$, $t/l = 0.04$

Figures 4 and 5 clearly show that for lower Reynolds numbers, i.e., when $Re_l < 10$, the Nusselt number becomes virtually independent of Re_l , as it is primarily determined by the constant A . At higher Reynolds numbers, when $Re_l > 100$, the influence of the Reynolds number Re_l on the Nusselt number becomes more significant through the linear term BRe_l .

The observed linear relationship between Nu_{unit} and Re_l is supported by the findings in various experimental and numerical performance studies for micro- and mini-channels applications in the literature (Refs. 5, 9–11, and 13). In addition, it closely resembles the form of the empirical correlations for the Nusselt number characterizing the convective heat transfer coefficient in porous media and arrays of circular and square cylinders: $Nu = A + BRe^b$ (Refs. 52–60). Nevertheless,

in these studies, the reported exponent b lies between 0.5 and 0.9. Moreover, many studies have suggested that $Nu \sim Re^b$ with $b < 1$, since they focused on the transitional regime in porous media and cylinder arrays. Indeed, the relation between the Nusselt number Nu and the Reynolds number Re , and thus the specific value of the exponent b , depends on the nature of the flow regime through the porous medium, as clarified in the study of Lu and Zhao (Refs. 60). Therefore, the influence of the flow regime on the precise relationship between Nu_{unit} and Re_l in arrays of offset strip fins is examined in more detail in Section III E. Here, we first show that the linear relationship (10) found for $b = 1$ is more accurate with respect to our data than the available correlations from the literature with $b < 1$.

In figures 6 and 7, the various Nusselt number correlations from the literature, listed in Tables I and II, are compared with the data from this work, for a single representative geometry. For the comparison, the different definitions of Nu and Re in the correlations from the literature, given in Section I, are converted to our definitions of Nu_{unit} and Re_l . Note that only an approximate conversion of the heat transfer coefficient is possible, due to the approximations made in the $\varepsilon - NTU$ and LMTD methods. This underlines again the importance of using an exact and physically meaningful definition of h_{unit} , as in equation (7).

As it can be seen in Figure 6, the correlations of Wieting (Refs. 24), Joshi and Webb (Refs. 26), and Manglik and Bergles (Refs. 27), all deviate significantly from our data, both in their predicted values and scaling with Re_l . They all predict a trend $Nu \sim Re^{0.5}$ in the laminar flow regime, while the trend in our data is $Nu \sim Re$. The reason is likely the fact that these correlations were fitted mainly to data points pertaining to the transitional and turbulent flow regime. As such, these correlations underestimate the Nusselt number data determined in this work with an average relative error of 70% and a maximum relative error of 90%, which occurs for $Re_l \simeq 1$.

The correlation from Dong et al. (Refs. 28), which predicts a trend $Nu \sim Re^{0.8}$, results in an even more considerable underestimation of our Nusselt number data, although an illustrative comparison has been omitted here. Again, this is most likely due to the fact that the latter authors only considered Reynolds numbers above 500, as shown in Table I. Also the correlation of Kim et al. (Ref. 29), which is illustrated in Figures 6 and 7, does not accurately capture the correct dependence of the Nusselt number on the Reynolds number for $Re_l < 100$ when $Pr_f = 0.7$ and $Pr_f = 7$, despite the fact it was obtained from a data set which did include lower Reynolds numbers. For $Re_l > 100$, it underestimates our Nusselt number data with an error similar to that of the correlations of Joshi and Webb, and Manglik and Bergles. It thus appears that the highly non-linear trend

$Nu \sim Re^{0.05\ln(Re)-0.1}$ proposed by Kim et al. does not apply to the steady laminar regime.

From the previous considerations, we conclude that the correlations from the literature cannot accurately capture the Reynolds number dependence of the Nusselt number for periodically developed flow and heat transfer in micro- and mini-channels with offset strip fins subject to an imposed heat flux.

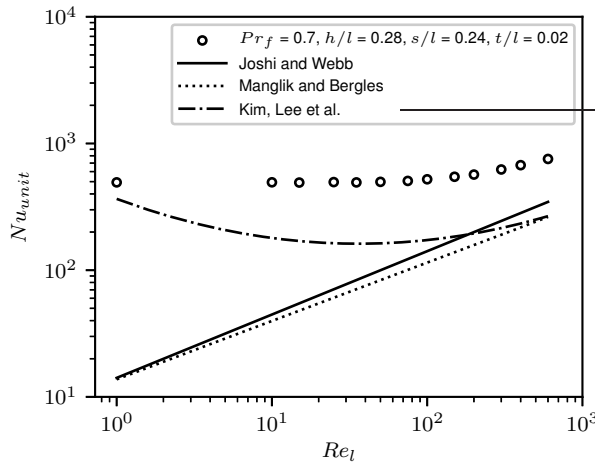


FIG. 6. A comparison between the Nusselt number correlations from the literature with the data from this work for steady periodically developed heat transfer at low Reynolds numbers, when $Pr_f = 0.7$, $t/l = 0.02$, $h/l = 0.28$, $s/l = 0.24$

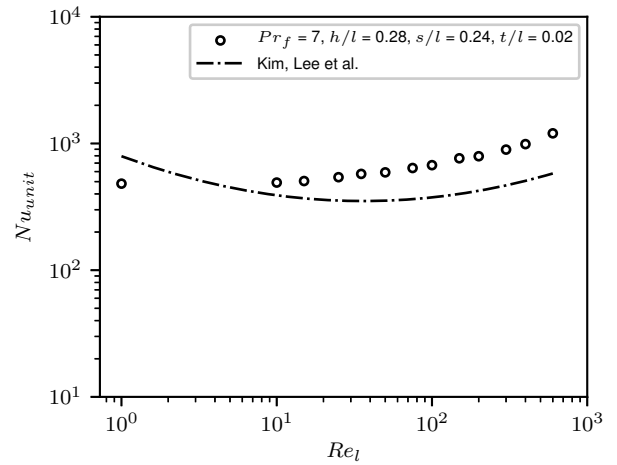


FIG. 7. A comparison between the Nusselt number correlations from the literature with the data from this work for steady periodically developed heat transfer at low Reynolds numbers, when $Pr_f = 7$, $t/l = 0.02$, $h/l = 0.28$, $s/l = 0.24$

B. The influence of the fin height-to-length ratio h/l on the Nusselt number

The influence of the fin height-to-length ratio h/l on the Nusselt number in the steady periodically developed heat transfer regime is illustrated in Figure 8. From our data set, it can be concluded that the Nusselt number Nu_{unit} becomes proportional to $(h/l)^{-2}$ for low values of h/l , in analogy to what is observed for developed heat transfer between two parallel plates. Notice that, in that case, the commonly used Nusselt number based on the channel height h is a constant (Refs. 17). This is consistent with our findings, as the Nusselt number in this work, Nu_{unit} , is based on the reference length l instead of h , and the heat transfer coefficient h_{unit} includes the

area of heat transfer surface per unit cell volume, given by $\langle \delta_b \rangle \simeq 1/h$. For developed heat transfer between two parallel plates with an imposed heat flux, this results in the analytical relation $Nu_{\text{unit}} = 10(h/l)^{-2}$. The asymptotic trend $Nu_{\text{unit}} \sim (h/l)^{-2}$ for $h/l \rightarrow 0$, thus can be explained by similarity with developed flow and heat transfer between two parallel plates. Indeed, as h/l decreases, the top and bottom plates become the main heat transfer surfaces, and the flow field resembles more and more the developed flow field between two parallel plates (Refs. 16).

On the other hand, when the fin height-to-length ratio is sufficiently large, the Nusselt number becomes independent of h/l , as Figure 8 shows. This asymptotic behaviour results from the fact that when h/l increases, the fins, but no longer the plates, become the main heat exchanging surface. For $h/l \rightarrow \infty$, the flow becomes more two-dimensional (Refs. 16). As a consequence, the temperature gradients at the fin sides will vary less along the direction \mathbf{e}_3 and therefore become independent of h/l .

The occurrence of the two asymptotic trends $Nu_{\text{unit}} \sim (h/l)^{-2}$ and $Nu_{\text{unit}} \sim (h/l)^0$ is greatly influenced by the fin pitch-to-length ratio s/l , and thus the aspect ratio s/h , as illustrated in Figure 8. More specifically, as s/h decreases, the contribution of the fin sides to the total transferred heat increases, so that the trend $Nu_{\text{unit}} \sim (h/l)^0$ starts to prevail at relatively lower h/l -ratios.

As a consequence of the former asymptotic trends, the influence of the fin height-to-length ratio on the Nusselt number is accurately described by

$$Nu_{\text{unit}} \simeq E \left(\frac{h}{l} \right)^{-2} + F. \quad (11)$$

Here, the parameters E and F depend on Re_l , Pr_f and k_s/k_f , as well as the geometrical parameters s/l and t/l . When E and F are determined by a least-squares fitting, the correlation (11) can predict all the Nusselt number data from this work with a mean relative error of 0.5%, and a maximum relative error of 8%.

In the literature, the influence of the fin height-to-length ratio on the Nusselt number has been taken into account by a factor of the form $(h/l)^c$, hence by means of a single exponent c . However, the existing correlations are also implicitly affected by the ratio h/l through the Reynolds number, via the specific definition of the hydraulic diameter. For the studies in Tables I and II, this leads to an effective exponent C , such that $Nu_{\text{unit}} \sim (h/l)^C$, which lies between -1.3 to -1.8 for small fin heights. As a result, the correlations from the literature, which mainly focus on conventional offset strip fin channels with larger fin height-to-length ratios, underestimate the Nusselt number for micro- and mini-channels. This statement is supported by Figure 9. Even when the least-

square differences with our data is minimized by rescaling the correlations from the literature with a constant to account for any incorrect scaling with the other parameters, our data is still underestimated with a mean relative error of 40%, and a maximum relative error of 85% near $h/l \simeq 0.1$. Furthermore, Figure 9 reveals that the correlation presented in the numerical study of Kim et al. (Refs. 29) does not even predict a continuous trend of the Nusselt number with respect to the height-to-length ratio, since the latter is based on a piecewise function of the porosity (see Table II).

Finally, all the available correlations from the literature for offset strip fins do not recover a constant Nusselt number Nu_{unit} for $h/l \rightarrow \infty$ as it can be seen in Figure 9, but instead predict a scaling close to $Nu_{unit} \sim (h/l)^{0.2}$ for $h/l \rightarrow \infty$.

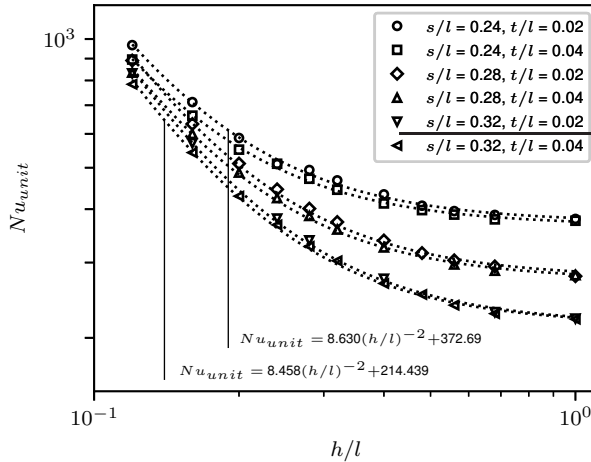


FIG. 8. Influence of the fin height-to-length ratio on the Nusselt number for steady periodically developed heat transfer, when $Re_l = 10$, $Pr_f = 0.7$, $k_s/k_f = 10^4$

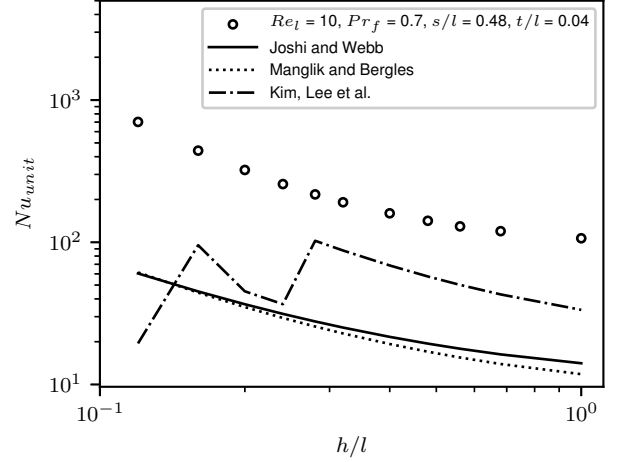


FIG. 9. A comparison between the Nusselt number correlations from the literature with the data from this work for steady periodically developed heat transfer at small fin heights, when $Re_l = 10$, $Pr_f = 0.7$, $s/l = 0.48$, $t/l = 0.04$

C. The influence of the fin pitch-to-length ratio s/l on the Nusselt number

Figure 10 illustrates the variation of the Nusselt number with the fin pitch-to-length ratio s/l . According to our data, the Nusselt number becomes infinite as s/l approaches a value close to that of the relative fin thickness t/l . In the limit $s = t$, the channel becomes fully blocked. This implies

that the fluid flows ever more slowly past the fins as $s \rightarrow t$. Consequently, the average temperature difference between the fluid and solid domain progressively decreases as $s \rightarrow t$, giving rise to an ever larger value of the Nusselt number. Therefore, we propose to capture the variation of the Nusselt number with the fin pitch-to-length ratio by means of a correlation of the form

$$Nu_{\text{unit}} \simeq G \left(\frac{s}{l} - \frac{t}{l} \right)^d + H. \quad (12)$$

Here, the parameters G , H and d are a function of Re_l , Pr_f and k_s/k_f , and the remaining geometrical parameters h/l and t/l .

As it is shown in Figure 10, the correlation form (12) results in a quite accurate fit of our Nusselt number data. However, the negative exponent d cannot be assumed to be constant over the entire data set. Nevertheless, the exponent d can be approximated by a constant over distinct ranges of the Reynolds number and the geometrical parameters. For example, for $Re_l \in (150, 600)$ and $h/l \in (0.3, 1)$, the correlation (12) results in a relative error below 5% with respect to our data, if $d = -1.29$, for all Prandtl numbers, thermal conductivity ratios and fin thickness-to-length ratios studied in this work.

Besides the asymptotic behaviour $Nu_{\text{unit}} \rightarrow \infty$ for $s/l \rightarrow t/l$, the relationship (12) is in line with our observation from Figure 10 that the Nusselt number becomes independent of the relative fin pitch for high values of s/l . This asymptotic trend for $s/l \rightarrow \infty$ corresponds to the case where less heat is transferred by the fin sides in comparison to the top and bottom plate. Therefore, the value of s/l after which the Nusselt number becomes independent of s/l depends significantly on how large the fin sides are compared to the plate surface. Such a characteristic is well represented by the fin aspect ratio s/h . More specifically, for lower values of s/h or smaller fin heights, the fin sides will inevitably contribute less to the total heat transfer surface area than the bottom and top plate. Thus, the Nusselt number will become independent of the relative fin pitch s/l at lower s/l -values.

The correlations from the literature typically express the influence of the fin pitch-to-length ratio on the Nusselt number as $Nu \sim (s/l)^k$ with $k < 0$. Of all correlations listed in Tables I and II, practically only the one proposed by Joshi and Webb (Refs. 26) complies with the limit of $Nu_{\text{unit}} \rightarrow \infty$ for $s/l \rightarrow t/l$. Nevertheless, this limit is incorporated implicitly through the definition of the hydraulic diameter $D_h \sim (s-t)$ and reference velocity $U_{\text{ref}} \sim (s-t)^{-1}$, so that the correlation becomes equivalent to the scaling law $Nu \sim (s/l - t/l)^{-0.85}$ when $s/l \rightarrow t/l$. Such a dependence leads to an overestimation of our Nusselt number data up to 50% for $s/l < 0.25$.

Strictly speaking, also the correlation of Bhowmik (Refs. 38) respects the limit of $Nu_{\text{unit}} \rightarrow \infty$ for $s/l \rightarrow t/l$, since the author used a definition of the hydraulic diameter identical to that of Joshi and Webb. However, the correlation of Bhowmik is only applicable to just a single offset strip fin geometry. The remaining correlations in Tables I and II typically underestimate our Nusselt number data by as much as 40% for $s/l < 0.25$, as we have illustrated in Figure 11. The correlation of Kim et al. (Refs. 29) in particular, shows the largest and most inconsistent deviations with our data, due to its discontinuous dependence on the fin porosity and thus the fin pitch-to-length ratio. We remark that, in the preceding discussion, all the reported errors have been computed after rescaling the correlations with a constant, to minimize the least-square differences with our data and compensate for any incorrect scaling with the other parameters. Lastly, we notice that the correlations from the literature fail to predict the correct limit of a constant Nusselt number for $s/l \rightarrow \infty$. On the contrary, they still show a dependence on s/l of the form $(s/l)^k$ with $k \in (-0.2, 0.1)$ for larger values of the fin pitch-to-length ratio,

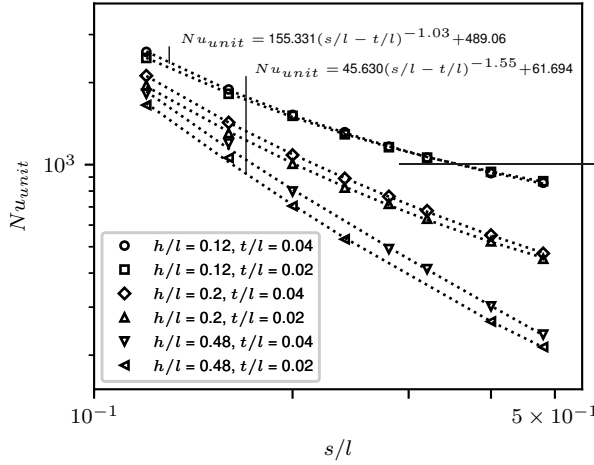


FIG. 10. Influence of the fin pitch-to-length ratio on the Nusselt number for steady periodically developed heat transfer, when $Re_l = 100$, $Pr_f = 7$, $k_s/k_f = 500$

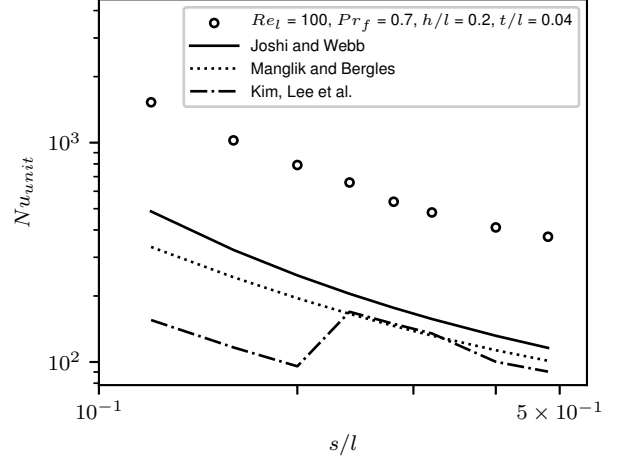


FIG. 11. A comparison between the Nusselt number correlations from the literature with the data from this work for steady periodically developed heat transfer at small fin heights, when $Re_l = 100$, $Pr_f = 0.7$, $t/l = 0.04$, $h/l = 0.20$

D. The influence of the fin thickness-to-length ratio t/l on the Nusselt number

The third and final geometrical parameter whose influence on the Nusselt number is assessed is the fin thickness-to-length ratio t/l . In Figure 12 we observe that, as the fin thickness decreases, the Nusselt number becomes independent of the fin thickness-to-length ratio t/l . This can be explained by the fact that the heat transfer at the fin sides normal to the main flow direction e_1 and parallel to e_2 , becomes negligible once the fin thickness t , and thus the width of these sides, is sufficiently small. This implies that the relative fin thickness t/l will no longer affect the heat transfer coefficient. We remark that the heat transfer at the fin sides mainly occurs at the leading edge of the fin, as little heat is transferred near the wake at the trailing edge of the fin. This is also visible from the closely spaced iso-lines at the leading edge in Figure 3, which indicate the presence of large temperature gradients. Additionally, we observe again in Figure 12 that the Nusselt number becomes infinite when t/l approaches the fin pitch-to-length ratio s/l , as discussed in the preceding subsection.

Based on our data, the dependence of the Nusselt number on the fin height-to-length ratio is accurately captured by a correlation of the form

$$Nu_{\text{unit}} \simeq J \left(\frac{t}{l} \right)^m + K, \quad (13)$$

where the parameters J , K and m depend on Re_l , Pr_f , k_s/k_f , as well as the other geometrical parameters s/l and t/l . It appears from Figure 12 that the exponent m cannot be treated as a constant over all our Nusselt number data. We found that $m = 0$ for $Pr_f = 0.7$ and $k_s/k_f = 10^4$, as Nu_{unit} appears to be virtually independent of the fin thickness-to-length ratio for all t/l -values considered in this work. On the other hand, for $Pr_f = 7$ and $k_s/k_f = 500$, the best fitting is obtained for $m > 0$. At the same time, m can be taken constant over wide intervals of the fin pitch-to-length ratio. For instance, the correlation form (13) holds within a relative error of 5% in the case that $Pr_f = 7$, $k_s/k_f = 500$, if $m = 0.50$, as long as $Re_l \in (1, 600)$, $h/l \in (0.1, 1)$ and $s/l \in (0.3, 0.5)$.

The correlations of Joshi and Webb (Refs. 26) and Bhowmik (Refs. 38) comply with the observation that Nu_{unit} becomes independent of the fin thickness-to-length ratio for small values of t/l . However, the other correlations from the literature express the influence of the fin thickness on the Nusselt number through a scaling law of the form $Nu_{\text{unit}} \sim (t/l)^m$ with $m \in (0.02, 0.2)$ for $t/l \rightarrow 0$. As a result, they underestimate the Nusselt number data from this work with a relative error up to 40% for $t/l < 0.02$, even after they are rescaled by a constant factor to minimize the least-square differences between each correlation and our data, and to compensate for their

incorrect scaling with other parameters. Moreover, the correlation of Kim et al. (Refs. 29) does not predict a continuous relationship between Nu and t/l as illustrated in Figure 13, for the same reason as discussed previously.

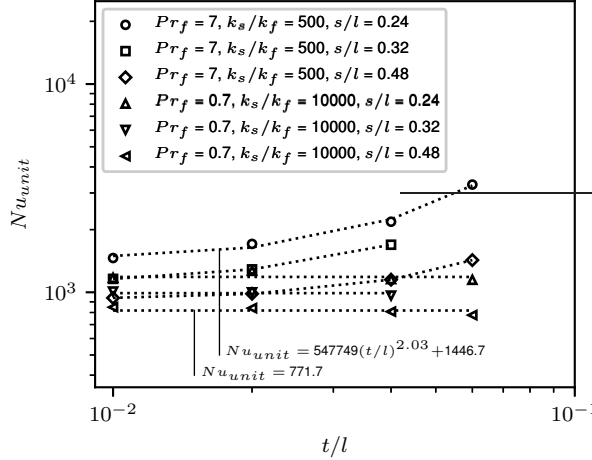


FIG. 12. Influence of the fin thickness-to-length ratio on the Nusselt number for steady periodically developed heat transfer, when $Re_l = 300$, $h/l = 0.12$

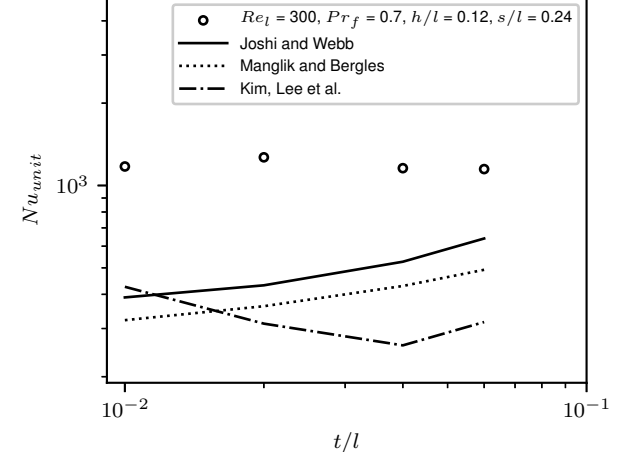


FIG. 13. A comparison between the Nusselt number correlations from the literature with the data from this work for steady periodically developed heat transfer at small fin heights, when $Re_l = 300$, $Pr_f = 0.7$, $h/l = 0.12$, $s/l = 0.24$

E. The influence of the critical Reynolds number

Despite the fact that our entire Nusselt number data set can be accurately captured by a linear relationship of the form $Nu_{\text{unit}} \simeq A + BRe_l$, a detailed analysis reveals a more complex scaling of Nu_{unit} with Re_l . Although the Nusselt number approximately becomes constant for $Re_l \rightarrow 0$, so $Nu_{\text{unit}} \rightarrow A$, the correction term $Nu_{\text{unit}} - A$ only approximately behaves as BRe_l for some constant B . In Figure 14, it is illustrated that the correction term $Nu_{\text{unit}} - A$ can only be considered to be linearly dependent on Re_l with a constant slope B over a specific Reynolds number range $Re_l \in (Re_{l,c}, Re_{l,c}^*)$. In this figure, the constant term A has been determined by fitting the Nusselt number in the lower Reynolds range, such that the fit $Nu_{\text{unit}} = A$ has a relative error below 1% over this Re_l -range. Furthermore, the critical Reynolds numbers $Re_{l,c}$ and $Re_{l,c}^*$ have been determined as the

values of Re_l for which the correction term $Nu_{\text{unit}} - A$ deviates 1% from the linear fit ($Nu_{\text{unit}} - A = BRe_l + D$). It should be noted that the offset D was added to ensure the robustness of the fitting procedure, since there is some numerical uncertainty on A . However, since $D \ll A$, the interval $Re_l \in (Re_{l,c}, Re_{l,c}^*)$ actually indicates the validity of the linear relationship $Nu_{\text{unit}} \simeq A + BRe_l$.

In our previous work (Ref. 16), two critical Reynolds numbers $Re_{l,ws}$ and $Re_{l,st}$ were introduced to indicate the transition from the weak inertia regime to the strong inertia regime and the transition from the strong inertia regime to the transitional regime, respectively. For the weak and strong inertia regime, the pressure drop deviates from Darcy's law with a term that is cubic and quadratic in the volume-averaged velocity, respectively (Refs. 16 and 61). This term is typically known as Forchheimer's correction. A comparison of the critical Reynolds numbers for these flow regimes, $Re_{l,ws}$ and $Re_{l,st}$, with the critical Reynolds numbers for the heat transfer regime, $Re_{l,c}$ and $Re_{l,c}^*$, indicates a strong correspondence between these quantities. More specifically, $Re_{l,c}$ and $Re_{l,ws}$ have been found to virtually coincide for all unit cell geometries, Prandtl numbers and thermal conductivity ratios investigated in this work, as their average and maximum relative difference are 1% and 10%, respectively. The same conclusion can be drawn for $Re_{l,c}^*$ and $Re_{l,st}$, whose average and maximum relative difference equal 3% and 10%, respectively. As a consequence, we can deduce that the critical Reynolds numbers $Re_{l,c}$ and $Re_{l,c}^*$ depend on the geometrical parameters in the same way as $Re_{l,ws}$ and $Re_{l,st}$, as discussed in (Refs. 16).

The coincidence of the critical Reynolds numbers suggests that distinguishable heat transfer regimes are directly linked to the underlying flow regimes. In the literature, similar observations have been made for the heat transfer regimes in porous media (Refs. 53, 54, 56, 59, and 60). For instance, in the work of Lu et al. (Refs. 60), it was empirically assessed that the scaling of the Nusselt number with the Reynolds number is given by $Nu_{\text{unit}} \sim Re_l^b$, where the exponent b can be considered a constant for each different flow regime. Besides the weak and strong inertia regime, they also considered the so-called pre-Darcy regime, which is not considered in this work. Nevertheless, as no analytical studies have been conducted on the theoretical scaling laws for the Nusselt number in porous media and fin arrays, the precise connection between the different flow and heat transfer regimes is currently not fully understood.

Finally, we remark that Figure 14 confirms that any deviation from the trends $Nu_{\text{unit}} = A$ and $Nu_{\text{unit}} = A + BRe_l$ remains small. This implies that, from a practical perspective, the linear correlation (10) is sufficiently accurate to model periodically developed heat transfer in offset strip fin arrays in micro- and mini-channels subject to a constant heat flux.

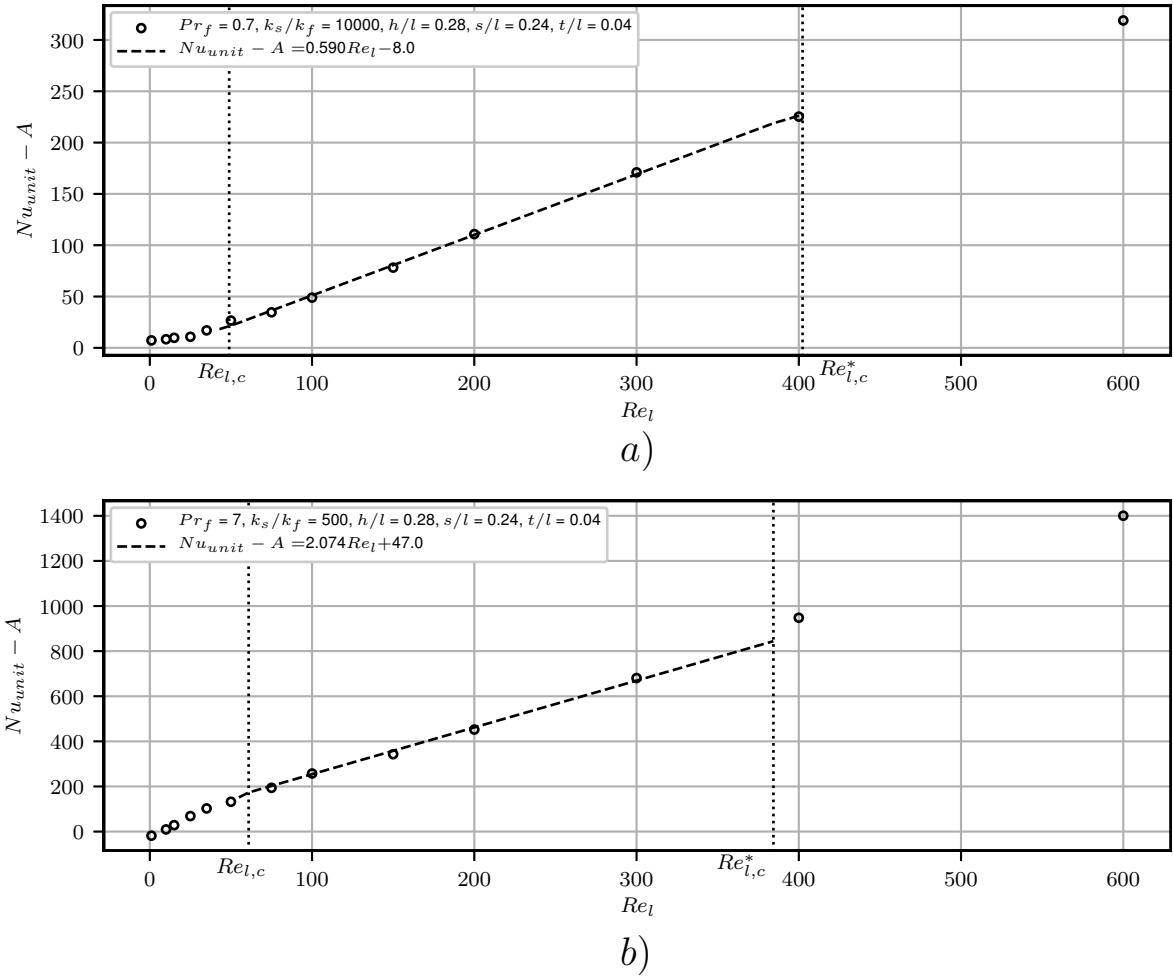


FIG. 14. Scaling of the correction term $Nu_{unit} - A$ with Re_l for steady periodically developed heat transfer with (a) $Pr_f = 0.7$ and $k_s/k_f = 10^4$, and (b) $Pr_f = 7$ and $k_s/k_f = 500$, when $h/l = 0.28$, $s/l = 0.24$, $t/l = 0.04$

F. The influence of the Prandtl number Pr_f and the thermal conductivity ratio k_s/k_f on the Nusselt number

So far, the Nusselt number was only investigated for two Prandtl numbers: $Pr_f = 0.7$ (air) and $Pr_f = 7$ (water), while the conductivity ratio was kept fixed to $k_s/k_f = 10^4$ and $k_s/k_f = 500$. Therefore, the influence of these material properties is now examined more thoroughly.

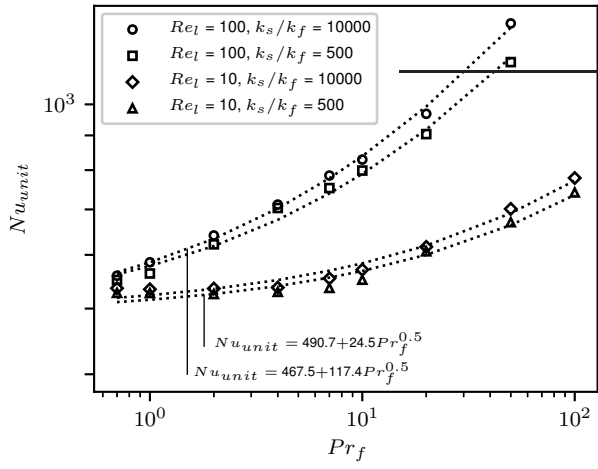


FIG. 15. Influence of the Prandtl number on the Nusselt number for steady periodically developed heat transfer, when $h/l = 0.24$, $s/l = 0.24$, $t/l = 0.02$

In Figure 15, the influence of the Prandtl number Pr_f is illustrated for a single unit cell geometry, for two conductivity ratios, $k_s/k_f = 500$ and $k_s/k_f = 10^4$, and two Reynolds numbers, $Re_l = 10$ and $Re_l = 100$. The range of Prandtl numbers displayed in this figure is relevant for thermal oils used in heat recuperators (Refs. 62). It can be observed that for the selected parameters, the Nusselt number correlates well with the Prandtl number according to a scaling law of the type

$$Nu_{\text{unit}} \simeq M + NP_r f^{0.5}, \quad (14)$$

where the standard deviation on the exponent of the Prandtl number equals 0.1. As a matter of fact, the correlation above predicts all the data points for the Nusselt number in Figure 15 with an average error of 2%, and a maximum relative error of 4%. It clearly reflects that for low Prandtl numbers, the Nusselt number becomes independent of Pr_f . In general, the parameters M and N in correlation (14) vary, of course, with the Reynolds number, the thermal conductivity ratio, and the offset strip fin geometry.

Figure 15 shows that the Nusselt number remains constant over a wider range of Prandtl numbers, when the Reynolds number decreases. This observation is predicted by the empirical correlations for convective heat transfer in porous media and cylinder arrays, which relate the Nusselt number to the Reynolds number and Prandtl number through a relationship of the form

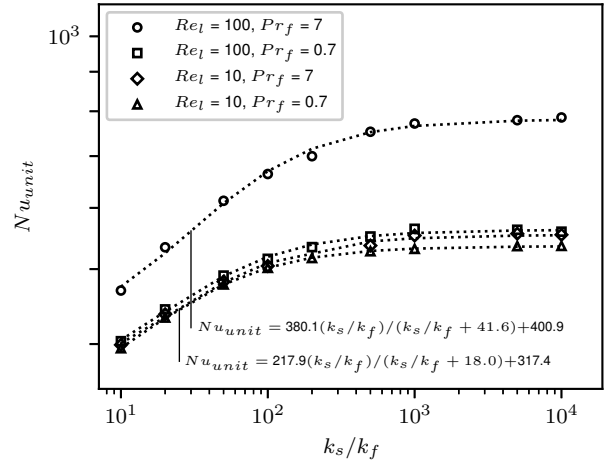


FIG. 16. Influence of the thermal conductivity ratio on the Nusselt number for steady periodically developed heat transfer, when $h/l = 0.24$, $s/l = 0.24$, $t/l = 0.02$

$Nu = M + NRe_l^bPr_f^n$. Commonly, the coefficients M and N in this relationship depend solely on the geometry, and the exponents satisfy $b \in (0.5, 0.9)$ and $n \in (0.2, 0.4)$ (Refs. 52, 53, 55–58). The finding that our data from Figure 15 indicates a larger exponent ($n = 0.5$) can be attributed to the different geometry of offset strip fins and the fact that we considered a limited number of data points for the Prandtl number.

It is worth pointing out that the scaling law (14) observed in Figure 15 deviates significantly from the correlations for offset strip fins in the literature. The latter all predict a trend $Nu \sim Pr_f^n$ with $n \in (0.3, 0.4)$ and thus fail to predict a constant limit of the Nusselt number for low Prandtl numbers and low Reynolds numbers, despite its relevance for micro- and mini-channels. Moreover, these correlations also underestimate our data in Figure 15 for larger Reynolds numbers, due to their lower exponent n for the Prandtl number. This mismatch is arguably caused by a different scaling of the Nusselt number with the Prandtl number in the transitional and turbulent flow regime, which most of the data in the literature belong to. For example, the correlation of Kim et al. (Refs. 29), which was constructed for Prandtl numbers ranging from 0.72 to 50 (see Table II), underestimates our data in Figure 15 with at least 20% for $Pr_f < 2$ and $Re_l = 100$, as well as $Pr_f < 7$ and $Re_l = 10$. Similar discrepancies are observed between our data and the correlations of Manglik and Bergles (Refs. 27) and Joshi and Webb (Refs. 26). For those correlations, it is assumed that the dependence of the Nusselt number on the Prandtl number is captured in the definition of the Colburn j-factor, through the factor $Pr^{1/3}$. This additional data set is tabulated in Appendix D.

The influence of the thermal conductivity ratio k_s/k_f on the Nusselt number is illustrated in Figure 16. For low values of k_s/k_f , the Nusselt number scales linearly with the thermal conductivity ratio k_s/k_f . On the contrary, for high values of k_s/k_f , in this case $k_s/k_f > 500$, the Nusselt number Nu_{unit} becomes independent of the thermal conductivity ratio. When the ratio k_s/k_f is high, the periodic temperature field T^* inside the solid domain becomes approximately uniform with a limited dependence on k_s/k_f , as discussed in (Refs. 31) in the context of conjugate heat transfer in pin-fin arrays. This means that the influence of the thermal conductivity ratio k_s/k_f on the temperature field in the fluid domain, and hence Nu_{unit} , is very weak in that case. As a result, when considering typical values for the material properties of air and water, namely $Pr_f < 10$ and $k_s/k_f > 500$, both the Prandtl number and the thermal conductivity ratio do not exert any significant influence on the Nusselt number at low Reynolds numbers. The same conclusions can be

drawn by observing Figures 4 and 5.

Based on the two observed trends for low and high k_s/k_f -ratios, the dependence of the Nusselt number on the thermal conductivity ratio is asymptotically equivalent to the form

$$Nu_{\text{unit}} \simeq P \frac{(k_s/k_f)}{(k_s/k_f) + R} + Q. \quad (15)$$

This expression results in an average relative error of 0.5% and a maximum relative error of 2% with respect to the data in Figure 16. As discussed in Section I, the influence of k_s/k_f on the Nusselt number for offset strip fins has not been reported in literature before. Therefore, the parameter k_s/k_f does not appear in the available correlations from the literature, and a comparison with our data could not be made.

IV. NUSSELT NUMBER CORRELATION

A. Fitting approach

To obtain a final correlation for the Nusselt number in the steady periodically developed heat transfer regime in micro- and mini-channels with offset strip fins, we followed the same two-step procedure as proposed for the friction factor in our previous work (Ref. 16). First, we determined the optimal parameter values for multiple heuristically chosen candidate correlations, complying with the forms (10)-(13). Hereto, we used a non-linear least-squares optimization method based on a trust region reflective algorithm (Refs. 63). Secondly, we calculated the most likely parameter values for each candidate correlation using the Bayesian approach for parameter estimation and model validation (Refs. 64). Through the Bayesian approach, we also obtained for each candidate correlation its log-evidence, which is a statistical measure to quantify the suitability of the correlation to represent the data. Finally, we selected the candidate correlation and its fitting parameters that resulted in the highest relative accuracy and the highest log-evidence value for our Nusselt number data. We note that both the optimal and most likely parameter values were found to be equal within their significant digits for the final Nusselt number correlations presented next.

B. Fitting result

The proposed correlation for the Nusselt number in the case of air ($Pr_f = 0.7$ and $k_s/k_f = 10^4$) is

$$Nu_{\text{unit}} = c_0 + c_1 Re_l,$$

with

$$\begin{aligned} c_0 &= 6.44(h/l)^{-2} + 9.60(h/l)^{-1.24} + 24.4(s/l)^{-1.85}, \\ c_1 &= 0.112(s/l - t/l)^{-0.61}(h/l)^{-0.48}. \end{aligned} \quad (16)$$

This correlation results in an average relative error of 3% with respect to the Nusselt number data in this work. The maximum relative error is below 6%, 8% and 12% for, respectively, 90%, 95%, 99% of the data points.

The proposed Nusselt number correlation in the case of water ($Pr_f = 7$ and $k_s/k_f = 500$), is

$$Nu_{\text{unit}} = d_0 + d_1 Re_l,$$

with

$$\begin{aligned} d_0 &= 3.84(h/l)^{-2} + 19.2(h/l)^{-1.39} + 22.3(s/l)^{-1.87}, \\ d_1 &= 1.26(s/l - t/l)^{-1.07}(t/l)^{0.54}(h/l)^{-0.56}. \end{aligned} \quad (17)$$

In this case, the average relative error is 4% with respect to our data, while the maximum relative error remains below 9%, 11% and 18% for, respectively, 90%, 95%, 99% of the data points.

The accuracy of correlations (16) and (17) is illustrated in Figures 17 and 18. For example, all candidate correlations of the form $Nu_{\text{unit}} = A + B Re_l$ resulted in log-evidence values two times larger than those of the form $Nu_{\text{unit}} = B Re_l^b$, despite the latter form is most frequently adopted in the literature.

The correlations (16) and (17) reflect that a linear relation between the Nusselt and the Reynolds number is very precise for Reynolds numbers Re_l ranging from 1 to 600. Furthermore, they are consistent with all the discussed trends (11)-(13) which characterize the influence of the geometrical parameters on Nu_{unit} .

With regard to the influence of the fin height-to-length ratio h/l , the final correlations respect the asymptotic trends $Nu_{\text{unit}} \sim (h/l)^{-2}$ for $h/l \rightarrow 0$ and $Nu_{\text{unit}} \sim (h/l)^0$ for $h/l \rightarrow \infty$. At the same time, they include some additional terms proportional to $(h/l)^b$ with $b \neq -2$ to better match our data for intermediate values of h/l . We remark that their limits $Nu_{\text{unit}} = 6.44(h/l)^{-2}$ (for air) and $Nu_{\text{unit}} = 3.84(h/l)^{-2}$ (for water), which are found for $h/l \rightarrow 0$, do not correspond to the Nusselt

number for fully-developed heat transfer between two parallel plates subject to a constant heat flux (Refs. 35). In contrast, the asymptotic value of the friction factor for offset strip fins in the limit of $h/l \rightarrow 0$ was found to agree well with the one for fully-developed flow between parallel plates (Refs. 16). This can be explained by the fact that the offset strip fins still thermally connect the top and bottom plates of the channel, even when the fin height-to-length ratio h/l and the fin thickness-to-length ratio t/l approach zero. As such, there remains a path of low thermal resistance in the solid fins, along which heat is more easily conducted from the bottom plate to the top plate, than through fluid. Nevertheless, the asymptotic scaling of Nu_{unit} with $(h/l)^{-2}$ for $h/l \rightarrow 0$ is in agreement with the Nusselt numbers for fully-developed heat transfer between two parallel plates with any type of thermal boundary condition (Refs. 35).

Concerning the fin pitch-to-length ratio s/l , the final correlations (16) and (17) reveal that Nu_{unit} becomes independent of s/l for $s/l \rightarrow \infty$. Besides, they indicate that $Nu_{\text{unit}} \rightarrow \infty$ for $s \rightarrow t$ and that the Nusselt number becomes directly proportional to the Reynolds number when $s \rightarrow t$. The reason is that the coefficients c_1 and d_1 in equations (16) and (17) become dominant in that limit. This prediction is in line with many empirical correlations from the literature (Refs. 54, 57, and 60), although it is still not clear whether it is justified from a theoretical perspective.

With respect to the fin thickness-to-length ratio t/l , the final correlations show that t/l barely affects the Nusselt number when t/l is small. Therefore, the correlation factors c_0 and d_0 are independent of t/l . In the case of air ($Pr_f = 0.7$ and $k_s/k_f = 10^4$), even the correlation term c_1 does not directly depend on t/l . On the contrary, for water ($Pr_f = 7$ and $k_s/k_f = 500$), the correlation term d_1 does scale with $(t/l)^{0.54}$, as it accounts for a more significant influence of the thickness-to-length ratio.

Finally, it is worth mentioning that the correlations (16) and (17) are valid for air at temperatures between 0°C and 500°C , and for water at temperatures between 15°C to 25°C , respectively. Yet, from the analysis in Section III F, it is expected that the value of Nu_{unit} , and in particular of the terms c_0 and d_0 , are not significantly influenced by Pr_f or k_s/k_f , as long as the Reynolds number remains below 10.

V. FINAL REMARKS

As the results from this work have been obtained under the condition of a uniform heat flux at the channel wall, while the correlations from the literature apply to the condition of a uniform

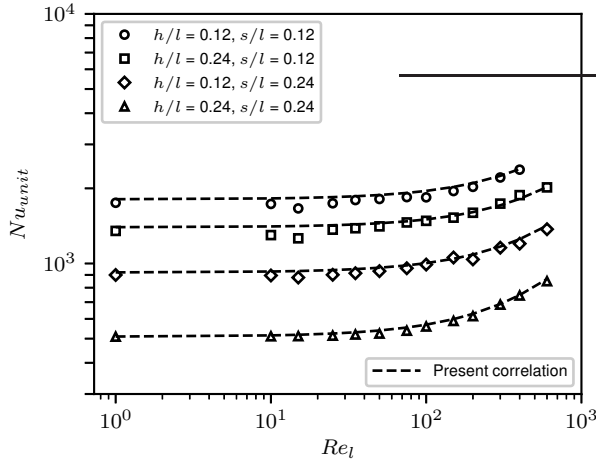


FIG. 17. A comparison between our final Nusselt number correlation and the data from this work, at small fin heights, when $Pr_f = 0.7$, $k_s/k_f = 10^4$, $t/l = 0.04$

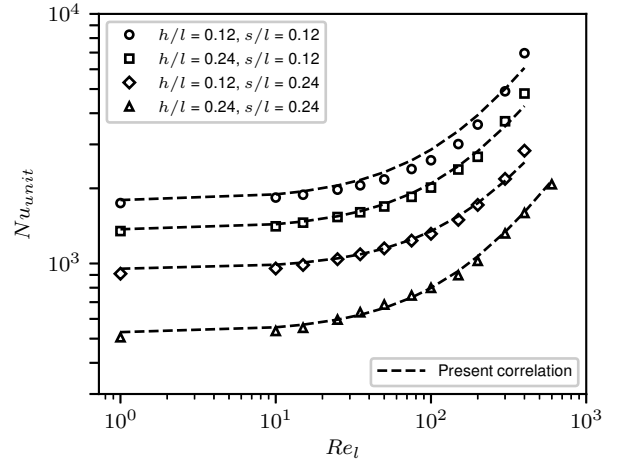


FIG. 18. A comparison between our final Nusselt number correlation and the data from this work, for at small fin heights, when $Pr_f = 7$, $k_s/k_f = 500$, $t/l = 0.04$

channel wall (and solid fin) temperature, the influence of the boundary condition deserves a closer inspection. Although an investigation of the Nusselt number for a uniform solid temperature falls beyond the scope of the present work, we do present a comparison between our data and a limited data set obtained for a uniform solid temperature. This comparison is made in Figure 19 and shows that the Nusselt number for a uniform solid temperature can be up to 23% smaller than for a uniform heat flux. Notably, this difference becomes even larger when the Reynolds number increases. The latter observations agree with the findings for straight channels without fins and arrays of pin-fins (Refs. 17 and 31). They suggest that the discrepancies between our Nusselt number correlations and the empirical correlations from the literature are largely, but not wholly, explained by the difference in the considered thermal boundary condition. We note that the necessary equations to compute Nu_{unit} for a uniform solid temperature boundary condition are included in Appendix A.

Another possible source of discrepancies between our correlations and those from the literature is the choice of the temperature difference ΔT_{ref} in the definition of the heat transfer coefficient: $h_{unit} = \langle q_{fs} \delta_{fs} \rangle_m / \Delta T_{ref}$. The heat transfer coefficient in the experimental correlations from the literature may be interpreted as a measure for the temperature difference between the average fluid

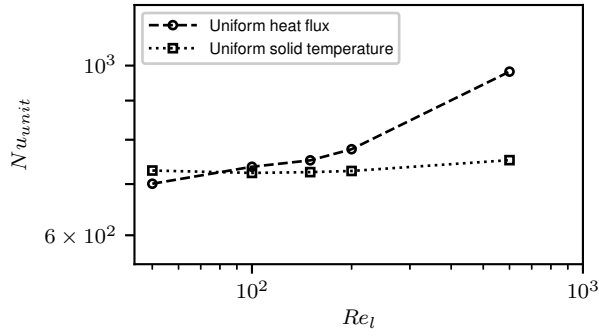


FIG. 19. Influence of the thermal boundary condition on the Nusselt number for steady periodically developed heat transfer, when $Pr_f = 0.7$, $k_s/k_f = 10^4$, $h/l = 0.12$, $s/l = 0.48$, $t/l = 0.04$

temperature and average bottom plate temperature: $\Delta T_{\text{ref}} = \overline{T}_f - \overline{T}_b$. However, it may also be interpreted as a measure for the difference in bulk temperatures $\Delta T_{\text{ref}} = \overline{T}_{f,\text{bulk}} - \overline{T}_b$, instead of the difference between the macro-scale temperatures of the fluid and solid, $\Delta T_{\text{ref}} = \langle T \rangle_m^f - \langle T \rangle_m^s$. The impact of the chosen temperature difference in the definition of the heat transfer coefficient is illustrated in Figures 20 and 21. The employed definitions of the various reference temperature differences are further clarified in Appendix B. Both figures show that the Nusselt numbers based on the difference in cross-sectional temperatures and the bulk temperatures exhibit spatial variations up to 20% within in a single fin unit, whereas the Nusselt numbers based on the macro-scale temperature difference are spatially constant. Furthermore, the offset between the Nusselt numbers for different reference temperatures can be as high as 50%.

VI. CONCLUSIONS

In this work, the Nusselt number for periodically developed conjugate heat transfer in micro- and mini-channels with offset strip fin arrays has been analyzed under the assumption of a constant heat flux at the channel wall. An extensive data set for the Nusselt number was collected through 2282 numerical simulations of the periodic temperature field on a unit cell of the array.

It was shown that the Nusselt number correlations from the literature primarily focus on the heat transfer for airflow through larger conventional offset strip fin arrays, subject to a constant channel wall temperature. Consequently, these correlations do not accurately predict the trends and limits

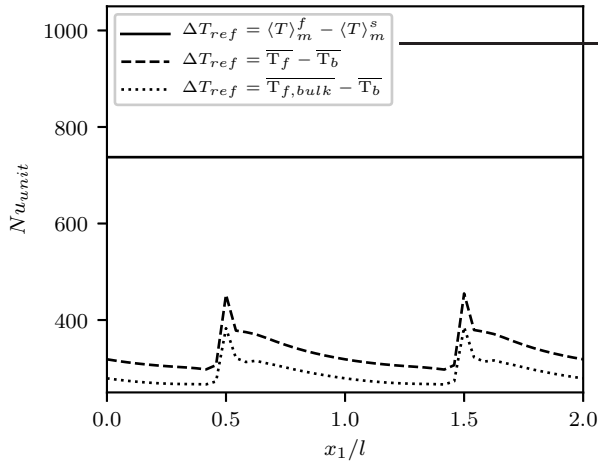


FIG. 20. Influence of the reference temperature difference on the Nusselt number for steady periodically developed heat transfer driven by a uniform heat flux, when $Re_l = 100$, $Pr_f = 0.7$, $k_s/k_f = 10^4$, $h/l = 0.12$, $s/l = 0.48$, $t/l = 0.04$

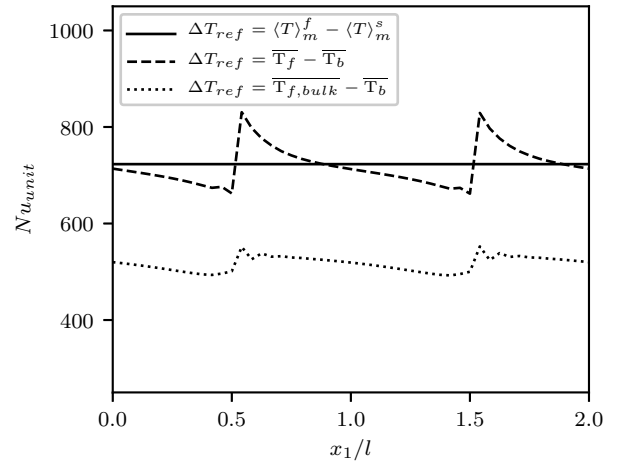


FIG. 21. Influence of the reference temperature difference on the Nusselt number for steady periodically developed heat transfer driven by a uniform solid temperature, when $Re_l = 100$, $Pr_f = 0.7$, $h/l = 0.12$, $s/l = 0.48$, $t/l = 0.04$

for the Nusselt number with respect to the Reynolds number and the geometrical parameters in micro- and mini-channels. At least, they result in discrepancies as large as 40-90% in the case of an imposed uniform heat flux.

For this reason, two new Nusselt number correlations have been presented, which apply to air and water in micro- and mini-channels with offset strip fins. They result in an average relative error of 4% with respect to the Nusselt number data from this work. The correlations were constructed through a least-squares fitting procedure, after which their suitability was assessed by the Bayesian approach for parameter estimation and model estimation.

The two new correlations predict a linear relationship between the Nusselt number and the Reynolds number. Yet, a more detailed analysis of the Nusselt number correction term has revealed a deviation from this linear scaling outside a specific range of Reynolds numbers bound by two critical Reynolds numbers. Within a relative margin of 10%, these critical Reynolds numbers were shown to correspond to the two critical Reynolds numbers which characterize the transition from the weak inertia regime to the strong inertia regime, and the transition from the strong inertia regime to the transitional regime. This result suggests a direct link between the flow regime and the heat transfer regime. Despite the observed deviation from a linear scaling, the linear relationship

still accurately captures all the Nusselt number data from this work.

In addition, the new correlations respect the asymptotic trends observed for each of the geometrical parameters of the offset strip fin array. More specifically, the correlations respect the observation that the Nusselt number scales with the inverse square of the relative fin-height-to-length ratio for small fin heights. The correlations also comply with the asymptotic limit of the Nusselt number becoming infinite when the fin pitch approaches the value of the fin thickness. Furthermore, the observation that the Nusselt number becomes independent of the fin height, fin pitch, and fin thickness for large fin heights, large fin pitches, and small fin thicknesses, respectively, is taken into account as well.

Finally, the influence of the Prandtl number and thermal conductivity ratio on the Nusselt number has been investigated via 62 additional simulations. We observed that the Nusselt number does not change with the Prandtl number over the lower Prandtl-number range, in particular at lower Reynolds numbers. Although this observation is contradicted by the available correlations for offset strip fins from the literature, it is in agreement with the empirical correlations for convective heat transfer in porous media and cylinder arrays. Furthermore, our simulations indicate that the Nusselt number scales linearly with the thermal conductivity ratio, as long as this ratio remains below 500. For larger values, the Nusselt number is no longer affected by the thermal conductivity ratio, as the periodic temperature becomes nearly uniform in the fins.

VII. CONTRIBUTIONS

The implementation and validation of the computational algorithms and software framework for the periodic flow and temperature equations were performed by G. Buckinx. All heat transfer simulations and post-processing calculations were carried out by A. Vangeffelen. The results were interpreted by A. Vangeffelen, with input from G. Buckinx regarding the existing literature. The paper was written by A. Vangeffelen and G. Buckinx with input from C. De Servi, M. R. Vetrano and M. Baelmans.

VIII. ACKNOWLEDGEMENTS

The work documented in this paper was funded by the Research Foundation — Flanders (FWO) through the post-doctoral project grant 12Y2919N of G. Buckinx, and by the Flemish Institute for Technological Research (VITO) through the Ph.D. grant 1810603 of A. Vangeffelen. The resources and services used in this work were provided by the VSC (Flemish Supercomputer Center), funded by the Research Foundation - Flanders (FWO) and the Flemish Government.

Appendix A: Nusselt number for a uniform solid temperature

When the solid temperature T_s is uniform, the Nusselt number in the steady periodically developed heat transfer regime is defined by the heat transfer coefficient

$$h_{\text{unit}} \triangleq \varepsilon_{fm}^{-1} \frac{\langle q_{fs} \delta_{fs} \rangle_m}{\langle T \rangle_m^f - \langle T \rangle_m^s} = -\langle \mathbf{n}_{fs} \cdot k_f \nabla \theta_f \delta_{fs} \rangle, \quad (\text{A1})$$

as the fluid temperature decays exponentially in the main flow direction \mathbf{e}_s with a spatially periodic amplitude θ_f : $T_f = T_0 \theta_f \exp(\lambda_T \mathbf{x} \cdot \mathbf{e}_s) + T_s$ for some constant T_0 (Refs. 40). The periodic amplitude θ_f is governed by the following energy conservation equation, if viscous dissipation is negligible, and other heat sources are absent (Refs. 40):

$$\rho_f c_f \nabla \cdot (\mathbf{u} \theta_f) = k_f \nabla^2 \theta_f + \sigma_T \quad \text{in } \Omega_f, \quad (\text{A2})$$

with

$$\sigma_T = (2k_f \nabla \theta_f - \rho_f c_f \mathbf{u} \theta_f) \cdot \mathbf{e}_s \lambda_T + k_f \theta_f \lambda_T^2. \quad (\text{A3})$$

The corresponding periodicity and boundary conditions are given by

$$\begin{aligned} \theta_f(\mathbf{x} + \mathbf{l}_j) &= \theta_f(\mathbf{x}) \quad \text{in } \Omega_f, \\ \theta_f &= 0 \quad \text{in } \Gamma_{fs} \cup \Gamma_t \cup \Gamma_b, \\ -\mathbf{n}_{fs} \cdot k_f \nabla \theta_f &= 0 \quad \text{in } \Gamma_t \cup \Gamma_b, \\ \langle \theta \rangle &= 1, \end{aligned} \quad (\text{A4})$$

with $j = \{1, 2\}$. The volume-average of the distribution θ , which equals θ_f in Ω_f and $\theta_s = 0$ in Ω_s needs to be imposed in order to find a unique solution, but does not affect Nu_{unit} . The temperature decay rate λ_T is the negative solution of the following eigenvalue problem:

$$\langle \mathbf{n}_{fs} \cdot k_f \nabla \theta_f \delta_{fs} \rangle - (\rho_f c_f \langle \mathbf{u} \theta \rangle \cdot \mathbf{e}_s) \lambda_T + k_f \lambda_T^2 = 0. \quad (\text{A5})$$

Appendix B: Reference temperature difference for the Nusselt number

The heat transfer coefficient for channel flows is commonly defined on the basis of a reference temperature difference ΔT_{ref} between cross-sectional averaged temperatures or bulk averaged temperatures. Any of these averaged temperatures can be defined as

$$\bar{T} \triangleq \frac{\int_{\mathbf{r} \in \Gamma^*(\mathbf{x})} T(\mathbf{r}) w_{\text{ref}}(\mathbf{r}) d\Gamma^*(\mathbf{r})}{\int_{\mathbf{r} \in \Gamma^*(\mathbf{x})} w_{\text{ref}}(\mathbf{r}) d\Gamma^*(\mathbf{r})}, \quad (\text{B1})$$

where w_{ref} is a weighting function, and Γ^* the cross-section given by

$$\Gamma^*(\mathbf{x}) \triangleq \left\{ \mathbf{r} \mid \exists c_j \in \left(-\frac{1}{2}, \frac{1}{2} \right) \Leftrightarrow \mathbf{r} = \mathbf{x} + \sum_{j=2}^3 c_j \mathbf{l}_j \right\}. \quad (\text{B2})$$

Often, the reference temperature difference is that between the average fluid temperature and average bottom plate temperature: $\Delta T_{\text{ref}} = \bar{T}_f - \bar{T}_b$, with $\bar{T}_f \triangleq (\bar{T} \mid w_{\text{ref}} = \gamma_f)$ and $\bar{T}_b \triangleq (\bar{T} \mid w_{\text{ref}} = \delta_b)$. On the other hand, the bulk-temperature difference is usually given by $\Delta T_{\text{ref}} = \overline{\bar{T}_{f,\text{bulk}}} - \bar{T}_b$, with $\overline{\bar{T}_{f,\text{bulk}}} \triangleq (\bar{T} \mid w_{\text{ref}} = \mathbf{u} \cdot \mathbf{e}_1)$.

Appendix C: Periodically developed Nusselt number data for air and water

t/l	h/l	s/l	ϵ	Re_l	Pr_f	k_s/k_f	Nu_{unit}	
1	0.01	0.12	0.24	0.88615	300	0.7	10000	1173.5
2	0.01	0.12	0.28	0.89125	300	0.7	10000	1074.9
3	0.01	0.12	0.32	0.8951	300	0.7	10000	1008.9
4	0.01	0.12	0.4	0.90056	300	0.7	10000	905.05
5	0.01	0.12	0.48	0.90424	300	0.7	10000	848.25
6	0.01	0.16	0.4	0.91822	300	0.7	10000	636.97
7	0.01	0.32	0.28	0.93626	300	0.7	10000	492.18
8	0.01	0.4	0.2	0.92915	100	0.7	10000	596.04
9	0.01	0.48	0.48	0.9596	100	0.7	10000	172.91
10	0.01	0.68	0.12	0.9097	300	0.7	10000	1416.7
11	0.02	0.12	0.12	0.73469	1	0.7	10000	1916.5
12	0.02	0.12	0.12	0.73469	10	0.7	10000	1912.3
13	0.02	0.12	0.12	0.73469	15	0.7	10000	1822.4
14	0.02	0.12	0.12	0.73469	25	0.7	10000	1892.2
15	0.02	0.12	0.12	0.73469	35	0.7	10000	1949.6
16	0.02	0.12	0.12	0.73469	50	0.7	10000	1906.9
17	0.02	0.12	0.12	0.73469	75	0.7	10000	2023.2
18	0.02	0.12	0.12	0.73469	100	0.7	10000	2063.2
19	0.02	0.12	0.12	0.73469	150	0.7	10000	2034.3
20	0.02	0.12	0.12	0.73469	200	0.7	10000	2130.7
21	0.02	0.12	0.12	0.73469	300	0.7	10000	2245.5
22	0.02	0.12	0.12	0.73469	400	0.7	10000	2398.7
23	0.02	0.12	0.12	0.73469	600	0.7	10000	2620
24	0.02	0.12	0.16	0.7619	1	0.7	10000	1388.1
25	0.02	0.12	0.16	0.7619	10	0.7	10000	1372.4
26	0.02	0.12	0.16	0.7619	15	0.7	10000	1320.9
27	0.02	0.12	0.16	0.7619	25	0.7	10000	1373.4
28	0.02	0.12	0.16	0.7619	35	0.7	10000	1388.3
29	0.02	0.12	0.16	0.7619	50	0.7	10000	1406.5
30	0.02	0.12	0.16	0.7619	75	0.7	10000	1434.9
31	0.02	0.12	0.16	0.7619	100	0.7	10000	1449.6
32	0.02	0.12	0.16	0.7619	150	0.7	10000	1505.3
33	0.02	0.12	0.16	0.7619	200	0.7	10000	1554
34	0.02	0.12	0.16	0.7619	300	0.7	10000	1676.1
35	0.02	0.12	0.16	0.7619	400	0.7	10000	1788.6
36	0.02	0.12	0.16	0.7619	600	0.7	10000	1990.2
37	0.02	0.12	0.2	0.77922	1	0.7	10000	1117.1
38	0.02	0.12	0.2	0.77922	10	0.7	10000	1093.7
39	0.02	0.12	0.2	0.77922	15	0.7	10000	1078.7
40	0.02	0.12	0.2	0.77922	25	0.7	10000	1103.1
41	0.02	0.12	0.2	0.77922	35	0.7	10000	1115.6
42	0.02	0.12	0.2	0.77922	50	0.7	10000	1133.6
43	0.02	0.12	0.2	0.77922	75	0.7	10000	1157.3
44	0.02	0.12	0.2	0.77922	100	0.7	10000	1188.2
45	0.02	0.12	0.2	0.77922	150	0.7	10000	1255.7
46	0.02	0.12	0.2	0.77922	200	0.7	10000	1306.1
47	0.02	0.12	0.2	0.77922	300	0.7	10000	1442.4
48	0.02	0.12	0.2	0.77922	400	0.7	10000	1322.1
49	0.02	0.12	0.2	0.77922	600	0.7	10000	1608.9
50	0.02	0.12	0.24	0.79121	1	0.7	10000	965.2
51	0.02	0.12	0.24	0.79121	10	0.7	10000	967.65
52	0.02	0.12	0.24	0.79121	15	0.7	10000	943.59
53	0.02	0.12	0.24	0.79121	25	0.7	10000	956.65
54	0.02	0.12	0.24	0.79121	35	0.7	10000	969.39
55	0.02	0.12	0.24	0.79121	50	0.7	10000	985.48
56	0.02	0.12	0.24	0.79121	75	0.7	10000	1010.7
57	0.02	0.12	0.24	0.79121	100	0.7	10000	1033.5
58	0.02	0.12	0.24	0.79121	150	0.7	10000	1089.8
59	0.02	0.12	0.24	0.79121	200	0.7	10000	1150.9
60	0.02	0.12	0.24	0.79121	300	0.7	10000	1267.6
61	0.02	0.12	0.24	0.79121	400	0.7	10000	1163.7
62	0.02	0.12	0.24	0.79121	600	0.7	10000	1415.3
63	0.02	0.12	0.28	0.8	1	0.7	10000	889.13
64	0.02	0.12	0.28	0.8	10	0.7	10000	890.67
65	0.02	0.12	0.28	0.8	15	0.7	10000	890.11
66	0.02	0.12	0.28	0.8	25	0.7	10000	889.46
67	0.02	0.12	0.28	0.8	35	0.7	10000	891.19
68	0.02	0.12	0.28	0.8	50	0.7	10000	903.34
69	0.02	0.12	0.28	0.8	75	0.7	10000	907.29
70	0.02	0.12	0.28	0.8	100	0.7	10000	925.59
71	0.02	0.12	0.28	0.8	150	0.7	10000	960.37
72	0.02	0.12	0.28	0.8	200	0.7	10000	1001.6
73	0.02	0.12	0.28	0.8	300	0.7	10000	1064.3
74	0.02	0.12	0.28	0.8	400	0.7	10000	1117.9
75	0.02	0.12	0.28	0.8	600	0.7	10000	1199.6
76	0.02	0.12	0.32	0.80672	10	0.7	10000	831.14
77	0.02	0.12	0.32	0.80672	100	0.7	10000	872.89
78	0.02	0.12	0.32	0.80672	300	0.7	10000	999.93
79	0.02	0.12	0.4	0.81633	10	0.7	10000	768.99
80	0.02	0.12	0.4	0.81633	100	0.7	10000	799.45

t/l	h/l	s/l	ϵ	Re_l	Pr_f	k_s/k_f	Nu_{unit}	
81	0.02	0.12	0.4	0.81633	300	0.7	10000	900.28
82	0.02	0.12	0.48	0.82286	10	0.7	10000	737.11
83	0.02	0.12	0.48	0.82286	100	0.7	10000	761.62
84	0.02	0.12	0.48	0.82286	300	0.7	10000	839.62
85	0.02	0.16	0.12	0.7619	1	0.7	10000	1658.7
86	0.02	0.16	0.12	0.7619	10	0.7	10000	1653.8
87	0.02	0.16	0.12	0.7619	15	0.7	10000	1564.2
88	0.02	0.16	0.12	0.7619	25	0.7	10000	1624.2
89	0.02	0.16	0.12	0.7619	35	0.7	10000	1678.3
90	0.02	0.16	0.12	0.7619	50	0.7	10000	1708.1
91	0.02	0.16	0.12	0.7619	75	0.7	10000	1769.4
92	0.02	0.16	0.12	0.7619	100	0.7	10000	1812.8
93	0.02	0.16	0.12	0.7619	150	0.7	10000	1828.9
94	0.02	0.16	0.12	0.7619	200	0.7	10000	1864.5
95	0.02	0.16	0.12	0.7619	300	0.7	10000	1938.7
96	0.02	0.16	0.12	0.7619	400	0.7	10000	2095.3
97	0.02	0.16	0.12	0.7619	600	0.7	10000	2255.5
98	0.02	0.16	0.16	0.79012	1	0.7	10000	1133.2
99	0.02	0.16	0.16	0.79012	10	0.7	10000	1120
100	0.02	0.16	0.16	0.79012	15	0.7	10000	1040
101	0.02	0.16	0.16	0.79012	25	0.7	10000	1116.2
102	0.02	0.16	0.16	0.79012	35	0.7	10000	1143
103	0.02	0.16	0.16	0.79012	50	0.7	10000	1159.7
104	0.02	0.16	0.16	0.79012	75	0.7	10000	1186.6
105	0.02	0.16	0.16	0.79012	100	0.7	10000	1205.2
106	0.02	0.16	0.16	0.79012	150	0.7	10000	1238.9
107	0.02	0.16	0.16	0.79012	200	0.7	10000	1304.7
108	0.02	0.16	0.16	0.79012	300	0.7	10000	1369.8
109	0.02	0.16	0.16	0.79012	400	0.7	10000	1481.5
110	0.02	0.16	0.16	0.79012	600	0.7	10000	1612.1
111	0.02	0.16	0.2	0.80808	10	0.7	10000	856.55
112	0.02	0.16	0.2	0.80808	15	0.7	10000	831.02
113	0.02	0.16	0.2	0.80808	25	0.7	10000	866.46
114	0.02	0.16	0.2	0.80808	35	0.7	10000	877.85
115	0.02	0.16	0.2	0.80808	50	0.7	10000	893.8
116	0.02	0.16	0.2	0.80808	75	0.7	10000	908.21
117	0.02	0.16	0.2	0.80808	100	0.7	10000	936.77
118	0.02	0.16	0.2	0.80808	150	0.7	10000	986.56
119	0.02	0.16	0.2	0.80808	200	0.7	10000	1045
120	0.02	0.16	0.2	0.80808	300	0.7	10000	1141.8
121	0.02	0.16	0.2	0.80808	400	0.7	10000	1141.3
122	0.02	0.16	0.2	0.80808	600	0.7	10000	1244.5
123	0.02	0.16	0.24	0.82051	1	0.7	10000	746.76
1								

	t/l	h/l	s/l	ϵ	Re_l	Pr_f	k_s/k_f	Nu_{unit}
161	0.02	0.2	0.12	0.77922	75	0.7	10000	1644.4
162	0.02	0.2	0.12	0.77922	100	0.7	10000	1663
163	0.02	0.2	0.12	0.77922	150	0.7	10000	1658.8
164	0.02	0.2	0.12	0.77922	200	0.7	10000	1709.6
165	0.02	0.2	0.12	0.77922	300	0.7	10000	1800.7
166	0.02	0.2	0.12	0.77922	400	0.7	10000	1912.3
167	0.02	0.2	0.12	0.77922	600	0.7	10000	2064.8
168	0.02	0.2	0.16	0.80808	1	0.7	10000	990.74
169	0.02	0.2	0.16	0.80808	10	0.7	10000	970.2
170	0.02	0.2	0.16	0.80808	15	0.7	10000	942.12
171	0.02	0.2	0.16	0.80808	25	0.7	10000	1021.5
172	0.02	0.2	0.16	0.80808	35	0.7	10000	1048.4
173	0.02	0.2	0.16	0.80808	50	0.7	10000	1071.6
174	0.02	0.2	0.16	0.80808	75	0.7	10000	1071.8
175	0.02	0.2	0.16	0.80808	100	0.7	10000	1077.3
176	0.02	0.2	0.16	0.80808	150	0.7	10000	1112
177	0.02	0.2	0.16	0.80808	200	0.7	10000	1172.4
178	0.02	0.2	0.16	0.80808	300	0.7	10000	1265.9
179	0.02	0.2	0.16	0.80808	400	0.7	10000	1344.3
180	0.02	0.2	0.16	0.80808	600	0.7	10000	1475.2
181	0.02	0.2	0.2	0.82645	1	0.7	10000	753.3
182	0.02	0.2	0.2	0.82645	10	0.7	10000	727.93
183	0.02	0.2	0.2	0.82645	15	0.7	10000	711.01
184	0.02	0.2	0.2	0.82645	25	0.7	10000	744.16
185	0.02	0.2	0.2	0.82645	35	0.7	10000	761.97
186	0.02	0.2	0.2	0.82645	75	0.7	10000	787.26
187	0.02	0.2	0.2	0.82645	100	0.7	10000	816.52
188	0.02	0.2	0.2	0.82645	150	0.7	10000	862.35
189	0.02	0.2	0.2	0.82645	200	0.7	10000	897.27
190	0.02	0.2	0.2	0.82645	300	0.7	10000	982.55
191	0.02	0.2	0.2	0.82645	400	0.7	10000	1060.9
192	0.02	0.2	0.2	0.82645	600	0.7	10000	1067.9
193	0.02	0.2	0.24	0.83916	1	0.7	10000	604.27
194	0.02	0.2	0.24	0.83916	10	0.7	10000	586.9
195	0.02	0.2	0.24	0.83916	15	0.7	10000	576.56
196	0.02	0.2	0.24	0.83916	25	0.7	10000	597.1
197	0.02	0.2	0.24	0.83916	35	0.7	10000	607.96
198	0.02	0.2	0.24	0.83916	50	0.7	10000	619.15
199	0.02	0.2	0.24	0.83916	75	0.7	10000	646.24
200	0.02	0.2	0.24	0.83916	100	0.7	10000	680.13
201	0.02	0.2	0.24	0.83916	150	0.7	10000	730.57
202	0.02	0.2	0.24	0.83916	200	0.7	10000	767.78
203	0.02	0.2	0.24	0.83916	300	0.7	10000	817.52
204	0.02	0.2	0.24	0.83916	400	0.7	10000	852.11
205	0.02	0.2	0.24	0.83916	600	0.7	10000	911.05
206	0.02	0.2	0.28	0.84848	1	0.7	10000	511.75
207	0.02	0.2	0.28	0.84848	10	0.7	10000	511.32
208	0.02	0.2	0.28	0.84848	15	0.7	10000	512.24
209	0.02	0.2	0.28	0.84848	25	0.7	10000	516.57
210	0.02	0.2	0.28	0.84848	35	0.7	10000	516.15
211	0.02	0.2	0.28	0.84848	50	0.7	10000	520.32
212	0.02	0.2	0.28	0.84848	75	0.7	10000	532.87
213	0.02	0.2	0.28	0.84848	100	0.7	10000	544.99
214	0.02	0.2	0.28	0.84848	150	0.7	10000	582.29
215	0.02	0.2	0.28	0.84848	200	0.7	10000	610.32
216	0.02	0.2	0.28	0.84848	300	0.7	10000	665.01
217	0.02	0.2	0.28	0.84848	400	0.7	10000	714.81
218	0.02	0.2	0.28	0.84848	600	0.7	10000	780.03
219	0.02	0.2	0.32	0.85561	100	0.7	10000	487.23
220	0.02	0.2	0.4	0.86558	10	0.7	10000	373.34
221	0.02	0.2	0.4	0.86558	100	0.7	10000	415.86
222	0.02	0.2	0.48	0.87273	10	0.7	10000	322.38
223	0.02	0.2	0.48	0.87273	100	0.7	10000	377.69
224	0.02	0.24	0.12	0.79121	1	0.7	10000	1470.5
225	0.02	0.24	0.12	0.79121	10	0.7	10000	1444.3
226	0.02	0.24	0.12	0.79121	15	0.7	10000	1373.8
227	0.02	0.24	0.12	0.79121	25	0.7	10000	1442.5
228	0.02	0.24	0.12	0.79121	35	0.7	10000	1506.7
229	0.02	0.24	0.12	0.79121	50	0.7	10000	1532.5
230	0.02	0.24	0.12	0.79121	75	0.7	10000	1546.4
231	0.02	0.24	0.12	0.79121	100	0.7	10000	1565.2
232	0.02	0.24	0.12	0.79121	150	0.7	10000	1570.4
233	0.02	0.24	0.12	0.79121	200	0.7	10000	1613.9
234	0.02	0.24	0.12	0.79121	300	0.7	10000	1708.4
235	0.02	0.24	0.12	0.79121	400	0.7	10000	1818.1
236	0.02	0.24	0.12	0.79121	600	0.7	10000	1973.8
237	0.02	0.24	0.16	0.82051	1	0.7	10000	931.53
238	0.02	0.24	0.16	0.82051	10	0.7	10000	904.23
239	0.02	0.24	0.16	0.82051	15	0.7	10000	863.53
240	0.02	0.24	0.16	0.82051	25	0.7	10000	938.78

	t/l	h/l	s/l	ϵ	Re_l	Pr_f	k_s/k_f	Nu_{unit}
241	0.02	0.24	0.16	0.82051	35	0.7	10000	970.72
242	0.02	0.24	0.16	0.82051	50	0.7	10000	986.79
243	0.02	0.24	0.16	0.82051	75	0.7	10000	998.54
244	0.02	0.24	0.16	0.82051	100	0.7	10000	1003.6
245	0.02	0.24	0.16	0.82051	150	0.7	10000	1031.5
246	0.02	0.24	0.16	0.82051	200	0.7	10000	1084.9
247	0.02	0.24	0.16	0.82051	300	0.7	10000	1167.2
248	0.02	0.24	0.16	0.82051	400	0.7	10000	1230.4
249	0.02	0.24	0.16	0.82051	600	0.7	10000	1379.6
250	0.02	0.24	0.2	0.83916	1	0.7	10000	685.1
251	0.02	0.24	0.2	0.83916	10	0.7	10000	655.63
252	0.02	0.24	0.2	0.83916	15	0.7	10000	650.68
253	0.02	0.24	0.2	0.83916	25	0.7	10000	684.26
254	0.02	0.24	0.2	0.83916	35	0.7	10000	702.25
255	0.02	0.24	0.2	0.83916	50	0.7	10000	714.92
256	0.02	0.24	0.2	0.83916	75	0.7	10000	719.61
257	0.02	0.24	0.2	0.83916	100	0.7	10000	745.67
258	0.02	0.24	0.2	0.83916	150	0.7	10000	797.59
259	0.02	0.24	0.2	0.83916	200	0.7	10000	849.18
260	0.02	0.24	0.2	0.83916	300	0.7	10000	869.68
261	0.02	0.24	0.2	0.83916	400	0.7	10000	921.21
262	0.02	0.24	0.2	0.83916	600	0.7	10000	987.12
263	0.02	0.24	0.24	0.85207	1	0.7	10000	539.43
264	0.02	0.24	0.24	0.85207	10	0.7	10000	509.84
265	0.02	0.24	0.24	0.85207	15	0.7	10000	511.99
266	0.02	0.24	0.24	0.85207	25	0.7	10000	532.81
267	0.02	0.24	0.24	0.85207	35	0.7	10000	542.78
268	0.02	0.24	0.24	0.85207	50	0.7	10000	548.11
269	0.02	0.24	0.24	0.85207	75	0.7	10000	574.39
270	0.02	0.24	0.24	0.85207	100	0.7	10000	607.32
271	0.02	0.24	0.24	0.85207	150	0.7	10000	648.03
272	0.02	0.24	0.24	0.85207	200	0.7	10000	686.06
273	0.02	0.24	0.24	0.85207	300	0.7	10000	685.35
274	0.02	0.24	0.24	0.85207	400	0.7	10000	704.71
275	0.02	0.24	0.24	0.85207	600	0.7	10000	812.44
276	0.02	0.24	0.28	0.86154	1	0.7	10000	444.05
277	0.02	0.24	0.28	0.86154	10	0.7	10000	445.08
278	0.02	0.24	0.28	0.86154	15	0.7	10000	445.45
279	0.02	0.24	0.28	0.86154	25	0.7	10000	446.28
280	0.02	0.24	0.28	0.86154	35	0.7	10000	447.21
281	0.02	0.24	0.28	0.86154	50	0.7	10000	451.25
282	0.02	0.24	0.28	0.86154	75	0.7	10000	465.41

t/l	h/l	s/l	ϵ	Re_l	Pr_f	k_s/k_f	Nu_{unit}
321	0.02	0.28	0.2	0.84848	1	0.7	10000 639.42
322	0.02	0.28	0.2	0.84848	10	0.7	10000 638.66
323	0.02	0.28	0.2	0.84848	15	0.7	10000 640.84
324	0.02	0.28	0.2	0.84848	25	0.7	10000 640.82
325	0.02	0.28	0.2	0.84848	35	0.7	10000 638.86
326	0.02	0.28	0.2	0.84848	50	0.7	10000 638.41
327	0.02	0.28	0.2	0.84848	75	0.7	10000 645.8
328	0.02	0.28	0.2	0.84848	100	0.7	10000 662.81
329	0.02	0.28	0.2	0.84848	150	0.7	10000 687.92
330	0.02	0.28	0.2	0.84848	200	0.7	10000 710.85
331	0.02	0.28	0.2	0.84848	300	0.7	10000 761.12
332	0.02	0.28	0.2	0.84848	400	0.7	10000 813.91
333	0.02	0.28	0.2	0.84848	600	0.7	10000 917.12
334	0.02	0.28	0.24	0.86154	1	0.7	10000 493.28
335	0.02	0.28	0.24	0.86154	10	0.7	10000 493.92
336	0.02	0.28	0.24	0.86154	15	0.7	10000 491.61
337	0.02	0.28	0.24	0.86154	25	0.7	10000 495.76
338	0.02	0.28	0.24	0.86154	35	0.7	10000 492.98
339	0.02	0.28	0.24	0.86154	50	0.7	10000 497.86
340	0.02	0.28	0.24	0.86154	75	0.7	10000 506.45
341	0.02	0.28	0.24	0.86154	100	0.7	10000 521.67
342	0.02	0.28	0.24	0.86154	150	0.7	10000 546.18
343	0.02	0.28	0.24	0.86154	200	0.7	10000 568.44
344	0.02	0.28	0.24	0.86154	300	0.7	10000 623.45
345	0.02	0.28	0.24	0.86154	400	0.7	10000 674.28
346	0.02	0.28	0.24	0.86154	600	0.7	10000 754.93
347	0.02	0.28	0.28	0.87111	1	0.7	10000 401.9
348	0.02	0.28	0.28	0.87111	10	0.7	10000 401.14
349	0.02	0.28	0.28	0.87111	15	0.7	10000 403.74
350	0.02	0.28	0.28	0.87111	25	0.7	10000 400.99
351	0.02	0.28	0.28	0.87111	35	0.7	10000 404.17
352	0.02	0.28	0.28	0.87111	50	0.7	10000 406.83
353	0.02	0.28	0.28	0.87111	75	0.7	10000 419.72
354	0.02	0.28	0.28	0.87111	100	0.7	10000 434.9
355	0.02	0.28	0.28	0.87111	150	0.7	10000 458.51
356	0.02	0.28	0.28	0.87111	200	0.7	10000 489.43
357	0.02	0.28	0.28	0.87111	300	0.7	10000 538.56
358	0.02	0.28	0.28	0.87111	400	0.7	10000 577.21
359	0.02	0.28	0.28	0.87111	600	0.7	10000 626.67
360	0.02	0.28	0.32	0.87843	10	0.7	10000 338.17
361	0.02	0.28	0.32	0.87843	15	0.7	10000 340.15
362	0.02	0.28	0.32	0.87843	25	0.7	10000 341.71
363	0.02	0.28	0.32	0.87843	35	0.7	10000 343.46
364	0.02	0.28	0.32	0.87843	50	0.7	10000 349.25
365	0.02	0.28	0.32	0.87843	75	0.7	10000 363.54
366	0.02	0.28	0.32	0.87843	100	0.7	10000 378.23
367	0.02	0.28	0.32	0.87843	150	0.7	10000 404.24
368	0.02	0.28	0.32	0.87843	200	0.7	10000 431.11
369	0.02	0.28	0.32	0.87843	400	0.7	10000 507.97
370	0.02	0.28	0.32	0.87843	600	0.7	10000 553.49
371	0.02	0.28	0.4	0.88889	1	0.7	10000 264.46
372	0.02	0.28	0.4	0.88889	10	0.7	10000 265.06
373	0.02	0.28	0.4	0.88889	15	0.7	10000 265.64
374	0.02	0.28	0.4	0.88889	35	0.7	10000 271.48
375	0.02	0.28	0.4	0.88889	50	0.7	10000 278.9
376	0.02	0.28	0.4	0.88889	100	0.7	10000 307.06
377	0.02	0.28	0.4	0.88889	200	0.7	10000 351.74
378	0.02	0.28	0.48	0.896	1	0.7	10000 222.93
379	0.02	0.28	0.48	0.896	10	0.7	10000 222.22
380	0.02	0.28	0.48	0.896	25	0.7	10000 226.06
381	0.02	0.28	0.48	0.896	50	0.7	10000 238.59
382	0.02	0.28	0.48	0.896	75	0.7	10000 253.9
383	0.02	0.28	0.48	0.896	200	0.7	10000 303.92
384	0.02	0.28	0.48	0.896	300	0.7	10000 319.18
385	0.02	0.32	0.12	0.80672	10	0.7	10000 1413.7
386	0.02	0.32	0.12	0.80672	100	0.7	10000 1388.2
387	0.02	0.32	0.16	0.8366	10	0.7	10000 869.43
388	0.02	0.32	0.16	0.8366	100	0.7	10000 882.09
389	0.02	0.32	0.2	0.85561	10	0.7	10000 607.15
390	0.02	0.32	0.24	0.86878	10	0.7	10000 467.07
391	0.02	0.32	0.24	0.86878	100	0.7	10000 491.01
392	0.02	0.32	0.28	0.87843	1	0.7	10000 373.64
393	0.02	0.32	0.28	0.87843	10	0.7	10000 373.24
394	0.02	0.32	0.28	0.87843	15	0.7	10000 372.19
395	0.02	0.32	0.28	0.87843	35	0.7	10000 371.35
396	0.02	0.32	0.28	0.87843	75	0.7	10000 387.73
397	0.02	0.32	0.28	0.87843	100	0.7	10000 401.3
398	0.02	0.32	0.28	0.87843	150	0.7	10000 427.88
399	0.02	0.32	0.28	0.87843	200	0.7	10000 451.84
400	0.02	0.32	0.28	0.87843	400	0.7	10000 543.48

t/l	h/l	s/l	ϵ	Re_l	Pr_f	k_s/k_f	Nu_{unit}
401	0.02	0.32	0.28	0.87843	600	0.7	10000 602.94
402	0.02	0.32	0.32	0.88581	25	0.7	10000 311.65
403	0.02	0.32	0.32	0.88581	35	0.7	10000 316.37
404	0.02	0.32	0.32	0.88581	100	0.7	10000 346.77
405	0.02	0.32	0.32	0.88581	200	0.7	10000 396.59
406	0.02	0.32	0.32	0.88581	300	0.7	10000 438.61
407	0.02	0.32	0.32	0.88581	600	0.7	10000 507.8
408	0.02	0.32	0.4	0.89636	1	0.7	10000 237.26
409	0.02	0.32	0.4	0.89636	75	0.7	10000 262.03
410	0.02	0.32	0.4	0.89636	100	0.7	10000 278.65
411	0.02	0.32	0.4	0.89636	300	0.7	10000 351.39
412	0.02	0.32	0.48	0.90353	10	0.7	10000 194.74
413	0.02	0.32	0.48	0.90353	15	0.7	10000 196.1
414	0.02	0.4	0.12	0.81633	10	0.7	10000 1387.5
415	0.02	0.4	0.12	0.81633	100	0.7	10000 1344.8
416	0.02	0.4	0.16	0.84656	10	0.7	10000 835.58
417	0.02	0.4	0.16	0.84656	100	0.7	10000 842.53
418	0.02	0.4	0.2	0.8658	10	0.7	10000 572.81
419	0.02	0.4	0.24	0.87912	10	0.7	10000 433.17
420	0.02	0.4	0.24	0.87912	100	0.7	10000 452.2
421	0.02	0.4	0.28	0.88888	10	0.7	10000 337.9
422	0.02	0.4	0.32	0.89636	10	0.7	10000 275
423	0.02	0.4	0.32	0.89636	100	0.7	10000 303.34
424	0.02	0.4	0.48	0.91429	10	0.7	10000 162
425	0.02	0.48	0.12	0.82286	100	0.7	10000 1319.1
426	0.02	0.48	0.16	0.85333	10	0.7	10000 830.66
427	0.02	0.48	0.16	0.85333	100	0.7	10000 815.4
428	0.02	0.48	0.2	0.87273	10	0.7	10000 554.1
429	0.02	0.48	0.2	0.87273	100	0.7	10000 571.82
430	0.02	0.48	0.24	0.88615	10	0.7	10000 407.51
431	0.02	0.48	0.24	0.88615	100	0.7	10000 426.27
432	0.02	0.48	0.28	0.896	10	0.7	10000 315.78
433	0.02	0.48	0.28	0.896	50	0.7	10000 316.09
434	0.02	0.48	0.28	0.896	200	0.7	10000 383.23
435	0.02	0.48	0.28	0.896	300	0.7	10000 429.28
436	0.02	0.48	0.28	0.896	400	0.7	10000 465.45
437	0.02	0.48	0.32	0.90353	25	0.7	10000 259.25
438	0.02	0.48	0.32	0.90353	200	0.7	10000 328.61
439	0.02	0.48	0.32	0.90353	300	0.7	10000 366.62
440	0.02	0.48	0.4	0.91429	1	0.7	10000 184.08
441	0.02	0.48	0.4	0.91429	10	0.7	10000 185.36
442	0.02	0.48	0.4	0.91429	15	0.7	10000 184.9
443	0.02	0.48	0.4	0.91429	35	0.7	10000 189.36
444	0.02	0.48	0.4	0.91429	50	0.7	10000 197.04
445	0.02	0.48	0.4	0.91429	100	0.7	10000 216.54
446	0.02	0.48	0.4	0.91429	150	0.7	10000 239.11
447	0.02	0.48	0.48	0.9216	1	0.7	10000 143.18
448	0.02	0.48	0.48	0.9216	10	0.7	10000 143.61
4							

	t/l	h/l	s/l	ϵ	Re_l	Pr_f	k_s/k_f	Nu_{unit}
481	0.02	0.56	0.48	0.9269	35	0.7	10000	139.12
482	0.02	0.56	0.48	0.9269	50	0.7	10000	145.57
483	0.02	0.56	0.48	0.9269	75	0.7	10000	156.25
484	0.02	0.56	0.48	0.9269	100	0.7	10000	166.07
485	0.02	0.56	0.48	0.9269	150	0.7	10000	182.05
486	0.02	0.56	0.48	0.9269	200	0.7	10000	192.57
487	0.02	0.56	0.48	0.9269	600	0.7	10000	229.84
488	0.02	0.68	0.12	0.83265	10	0.7	10000	1403
489	0.02	0.68	0.12	0.83265	100	0.7	10000	1286.3
490	0.02	0.68	0.12	0.83265	300	0.7	10000	1456.1
491	0.02	0.68	0.16	0.86349	10	0.7	10000	842.13
492	0.02	0.68	0.2	0.88312	10	0.7	10000	541.55
493	0.02	0.68	0.2	0.88312	100	0.7	10000	541.39
494	0.02	0.68	0.24	0.8967	10	0.7	10000	387.77
495	0.02	0.68	0.28	0.90667	1	0.7	10000	295.14
496	0.02	0.68	0.28	0.90667	10	0.7	10000	293.89
497	0.02	0.68	0.28	0.90667	15	0.7	10000	292.26
498	0.02	0.68	0.28	0.90667	50	0.7	10000	293.66
499	0.02	0.68	0.28	0.90667	75	0.7	10000	301.76
500	0.02	0.68	0.28	0.90667	100	0.7	10000	310.01
501	0.02	0.68	0.28	0.90667	150	0.7	10000	326.51
502	0.02	0.68	0.28	0.90667	200	0.7	10000	352.33
503	0.02	0.68	0.28	0.90667	300	0.7	10000	395.84
504	0.02	0.68	0.32	0.91429	10	0.7	10000	229.75
505	0.02	0.68	0.32	0.91429	15	0.7	10000	234.12
506	0.02	0.68	0.32	0.91429	25	0.7	10000	233.75
507	0.02	0.68	0.32	0.91429	35	0.7	10000	232.55
508	0.02	0.68	0.32	0.91429	50	0.7	10000	235.34
509	0.02	0.68	0.32	0.91429	75	0.7	10000	243.62
510	0.02	0.68	0.32	0.91429	100	0.7	10000	255.66
511	0.02	0.68	0.32	0.91429	200	0.7	10000	298.35
512	0.02	0.68	0.32	0.91429	300	0.7	10000	334.64
513	0.02	0.68	0.32	0.91429	600	0.7	10000	390.43
514	0.02	0.68	0.4	0.92517	1	0.7	10000	160.58
515	0.02	0.68	0.4	0.92517	10	0.7	10000	159.71
516	0.02	0.68	0.4	0.92517	15	0.7	10000	161.96
517	0.02	0.68	0.4	0.92517	25	0.7	10000	162.81
518	0.02	0.68	0.4	0.92517	50	0.7	10000	170.79
519	0.02	0.68	0.4	0.92517	75	0.7	10000	179.61
520	0.02	0.68	0.4	0.92517	100	0.7	10000	188.76
521	0.02	0.68	0.4	0.92517	200	0.7	10000	226.68
522	0.02	0.68	0.4	0.92517	300	0.7	10000	249.54
523	0.02	0.68	0.48	0.93257	1	0.7	10000	120.22
524	0.02	0.68	0.48	0.93257	10	0.7	10000	120.86
525	0.02	0.68	0.48	0.93257	35	0.7	10000	127.79
526	0.02	0.68	0.48	0.93257	150	0.7	10000	168.95
527	0.02	0.68	0.48	0.93257	200	0.7	10000	179.31
528	0.02	1.0	0.12	0.84034	10	0.7	10000	1519.4
529	0.02	1.0	0.16	0.87146	10	0.7	10000	870.6
530	0.02	1.0	0.16	0.87146	100	0.7	10000	763.13
531	0.02	1.0	0.2	0.89127	10	0.7	10000	545.89
532	0.02	1.0	0.2	0.89127	100	0.7	10000	523.09
533	0.02	1.0	0.24	0.90498	10	0.7	10000	379.51
534	0.02	1.0	0.28	0.91503	1	0.7	10000	285.86
535	0.02	1.0	0.28	0.91503	10	0.7	10000	278.77
536	0.02	1.0	0.28	0.91503	25	0.7	10000	274.01
537	0.02	1.0	0.28	0.91503	75	0.7	10000	285.85
538	0.02	1.0	0.28	0.91503	100	0.7	10000	291.84
539	0.02	1.0	0.28	0.91503	150	0.7	10000	309.45
540	0.02	1.0	0.28	0.91503	200	0.7	10000	327.97
541	0.02	1.0	0.32	0.92272	10	0.7	10000	221.89
542	0.02	1.0	0.32	0.92272	25	0.7	10000	216.04
543	0.02	1.0	0.32	0.92272	75	0.7	10000	229.35
544	0.02	1.0	0.32	0.92272	100	0.7	10000	236.98
545	0.02	1.0	0.32	0.92272	200	0.7	10000	276.99
546	0.02	1.0	0.32	0.92272	600	0.7	10000	361.2
547	0.02	1.0	0.4	0.93371	10	0.7	10000	146.44
548	0.02	1.0	0.4	0.93371	15	0.7	10000	146.23
549	0.02	1.0	0.4	0.93371	35	0.7	10000	150.38
550	0.02	1.0	0.4	0.93371	75	0.7	10000	163.57
551	0.02	1.0	0.4	0.93371	200	0.7	10000	207.45
552	0.02	1.0	0.4	0.93371	400	0.7	10000	237.47
553	0.02	1.0	0.4	0.93371	600	0.7	10000	258.82
554	0.02	1.0	0.48	0.94118	10	0.7	10000	106.72
555	0.02	1.0	0.48	0.94118	15	0.7	10000	107.1
556	0.02	1.0	0.48	0.94118	25	0.7	10000	107.49
557	0.02	1.0	0.48	0.94118	50	0.7	10000	116.24
558	0.02	1.0	0.48	0.94118	75	0.7	10000	126.33
559	0.02	1.0	0.48	0.94118	400	0.7	10000	182.05
560	0.04	0.12	0.12	0.5625	1	0.7	10000	1751

	t/l	h/l	s/l	ϵ	Re_l	Pr_f	k_s/k_f	Nu_{unit}
561	0.04	0.12	0.12	0.5625	10	0.7	10000	1732.4
562	0.04	0.12	0.12	0.5625	15	0.7	10000	1662.4
563	0.04	0.12	0.12	0.5625	25	0.7	10000	1742.7
564	0.04	0.12	0.12	0.5625	35	0.7	10000	1795.6
565	0.04	0.12	0.12	0.5625	50	0.7	10000	1813.1
566	0.04	0.12	0.12	0.5625	75	0.7	10000	1844.8
567	0.04	0.12	0.12	0.5625	100	0.7	10000	1841.2
568	0.04	0.12	0.12	0.5625	150	0.7	10000	1951
569	0.04	0.12	0.12	0.5625	200	0.7	10000	2028.1
570	0.04	0.12	0.12	0.5625	300	0.7	10000	2211.1
571	0.04	0.12	0.12	0.5625	400	0.7	10000	2376.6
572	0.04	0.12	0.16	0.6	1	0.7	10000	1271.6
573	0.04	0.12	0.16	0.6	10	0.7	10000	1247.4
574	0.04	0.12	0.16	0.6	15	0.7	10000	1219.5
575	0.04	0.12	0.16	0.6	25	0.7	10000	1264.5
576	0.04	0.12	0.16	0.6	35	0.7	10000	1298.2
577	0.04	0.12	0.16	0.6	50	0.7	10000	1320.6
578	0.04	0.12	0.16	0.6	75	0.7	10000	1334.6
579	0.04	0.12	0.16	0.6	100	0.7	10000	1379
580	0.04	0.12	0.16	0.6	150	0.7	10000	1435.7
581	0.04	0.12	0.16	0.6	200	0.7	10000	1494.7
582	0.04	0.12	0.16	0.6	300	0.7	10000	1591.7
583	0.04	0.12	0.16	0.6	400	0.7	10000	1696.6
584	0.04	0.12	0.16	0.6	600	0.7	10000	1929.4
585	0.04	0.12	0.2	0.625	1	0.7	10000	1025.9
586	0.04	0.12	0.2	0.625	10	0.7	10000	1020.6
587	0.04	0.12	0.2	0.625	15	0.7	10000	999.01
588	0.04	0.12	0.2	0.625	25	0.7	10000	1026.4
589	0.04	0.12	0.2	0.625	35	0.7	10000	1041.1
590	0.04	0.12	0.2	0.625	50	0.7	10000	1059.9
591	0.04	0.12	0.2	0.625	75	0.7	10000	1090.8
592	0.04	0.12	0.2	0.625	100	0.7	10000	1119.5
593	0.04	0.12	0.2	0.625	150	0.7	10000	1198.4
594	0.04	0.12	0.2	0.625	200	0.7	10000	1278.7
595	0.04	0.12	0.2	0.625	300	0.7	10000	1239.2
596	0.04	0.12	0.2	0.625	400	0.7	10000	1366.4
597	0.04	0.12	0.2	0.625	600	0.7	10000	1572.6
598	0.04	0.12	0.24	0.64286	1	0.7	10000	899.48
599	0.04	0.12	0.24	0.64286	10	0.7	10000	895.37
600	0.04	0.12	0.24	0.64286	15	0.7	10000	878.51
601	0.04	0.12	0.24	0.64286	25	0.7	10000	900.95
602	0.04	0.12	0.24	0.64286	35	0.7	10000	914.24
603	0.04	0.12	0.24	0.64286	50	0.7	10000	931.96

t/l	h/l	s/l	ϵ	Re_l	Pr_f	k_s/k_f	Nu_{unit}	
641	0.04	0.16	0.12	0.6	150	0.7	10000	1720.2
642	0.04	0.16	0.12	0.6	200	0.7	10000	1801
643	0.04	0.16	0.12	0.6	300	0.7	10000	1974.7
644	0.04	0.16	0.12	0.6	400	0.7	10000	2121
645	0.04	0.16	0.16	0.64	1	0.7	10000	1052.7
646	0.04	0.16	0.16	0.64	10	0.7	10000	1028
647	0.04	0.16	0.16	0.64	15	0.7	10000	996.02
648	0.04	0.16	0.16	0.64	25	0.7	10000	1051.3
649	0.04	0.16	0.16	0.64	35	0.7	10000	1068.9
650	0.04	0.16	0.16	0.64	50	0.7	10000	1090.9
651	0.04	0.16	0.16	0.64	75	0.7	10000	1115.8
652	0.04	0.16	0.16	0.64	100	0.7	10000	1150
653	0.04	0.16	0.16	0.64	150	0.7	10000	1183.2
654	0.04	0.16	0.16	0.64	200	0.7	10000	1258.3
655	0.04	0.16	0.16	0.64	300	0.7	10000	1342.9
656	0.04	0.16	0.16	0.64	400	0.7	10000	1460.7
657	0.04	0.16	0.16	0.64	600	0.7	10000	1693.3
658	0.04	0.16	0.2	0.66667	1	0.7	10000	815.95
659	0.04	0.16	0.2	0.66667	10	0.7	10000	795.48
660	0.04	0.16	0.2	0.66667	15	0.7	10000	779.61
661	0.04	0.16	0.2	0.66667	25	0.7	10000	811.48
662	0.04	0.16	0.2	0.66667	35	0.7	10000	826.33
663	0.04	0.16	0.2	0.66667	50	0.7	10000	841.33
664	0.04	0.16	0.2	0.66667	75	0.7	10000	871.83
665	0.04	0.16	0.2	0.66667	100	0.7	10000	894.16
666	0.04	0.16	0.2	0.66667	150	0.7	10000	964.58
667	0.04	0.16	0.2	0.66667	200	0.7	10000	1019
668	0.04	0.16	0.2	0.66667	300	0.7	10000	1083.5
669	0.04	0.16	0.2	0.66667	400	0.7	10000	1098.7
670	0.04	0.16	0.2	0.66667	600	0.7	10000	1257.4
671	0.04	0.16	0.24	0.68571	1	0.7	10000	697.34
672	0.04	0.16	0.24	0.68571	10	0.7	10000	661.9
673	0.04	0.16	0.24	0.68571	15	0.7	10000	652.8
674	0.04	0.16	0.24	0.68571	25	0.7	10000	673.02
675	0.04	0.16	0.24	0.68571	35	0.7	10000	686.54
676	0.04	0.16	0.24	0.68571	50	0.7	10000	701.85
677	0.04	0.16	0.24	0.68571	75	0.7	10000	736.73
678	0.04	0.16	0.24	0.68571	100	0.7	10000	772.01
679	0.04	0.16	0.24	0.68571	150	0.7	10000	829.62
680	0.04	0.16	0.24	0.68571	200	0.7	10000	769.58
681	0.04	0.16	0.24	0.68571	300	0.7	10000	885.58
682	0.04	0.16	0.24	0.68571	400	0.7	10000	983.43
683	0.04	0.16	0.24	0.68571	600	0.7	10000	1073.8
684	0.04	0.16	0.28	0.7	1	0.7	10000	597.28
685	0.04	0.16	0.28	0.7	10	0.7	10000	599.83
686	0.04	0.16	0.28	0.7	15	0.7	10000	603.46
687	0.04	0.16	0.28	0.7	25	0.7	10000	602.93
688	0.04	0.16	0.28	0.7	35	0.7	10000	606.89
689	0.04	0.16	0.28	0.7	50	0.7	10000	616.07
690	0.04	0.16	0.28	0.7	75	0.7	10000	633.3
691	0.04	0.16	0.28	0.7	100	0.7	10000	653.92
692	0.04	0.16	0.28	0.7	150	0.7	10000	691.51
693	0.04	0.16	0.28	0.7	200	0.7	10000	727.8
694	0.04	0.16	0.28	0.7	300	0.7	10000	793.76
695	0.04	0.16	0.28	0.7	400	0.7	10000	855.87
696	0.04	0.16	0.28	0.7	600	0.7	10000	961.19
697	0.04	0.16	0.32	0.71111	10	0.7	10000	542.44
698	0.04	0.16	0.32	0.71111	100	0.7	10000	598.52
699	0.04	0.16	0.4	0.72727	10	0.7	10000	476.33
700	0.04	0.16	0.4	0.72727	300	0.7	10000	626.25
701	0.04	0.16	0.48	0.73846	10	0.7	10000	441.14
702	0.04	0.16	0.48	0.73846	100	0.7	10000	488.98
703	0.04	0.2	0.12	0.625	1	0.7	10000	1419.7
704	0.04	0.2	0.12	0.625	10	0.7	10000	1363.5
705	0.04	0.2	0.12	0.625	15	0.7	10000	1338.6
706	0.04	0.2	0.12	0.625	25	0.7	10000	1415.2
707	0.04	0.2	0.12	0.625	35	0.7	10000	1477.4
708	0.04	0.2	0.12	0.625	50	0.7	10000	1489.9
709	0.04	0.2	0.12	0.625	75	0.7	10000	1542.5
710	0.04	0.2	0.12	0.625	100	0.7	10000	1527.3
711	0.04	0.2	0.12	0.625	150	0.7	10000	1613.6
712	0.04	0.2	0.12	0.625	200	0.7	10000	1680.9
713	0.04	0.2	0.12	0.625	300	0.7	10000	1831.6
714	0.04	0.2	0.12	0.625	400	0.7	10000	1955.3
715	0.04	0.2	0.12	0.625	600	0.7	10000	2067.8
716	0.04	0.2	0.16	0.66667	1	0.7	10000	938.76
717	0.04	0.2	0.16	0.66667	10	0.7	10000	893.71
718	0.04	0.2	0.16	0.66667	15	0.7	10000	878.66
719	0.04	0.2	0.16	0.66667	25	0.7	10000	952.55
720	0.04	0.2	0.16	0.66667	35	0.7	10000	979.7

t/l	h/l	s/l	ϵ	Re_l	Pr_f	k_s/k_f	Nu_{unit}	
721	0.04	0.2	0.16	0.66667	50	0.7	10000	988.37
722	0.04	0.2	0.16	0.66667	75	0.7	10000	981.32
723	0.04	0.2	0.16	0.66667	100	0.7	10000	1023.9
724	0.04	0.2	0.16	0.66667	150	0.7	10000	1096.7
725	0.04	0.2	0.16	0.66667	200	0.7	10000	1167.8
726	0.04	0.2	0.16	0.66667	300	0.7	10000	1262
727	0.04	0.2	0.16	0.66667	400	0.7	10000	1302
728	0.04	0.2	0.16	0.66667	600	0.7	10000	1489.5
729	0.04	0.2	0.2	0.69444	1	0.7	10000	707.44
730	0.04	0.2	0.2	0.69444	10	0.7	10000	679.64
731	0.04	0.2	0.2	0.69444	15	0.7	10000	672.24
732	0.04	0.2	0.2	0.69444	35	0.7	10000	708.43
733	0.04	0.2	0.2	0.69444	50	0.7	10000	722.63
734	0.04	0.2	0.2	0.69444	600	0.7	10000	725.73
735	0.04	0.2	0.2	0.69444	75	0.7	10000	763.48
736	0.04	0.2	0.2	0.69444	100	0.7	10000	790.55
737	0.04	0.2	0.2	0.69444	150	0.7	10000	841.82
738	0.04	0.2	0.2	0.69444	200	0.7	10000	876.81
739	0.04	0.2	0.2	0.69444	300	0.7	10000	979.7
740	0.04	0.2	0.2	0.69444	400	0.7	10000	1001.4
741	0.04	0.2	0.2	0.69444	600	0.7	10000	1115.1
742	0.04	0.2	0.24	0.71429	1	0.7	10000	575.44
743	0.04	0.2	0.24	0.71429	10	0.7	10000	551.17
744	0.04	0.2	0.24	0.71429	15	0.7	10000	547.89
745	0.04	0.2	0.24	0.71429	25	0.7	10000	570.12
746	0.04	0.2	0.24	0.71429	35	0.7	10000	579.58
747	0.04	0.2	0.24	0.71429	50	0.7	10000	599.46
748	0.04	0.2	0.24	0.71429	75	0.7	10000	623.98
749	0.04	0.2	0.24	0.71429	100	0.7	10000	658.01
750	0.04	0.2	0.24	0.71429	150	0.7	10000	699.07
751	0.04	0.2	0.24	0.71429	200	0.7	10000	749.04
752	0.04	0.2	0.24	0.71429	300	0.7	10000	758.61
753	0.04	0.2	0.24	0.71429	400	0.7	10000	846.64
754	0.04	0.2	0.24	0.71429	600	0.7	10000	967.98
755	0.04	0.2	0.28	0.72917	1	0.7	10000	487.15
756	0.04	0.2	0.28	0.72917	10	0.7	10000	487.04
757	0.04	0.2	0.28	0.72917	15	0.7	10000	488.38
758	0.04	0.2	0.28	0.72917	25	0.7	10000	492.28
759	0.04	0.2	0.28	0.72917	35	0.7	10000	496.23
760	0.04	0.2	0.28	0.72917	50	0.7	10000	503.75
761	0.04	0.2	0.28	0.72917	75	0.7	10000	520.73
762	0.04	0.2	0.28	0.72917	100	0.7	10000	537.71
763	0.04	0.2	0.28	0.72917	150	0.7	10000	572.87
764	0.04	0.2	0.28	0.72917	200	0.7	10000	

t/l	h/l	s/l	ϵ	Re_l	Pr_f	k_s/k_f	Nu_{unit}
801	0.04	0.24	0.2	0.71429	10	0.7	10000 613.61
802	0.04	0.24	0.2	0.71429	15	0.7	10000 602.71
803	0.04	0.24	0.2	0.71429	25	0.7	10000 639.32
804	0.04	0.24	0.2	0.71429	35	0.7	10000 653.97
805	0.04	0.24	0.2	0.71429	50	0.7	10000 661.15
806	0.04	0.24	0.2	0.71429	75	0.7	10000 696.2
807	0.04	0.24	0.2	0.71429	100	0.7	10000 733.48
808	0.04	0.24	0.2	0.71429	150	0.7	10000 790.17
809	0.04	0.24	0.2	0.71429	200	0.7	10000 808.54
810	0.04	0.24	0.2	0.71429	300	0.7	10000 887.69
811	0.04	0.24	0.2	0.71429	400	0.7	10000 957.75
812	0.04	0.24	0.2	0.71429	600	0.7	10000 1046
813	0.04	0.24	0.24	0.73469	1	0.7	10000 509.19
814	0.04	0.24	0.24	0.73469	10	0.7	10000 510.83
815	0.04	0.24	0.24	0.73469	15	0.7	10000 511.49
816	0.04	0.24	0.24	0.73469	25	0.7	10000 513.83
817	0.04	0.24	0.24	0.73469	35	0.7	10000 519.18
818	0.04	0.24	0.24	0.73469	50	0.7	10000 523.78
819	0.04	0.24	0.24	0.73469	75	0.7	10000 537.79
820	0.04	0.24	0.24	0.73469	100	0.7	10000 559.02
821	0.04	0.24	0.24	0.73469	150	0.7	10000 588.46
822	0.04	0.24	0.24	0.73469	200	0.7	10000 615.14
823	0.04	0.24	0.24	0.73469	300	0.7	10000 684.21
824	0.04	0.24	0.24	0.73469	400	0.7	10000 744.07
825	0.04	0.24	0.24	0.73469	600	0.7	10000 849.1
826	0.04	0.24	0.28	0.75	1	0.7	10000 423.65
827	0.04	0.24	0.28	0.75	10	0.7	10000 424.52
828	0.04	0.24	0.28	0.75	15	0.7	10000 427.74
829	0.04	0.24	0.28	0.75	25	0.7	10000 428.38
830	0.04	0.24	0.28	0.75	35	0.7	10000 433.03
831	0.04	0.24	0.28	0.75	50	0.7	10000 440.98
832	0.04	0.24	0.28	0.75	75	0.7	10000 455.45
833	0.04	0.24	0.28	0.75	100	0.7	10000 471.67
834	0.04	0.24	0.28	0.75	150	0.7	10000 504.25
835	0.04	0.24	0.28	0.75	200	0.7	10000 533.89
836	0.04	0.24	0.28	0.75	300	0.7	10000 595.92
837	0.04	0.24	0.28	0.75	400	0.7	10000 649.17
838	0.04	0.24	0.28	0.75	600	0.7	10000 732.2
839	0.04	0.24	0.32	0.7619	10	0.7	10000 367.52
840	0.04	0.24	0.32	0.7619	100	0.7	10000 413.16
841	0.04	0.24	0.4	0.77922	10	0.7	10000 297.31
842	0.04	0.24	0.48	0.79121	10	0.7	10000 256.64
843	0.04	0.28	0.12	0.65625	1	0.7	10000 1336.1
844	0.04	0.28	0.12	0.65625	10	0.7	10000 1337.6
845	0.04	0.28	0.12	0.65625	15	0.7	10000 1338.4
846	0.04	0.28	0.12	0.65625	25	0.7	10000 1347.8
847	0.04	0.28	0.12	0.65625	35	0.7	10000 1344.1
848	0.04	0.28	0.12	0.65625	50	0.7	10000 1379.2
849	0.04	0.28	0.12	0.65625	75	0.7	10000 1420.9
850	0.04	0.28	0.12	0.65625	100	0.7	10000 1452.7
851	0.04	0.28	0.12	0.65625	150	0.7	10000 1455.4
852	0.04	0.28	0.12	0.65625	200	0.7	10000 1513
853	0.04	0.28	0.12	0.65625	300	0.7	10000 1616.9
854	0.04	0.28	0.12	0.65625	400	0.7	10000 1709.8
855	0.04	0.28	0.12	0.65625	600	0.7	10000 1861.7
856	0.04	0.28	0.16	0.7	1	0.7	10000 845.59
857	0.04	0.28	0.16	0.7	10	0.7	10000 845.97
858	0.04	0.28	0.16	0.7	15	0.7	10000 848.31
859	0.04	0.28	0.16	0.7	25	0.7	10000 858.89
860	0.04	0.28	0.16	0.7	35	0.7	10000 857.98
861	0.04	0.28	0.16	0.7	50	0.7	10000 866.53
862	0.04	0.28	0.16	0.7	75	0.7	10000 901.46
863	0.04	0.28	0.16	0.7	100	0.7	10000 895.43
864	0.04	0.28	0.16	0.7	150	0.7	10000 937.05
865	0.04	0.28	0.16	0.7	200	0.7	10000 977.15
866	0.04	0.28	0.16	0.7	300	0.7	10000 1044.1
867	0.04	0.28	0.16	0.7	400	0.7	10000 1113.2
868	0.04	0.28	0.16	0.7	600	0.7	10000 1238.5
869	0.04	0.28	0.2	0.72917	1	0.7	10000 605.99
870	0.04	0.28	0.2	0.72917	10	0.7	10000 609.8
871	0.04	0.28	0.2	0.72917	15	0.7	10000 612.63
872	0.04	0.28	0.2	0.72917	25	0.7	10000 610.01
873	0.04	0.28	0.2	0.72917	35	0.7	10000 613.89
874	0.04	0.28	0.2	0.72917	50	0.7	10000 619.82
875	0.04	0.28	0.2	0.72917	75	0.7	10000 634.46
876	0.04	0.28	0.2	0.72917	100	0.7	10000 652.14
877	0.04	0.28	0.2	0.72917	150	0.7	10000 682.92
878	0.04	0.28	0.2	0.72917	200	0.7	10000 707.49
879	0.04	0.28	0.2	0.72917	300	0.7	10000 772.16
880	0.04	0.28	0.2	0.72917	400	0.7	10000 836.52

t/l	h/l	s/l	ϵ	Re_l	Pr_f	k_s/k_f	Nu_{unit}
881	0.04	0.28	0.2	0.72917	600	0.7	10000 949.26
882	0.04	0.28	0.24	0.75	1	0.7	10000 470.09
883	0.04	0.28	0.24	0.75	10	0.7	10000 471.22
884	0.04	0.28	0.24	0.75	15	0.7	10000 472.61
885	0.04	0.28	0.24	0.75	25	0.7	10000 473.63
886	0.04	0.28	0.24	0.75	35	0.7	10000 479.88
887	0.04	0.28	0.24	0.75	50	0.7	10000 489.43
888	0.04	0.28	0.24	0.75	75	0.7	10000 497.46
889	0.04	0.28	0.24	0.75	100	0.7	10000 511.8
890	0.04	0.28	0.24	0.75	150	0.7	10000 541.02
891	0.04	0.28	0.24	0.75	200	0.7	10000 573.67
892	0.04	0.28	0.24	0.75	300	0.7	10000 633.82
893	0.04	0.28	0.24	0.75	400	0.7	10000 688.16
894	0.04	0.28	0.24	0.75	600	0.7	10000 781.86
895	0.04	0.28	0.28	0.76563	1	0.7	10000 385.12
896	0.04	0.28	0.28	0.76563	10	0.7	10000 385.59
897	0.04	0.28	0.28	0.76563	15	0.7	10000 386.88
898	0.04	0.28	0.28	0.76563	35	0.7	10000 393.14
899	0.04	0.28	0.28	0.76563	75	0.7	10000 415.72
900	0.04	0.28	0.28	0.76563	100	0.7	10000 423.03
901	0.04	0.28	0.28	0.76563	150	0.7	10000 460.43
902	0.04	0.28	0.28	0.76563	200	0.7	10000 487
903	0.04	0.28	0.28	0.76563	300	0.7	10000 546.18
904	0.04	0.28	0.28	0.76563	400	0.7	10000 596.39
905	0.04	0.28	0.28	0.76563	600	0.7	10000 671.54
906	0.04	0.28	0.32	0.77778	1	0.7	10000 328.27
907	0.04	0.28	0.32	0.77778	10	0.7	10000 327.42
908	0.04	0.28	0.32	0.77778	15	0.7	10000 327.9
909	0.04	0.28	0.32	0.77778	25	0.7	10000 331.12
910	0.04	0.28	0.32	0.77778	35	0.7	10000 337.53
911	0.04	0.28	0.32	0.77778	50	0.7	10000 341.61
912	0.04	0.28	0.32	0.77778	100	0.7	10000 369.77
913	0.04	0.28	0.32	0.77778	200	0.7	10000 431.26
914	0.04	0.28	0.32	0.77778	300	0.7	10000 483.6
915	0.04	0.28	0.32	0.77778	400	0.7	10000 517.21
916	0.04	0.28	0.4	0.79545	10	0.7	10000 258.83
917	0.04	0.28	0.4	0.79545	15	0.7	10000 259.16
918	0.04	0.28	0.4	0.79545	25	0.7	10000 260.33
919	0.04	0.28	0.4	0.79545	150	0.7	10000 332.75
920	0.04	0.28	0.4	0.79545	400	0.7	10000 423.31
921	0.04	0.28	0.48	0.80769	10	0.7	10000 217.15
922	0.04	0.28	0.48	0.80769	25	0.7	10000 221.81
923	0.04	0.28	0.48	0.80769	35	0.7	10000 229.05
924	0.04	0.32	0.12	0.66667	10	0.7	10000 444.1
925	0.04	0.32	0.12	0.66667	100	0.7	10000 1313.7
926	0.04	0.32	0.16	0.71111	100	0.7	10000 668.07
927	0.04	0.32	0.2	0.74074	10	0.7	10000 578.31
928	0.04	0.32	0.2	0.74074	100	0.7	10000 627.22
929	0.04	0.32	0.24	0.7619	10	0.7	10000 444.1
930							

	t/l	h/l	s/l	ϵ	Re_l	Pr_f	k_s/k_f	Nu_{unit}
961	0.04	0.4	0.28	0.79545	10	0.7	10000	325.44
962	0.04	0.4	0.32	0.80808	10	0.7	10000	268.07
963	0.04	0.4	0.32	0.80808	100	0.7	10000	305.76
964	0.04	0.4	0.48	0.83916	10	0.7	10000	159.87
965	0.04	0.48	0.16	0.73846	10	0.7	10000	782.23
966	0.04	0.48	0.2	0.76923	10	0.7	10000	534.92
967	0.04	0.48	0.24	0.79121	10	0.7	10000	397.94
968	0.04	0.48	0.28	0.80769	100	0.7	10000	343.52
969	0.04	0.48	0.28	0.80769	200	0.7	10000	387.88
970	0.04	0.48	0.28	0.80769	300	0.7	10000	437.22
971	0.04	0.48	0.32	0.82051	10	0.7	10000	252.59
972	0.04	0.48	0.32	0.82051	15	0.7	10000	250.05
973	0.04	0.48	0.32	0.82051	25	0.7	10000	254.78
974	0.04	0.48	0.32	0.82051	35	0.7	10000	257.59
975	0.04	0.48	0.32	0.82051	100	0.7	10000	285.13
976	0.04	0.48	0.32	0.82051	200	0.7	10000	334.11
977	0.04	0.48	0.32	0.82051	600	0.7	10000	446.56
978	0.04	0.48	0.4	0.83916	1	0.7	10000	180.1
979	0.04	0.48	0.4	0.83916	10	0.7	10000	181.08
980	0.04	0.48	0.4	0.83916	200	0.7	10000	260.9
981	0.04	0.48	0.4	0.83916	300	0.7	10000	285.14
982	0.04	0.48	0.48	0.85207	1	0.7	10000	140.77
983	0.04	0.48	0.48	0.85207	10	0.7	10000	141.63
984	0.04	0.48	0.48	0.85207	15	0.7	10000	143.59
985	0.04	0.48	0.48	0.85207	25	0.7	10000	146.13
986	0.04	0.48	0.48	0.85207	35	0.7	10000	152.19
987	0.04	0.48	0.48	0.85207	75	0.7	10000	170.81
988	0.04	0.48	0.48	0.85207	100	0.7	10000	182.16
989	0.04	0.48	0.48	0.85207	200	0.7	10000	213.99
990	0.04	0.48	0.48	0.85207	300	0.7	10000	232.95
991	0.04	0.48	0.48	0.85207	400	0.7	10000	243.98
992	0.04	0.48	0.48	0.85207	600	0.7	10000	259.76
993	0.04	0.56	0.16	0.74667	10	0.7	10000	783.23
994	0.04	0.56	0.2	0.77778	10	0.7	10000	540.86
995	0.04	0.56	0.2	0.77778	100	0.7	10000	554.1
996	0.04	0.56	0.24	0.8	10	0.7	10000	388.45
997	0.04	0.56	0.28	0.81667	10	0.7	10000	296.89
998	0.04	0.56	0.28	0.81667	300	0.7	10000	416.74
999	0.04	0.56	0.28	0.81667	600	0.7	10000	514.45
1000	0.04	0.56	0.32	0.82963	10	0.7	10000	238.49
1001	0.04	0.56	0.32	0.82963	15	0.7	10000	238.53
1002	0.04	0.56	0.32	0.82963	25	0.7	10000	240.77
1003	0.04	0.56	0.32	0.82963	35	0.7	10000	245.74
1004	0.04	0.56	0.32	0.82963	50	0.7	10000	250.76
1005	0.04	0.56	0.32	0.82963	100	0.7	10000	269.13
1006	0.04	0.56	0.32	0.82963	200	0.7	10000	318.26
1007	0.04	0.56	0.32	0.82963	300	0.7	10000	354.03
1008	0.04	0.56	0.32	0.82963	600	0.7	10000	427.59
1009	0.04	0.56	0.4	0.84848	1	0.7	10000	166.39
1010	0.04	0.56	0.4	0.84848	15	0.7	10000	170.7
1011	0.04	0.56	0.4	0.84848	75	0.7	10000	193.54
1012	0.04	0.56	0.4	0.84848	100	0.7	10000	205.25
1013	0.04	0.56	0.4	0.84848	150	0.7	10000	227.07
1014	0.04	0.56	0.4	0.84848	200	0.7	10000	243.75
1015	0.04	0.56	0.4	0.84848	300	0.7	10000	268.39
1016	0.04	0.56	0.4	0.84848	400	0.7	10000	286.98
1017	0.04	0.56	0.48	0.86154	1	0.7	10000	129.19
1018	0.04	0.56	0.48	0.86154	10	0.7	10000	129.4
1019	0.04	0.56	0.48	0.86154	50	0.7	10000	145.01
1020	0.04	0.56	0.48	0.86154	75	0.7	10000	157.21
1021	0.04	0.56	0.48	0.86154	100	0.7	10000	168.38
1022	0.04	0.56	0.48	0.86154	150	0.7	10000	185.82
1023	0.04	0.56	0.48	0.86154	200	0.7	10000	197.22
1024	0.04	0.56	0.48	0.86154	400	0.7	10000	225.9
1025	0.04	0.68	0.12	0.70833	10	0.7	10000	1353.3
1026	0.04	0.68	0.12	0.70833	100	0.7	10000	1258.4
1027	0.04	0.68	0.16	0.75556	10	0.7	10000	807.97
1028	0.04	0.68	0.2	0.78704	10	0.7	10000	521.35
1029	0.04	0.68	0.24	0.80952	10	0.7	10000	378.56
1030	0.04	0.68	0.24	0.80952	100	0.7	10000	403.33
1031	0.04	0.68	0.28	0.82639	10	0.7	10000	267.08
1032	0.04	0.68	0.28	0.82639	75	0.7	10000	304.43
1033	0.04	0.68	0.28	0.82639	400	0.7	10000	439.87
1034	0.04	0.68	0.32	0.83951	1	0.7	10000	225.59
1035	0.04	0.68	0.32	0.83951	10	0.7	10000	227.85
1036	0.04	0.68	0.32	0.83951	15	0.7	10000	227.56
1037	0.04	0.68	0.32	0.83951	35	0.7	10000	233.46
1038	0.04	0.68	0.32	0.83951	75	0.7	10000	248.29
1039	0.04	0.68	0.32	0.83951	200	0.7	10000	301.4
1040	0.04	0.68	0.32	0.83951	300	0.7	10000	337.63

	t/l	h/l	s/l	ϵ	Re_l	Pr_f	k_s/k_f	Nu_{unit}
1041	0.04	0.68	0.32	0.83951	400	0.7	10000	367.06
1042	0.04	0.68	0.32	0.83951	600	0.7	10000	407.22
1043	0.04	0.68	0.4	0.85859	10	0.7	10000	157.66
1044	0.04	0.68	0.4	0.85859	25	0.7	10000	161.57
1045	0.04	0.68	0.4	0.85859	75	0.7	10000	180.65
1046	0.04	0.68	0.4	0.85859	100	0.7	10000	191.44
1047	0.04	0.68	0.4	0.85859	150	0.7	10000	212.67
1048	0.04	0.68	0.4	0.85859	600	0.7	10000	291.77
1049	0.04	0.68	0.48	0.87179	1	0.7	10000	118.7
1050	0.04	0.68	0.48	0.87179	10	0.7	10000	119.7
1051	0.04	0.68	0.48	0.87179	25	0.7	10000	124.15
1052	0.04	0.68	0.48	0.87179	50	0.7	10000	134.56
1053	0.04	0.68	0.48	0.87179	75	0.7	10000	144.01
1054	0.04	0.68	0.48	0.87179	150	0.7	10000	171.04
1055	0.04	0.68	0.48	0.87179	200	0.7	10000	180.64
1056	0.04	0.68	0.48	0.87179	300	0.7	10000	198.17
1057	0.04	0.68	0.48	0.87179	600	0.7	10000	221.01
1058	0.04	1.0	0.16	0.76923	10	0.7	10000	827.01
1059	0.04	1.0	0.2	0.80128	10	0.7	10000	527.5
1060	0.04	1.0	0.2	0.80128	100	0.7	10000	521.58
1061	0.04	1.0	0.24	0.82418	10	0.7	10000	375.84
1062	0.04	1.0	0.24	0.82418	100	0.7	10000	387.63
1063	0.04	1.0	0.28	0.84135	1	0.7	10000	282.68
1064	0.04	1.0	0.28	0.84135	10	0.7	10000	280.26
1065	0.04	1.0	0.28	0.84135	300	0.7	10000	380.48
1066	0.04	1.0	0.28	0.84135	600	0.7	10000	467.13
1067	0.04	1.0	0.32	0.8547	1	0.7	10000	222.04
1068	0.04	1.0	0.32	0.8547	10	0.7	10000	221.19
1069	0.04	1.0	0.32	0.8547	15	0.7	10000	216.67
1070	0.04	1.0	0.32	0.8547	35	0.7	10000	218.79
1071	0.04	1.0	0.32	0.8547	75	0.7	10000	232.49
1072	0.04	1.0	0.32	0.8547	100	0.7	10000	241.94
1073	0.04	1.0	0.32	0.8547	200	0.7	10000	280.87
1074	0.04	1.0	0.4	0.87413	1	0.7	10000	143.97
1075	0.04	1.0	0.4	0.87413	15	0.7	10000	147.24
1076	0.04	1.0	0.4	0.87413	35	0.7	10000	151.61
1077	0.04	1.0	0.4	0.87413	50	0.7	10000	157.18
1078	0.04	1.0	0.4	0.87413	75	0.7	10000	165.55
1079	0.04	1.0	0.4	0.87413	300	0.7	10000	233.1
1080	0.04	1.0	0.4	0.87413	600	0.7	10000	263.89
1081	0.04	1.0	0.48	0.88757	1	0.7	10000	105.25</

t/l	h/l	s/l	ϵ	Re_l	Pr_f	k_s/k_f	Nu_{unit}
1121	0.06	0.24	0.12	0.53333	1	0.7	10000 1291.5
1122	0.06	0.24	0.12	0.53333	10	0.7	10000 1298.8
1123	0.06	0.24	0.12	0.53333	15	0.7	10000 1200.1
1124	0.06	0.24	0.12	0.53333	25	0.7	10000 1284.8
1125	0.06	0.24	0.12	0.53333	35	0.7	10000 1339.4
1126	0.06	0.24	0.12	0.53333	50	0.7	10000 1361.1
1127	0.06	0.24	0.12	0.53333	75	0.7	10000 1400
1128	0.06	0.24	0.12	0.53333	100	0.7	10000 1431.1
1129	0.06	0.24	0.12	0.53333	150	0.7	10000 1478.7
1130	0.06	0.24	0.12	0.53333	200	0.7	10000 1668.8
1131	0.06	0.24	0.12	0.53333	300	0.7	10000 1630.3
1132	0.06	0.24	0.12	0.53333	400	0.7	10000 2068.9
1133	0.06	0.24	0.12	0.53333	600	0.7	10000 2278.3
1134	0.06	0.24	0.24	0.64	1	0.7	10000 487.41
1135	0.06	0.24	0.24	0.64	10	0.7	10000 489.43
1136	0.06	0.24	0.24	0.64	15	0.7	10000 491.68
1137	0.06	0.24	0.24	0.64	25	0.7	10000 498.25
1138	0.06	0.24	0.24	0.64	35	0.7	10000 505.43
1139	0.06	0.24	0.24	0.64	50	0.7	10000 513.87
1140	0.06	0.24	0.24	0.64	75	0.7	10000 535.06
1141	0.06	0.24	0.24	0.64	100	0.7	10000 552.51
1142	0.06	0.24	0.24	0.64	150	0.7	10000 587.14
1143	0.06	0.24	0.24	0.64	200	0.7	10000 623.36
1144	0.06	0.24	0.24	0.64	300	0.7	10000 687.95
1145	0.06	0.24	0.24	0.64	400	0.7	10000 748.34
1146	0.06	0.24	0.24	0.64	600	0.7	10000 854.37
1147	0.06	0.24	0.48	0.71111	100	0.7	10000 304.56
1148	0.06	0.48	0.12	0.59259	10	0.7	10000 1251.2
1149	0.06	0.48	0.12	0.59259	15	0.7	10000 1256.1
1150	0.06	0.48	0.12	0.59259	25	0.7	10000 1269.1
1151	0.06	0.48	0.12	0.59259	35	0.7	10000 1283.4
1152	0.06	0.48	0.12	0.59259	50	0.7	10000 1301.9
1153	0.06	0.48	0.12	0.59259	100	0.7	10000 1343.9
1154	0.06	0.48	0.12	0.59259	150	0.7	10000 1369.9
1155	0.06	0.48	0.12	0.59259	200	0.7	10000 1397.9
1156	0.06	0.48	0.12	0.59259	300	0.7	10000 1454.9
1157	0.06	0.48	0.12	0.59259	400	0.7	10000 1517.5
1158	0.06	0.48	0.48	0.79012	15	0.7	10000 142.54
1159	0.06	0.48	0.48	0.79012	25	0.7	10000 146.61
1160	0.06	0.48	0.48	0.79012	35	0.7	10000 152.79
1161	0.06	0.48	0.48	0.79012	50	0.7	10000 160.3
1162	0.06	0.48	0.48	0.79012	75	0.7	10000 172.66
1163	0.06	0.48	0.48	0.79012	100	0.7	10000 184.32
1164	0.06	0.48	0.48	0.79012	150	0.7	10000 203.98
1165	0.06	0.48	0.48	0.79012	200	0.7	10000 216.58
1166	0.06	0.48	0.48	0.79012	300	0.7	10000 234.81
1167	0.06	0.48	0.48	0.79012	400	0.7	10000 251.61
1168	0.06	0.48	0.48	0.79012	600	0.7	10000 268.43
1169	0.01	0.12	0.16	0.86878	300	7	500 2091.7
1170	0.01	0.12	0.24	0.88615	300	7	500 1460.7
1171	0.01	0.12	0.28	0.89125	300	7	500 1272.2
1172	0.01	0.12	0.32	0.8951	300	7	500 1160
1173	0.01	0.12	0.4	0.90056	300	7	500 1012.7
1174	0.01	0.12	0.48	0.90424	300	7	500 939.78
1175	0.01	0.16	0.32	0.91266	400	7	500 911.74
1176	0.01	0.16	0.4	0.91822	300	7	500 727.14
1177	0.01	0.32	0.28	0.93626	300	7	500 552.25
1178	0.01	0.32	0.48	0.94991	100	7	500 266.77
1179	0.01	0.48	0.48	0.9596	100	7	500 192.27
1180	0.01	0.56	0.12	0.90688	300	7	500 1504.1
1181	0.01	1.0	0.12	0.91394	300	7	500 1354.9
1182	0.02	0.12	0.12	0.73469	1	7	500 1911.3
1183	0.02	0.12	0.12	0.73469	10	7	500 1939.7
1184	0.02	0.12	0.12	0.73469	15	7	500 1974.8
1185	0.02	0.12	0.12	0.73469	25	7	500 2036.1
1186	0.02	0.12	0.12	0.73469	35	7	500 2067.3
1187	0.02	0.12	0.12	0.73469	50	7	500 2164.9
1188	0.02	0.12	0.12	0.73469	75	7	500 2307.4
1189	0.02	0.12	0.12	0.73469	100	7	500 2462.3
1190	0.02	0.12	0.12	0.73469	150	7	500 2718.1
1191	0.02	0.12	0.12	0.73469	200	7	500 2942.1
1192	0.02	0.12	0.12	0.73469	300	7	500 3356.2
1193	0.02	0.12	0.12	0.73469	400	7	500 3826.4
1194	0.02	0.12	0.16	0.7619	1	7	500 1380
1195	0.02	0.12	0.16	0.7619	10	7	500 1403.5
1196	0.02	0.12	0.16	0.7619	15	7	500 1437.1
1197	0.02	0.12	0.16	0.7619	25	7	500 1487.2
1198	0.02	0.12	0.16	0.7619	35	7	500 1533.4
1199	0.02	0.12	0.16	0.7619	50	7	500 1600.5
1200	0.02	0.12	0.16	0.7619	75	7	500 1731.1

t/l	h/l	s/l	ϵ	Re_l	Pr_f	k_s/k_f	Nu_{unit}
1201	0.02	0.12	0.16	0.7619	100	7	500 1819.4
1202	0.02	0.12	0.16	0.7619	150	7	500 2010.3
1203	0.02	0.12	0.16	0.7619	200	7	500 2114.5
1204	0.02	0.12	0.16	0.7619	300	7	500 2498.9
1205	0.02	0.12	0.16	0.7619	400	7	500 2865.6
1206	0.02	0.12	0.16	0.7619	600	7	500 4199.5
1207	0.02	0.12	0.2	0.77922	1	7	500 1120.2
1208	0.02	0.12	0.2	0.77922	10	7	500 1145.1
1209	0.02	0.12	0.2	0.77922	15	7	500 1177.4
1210	0.02	0.12	0.2	0.77922	25	7	500 1224.2
1211	0.02	0.12	0.2	0.77922	35	7	500 1274.3
1212	0.02	0.12	0.2	0.77922	50	7	500 1340.8
1213	0.02	0.12	0.2	0.77922	75	7	500 1429.3
1214	0.02	0.12	0.2	0.77922	100	7	500 1510.4
1215	0.02	0.12	0.2	0.77922	150	7	500 1605
1216	0.02	0.12	0.2	0.77922	200	7	500 1754.2
1217	0.02	0.12	0.2	0.77922	300	7	500 2033.7
1218	0.02	0.12	0.2	0.77922	400	7	500 2393.3
1219	0.02	0.12	0.2	0.77922	600	7	500 3161.1
1220	0.02	0.12	0.24	0.79121	1	7	500 975.16
1221	0.02	0.12	0.24	0.79121	10	7	500 999.9
1222	0.02	0.12	0.24	0.79121	15	7	500 1028.7
1223	0.02	0.12	0.24	0.79121	25	7	500 1074.3
1224	0.02	0.12	0.24	0.79121	35	7	500 1118.2
1225	0.02	0.12	0.24	0.79121	50	7	500 1178.4
1226	0.02	0.12	0.24	0.79121	75	7	500 1242
1227	0.02	0.12	0.24	0.79121	100	7	500 1291.9
1228	0.02	0.12	0.24	0.79121	150	7	500 1388.8
1229	0.02	0.12	0.24	0.79121	200	7	500 1490.6
1230	0.02	0.12	0.24	0.79121	300	7	500 1707.9
1231	0.02	0.12	0.24	0.79121	400	7	500 1930.9
1232	0.02	0.12	0.24	0.79121	600	7	500 2309.2
1233	0.02	0.12	0.28	0.8	1	7	500 886.66
1234	0.02	0.12	0.28	0.8	10	7	500 909.41
1235	0.02	0.12	0.28	0.8	15	7	500 936.08
1236	0.02	0.12	0.28	0.8	25	7	500 983.85
1237	0.02	0.12	0.28	0.8	35	7	500 1025.1
1238	0.02	0.12	0.28	0.8	50	7	500 1072.1
1239	0.02	0.12	0.28	0.8	75	7	500 1114.6
1240	0.02	0.12	0.28	0.8	100	7	500 1158.6
1241	0.02	0.12	0.28	0.8	150	7	500 1231.2
1242	0.02	0.12	0.28	0.8	200	7	500 1301.8
1243	0.02	0.12	0.28	0.8	300	7	500 1486.4
1244	0.02	0.12	0.28	0.8	400	7	500 1691.8
1245	0.02	0.12	0.28	0.8	600	7	500 2124.1
1246	0.02	0.12	0.32	0.80672	10	7	500 857.67
1247	0.02	0.12	0.32	0.80672	100	7	500 1061.3
1248	0.02	0.12	0.32	0.80672	300	7	500 1288.4
1249	0.02	0.12	0.4	0.81633	10	7	500 785.22
1250	0.02	0.12	0.4	0.81633	100	7	500 940.55
1251	0.02	0.12	0.4	0.81633	300	7</td	

t/l	h/l	s/l	ϵ	Re_l	Pr_f	k_s/k_f	Nu_{unit}	
1281	0.02	0.16	0.2	0.80808	15	7	500	912.03
1282	0.02	0.16	0.2	0.80808	25	7	500	953.86
1283	0.02	0.16	0.2	0.80808	35	7	500	988.99
1284	0.02	0.16	0.2	0.80808	50	7	500	1050.7
1285	0.02	0.16	0.2	0.80808	75	7	500	1110.9
1286	0.02	0.16	0.2	0.80808	100	7	500	1176.1
1287	0.02	0.16	0.2	0.80808	150	7	500	1280.8
1288	0.02	0.16	0.2	0.80808	200	7	500	1363.1
1289	0.02	0.16	0.2	0.80808	300	7	500	1554.6
1290	0.02	0.16	0.2	0.80808	400	7	500	1932.6
1291	0.02	0.16	0.2	0.80808	600	7	500	2214.2
1292	0.02	0.16	0.24	0.82051	1	7	500	720.32
1293	0.02	0.16	0.24	0.82051	10	7	500	742.79
1294	0.02	0.16	0.24	0.82051	15	7	500	763.49
1295	0.02	0.16	0.24	0.82051	25	7	500	804.41
1296	0.02	0.16	0.24	0.82051	35	7	500	848.28
1297	0.02	0.16	0.24	0.82051	50	7	500	888.73
1298	0.02	0.16	0.24	0.82051	75	7	500	943.65
1299	0.02	0.16	0.24	0.82051	100	7	500	998.32
1300	0.02	0.16	0.24	0.82051	150	7	500	1087.8
1301	0.02	0.16	0.24	0.82051	200	7	500	1184.2
1302	0.02	0.16	0.24	0.82051	300	7	500	1300.8
1303	0.02	0.16	0.24	0.82051	400	7	500	1535.9
1304	0.02	0.16	0.24	0.82051	600	7	500	1900.8
1305	0.02	0.16	0.28	0.82963	1	7	500	628.84
1306	0.02	0.16	0.28	0.82963	10	7	500	651.43
1307	0.02	0.16	0.28	0.82963	15	7	500	676.84
1308	0.02	0.16	0.28	0.82963	25	7	500	714.99
1309	0.02	0.16	0.28	0.82963	35	7	500	750.6
1310	0.02	0.16	0.28	0.82963	50	7	500	777.99
1311	0.02	0.16	0.28	0.82963	75	7	500	827.44
1312	0.02	0.16	0.28	0.82963	100	7	500	864.57
1313	0.02	0.16	0.28	0.82963	200	7	500	1003.4
1314	0.02	0.16	0.28	0.82963	300	7	500	1127
1315	0.02	0.16	0.28	0.82963	400	7	500	1297.3
1316	0.02	0.16	0.28	0.82963	600	7	500	1575.2
1317	0.02	0.16	0.32	0.8366	10	7	500	599.85
1318	0.02	0.16	0.32	0.8366	100	7	500	780.26
1319	0.02	0.16	0.32	0.8366	400	7	500	1122.5
1320	0.02	0.16	0.4	0.84656	10	7	500	520.63
1321	0.02	0.16	0.4	0.84656	100	7	500	658.31
1322	0.02	0.16	0.4	0.84656	300	7	500	833.04
1323	0.02	0.16	0.48	0.85333	10	7	500	484.73
1324	0.02	0.16	0.48	0.85333	100	7	500	586.28
1325	0.02	0.2	0.12	0.77922	1	7	500	1521.2
1326	0.02	0.2	0.12	0.77922	10	7	500	1523.9
1327	0.02	0.2	0.12	0.77922	15	7	500	1543.8
1328	0.02	0.2	0.12	0.77922	25	7	500	1600.8
1329	0.02	0.2	0.12	0.77922	35	7	500	1624.2
1330	0.02	0.2	0.12	0.77922	50	7	500	1698.2
1331	0.02	0.2	0.12	0.77922	75	7	500	1813.4
1332	0.02	0.2	0.12	0.77922	100	7	500	1954.4
1333	0.02	0.2	0.12	0.77922	150	7	500	2108.3
1334	0.02	0.2	0.12	0.77922	200	7	500	2298
1335	0.02	0.2	0.12	0.77922	300	7	500	2701.1
1336	0.02	0.2	0.12	0.77922	400	7	500	3079.9
1337	0.02	0.2	0.16	0.80808	1	7	500	997.11
1338	0.02	0.2	0.16	0.80808	10	7	500	1004.6
1339	0.02	0.2	0.16	0.80808	15	7	500	1024.6
1340	0.02	0.2	0.16	0.80808	25	7	500	1057.6
1341	0.02	0.2	0.16	0.80808	35	7	500	1099.1
1342	0.02	0.2	0.16	0.80808	50	7	500	1165.6
1343	0.02	0.2	0.16	0.80808	75	7	500	1273.1
1344	0.02	0.2	0.16	0.80808	100	7	500	1305.4
1345	0.02	0.2	0.16	0.80808	150	7	500	1442.9
1346	0.02	0.2	0.16	0.80808	200	7	500	1552.4
1347	0.02	0.2	0.16	0.80808	300	7	500	1927.5
1348	0.02	0.2	0.16	0.80808	400	7	500	2268.3
1349	0.02	0.2	0.2	0.82645	1	7	500	742.01
1350	0.02	0.2	0.2	0.82645	10	7	500	761.38
1351	0.02	0.2	0.2	0.82645	15	7	500	774.59
1352	0.02	0.2	0.2	0.82645	25	7	500	805.01
1353	0.02	0.2	0.2	0.82645	35	7	500	843.99
1354	0.02	0.2	0.2	0.82645	75	7	500	978.39
1355	0.02	0.2	0.2	0.82645	100	7	500	1007.1
1356	0.02	0.2	0.2	0.82645	150	7	500	1100.7
1357	0.02	0.2	0.2	0.82645	200	7	500	1224.8
1358	0.02	0.2	0.2	0.82645	300	7	500	1352.7
1359	0.02	0.2	0.2	0.82645	400	7	500	1650.3
1360	0.02	0.2	0.2	0.82645	600	7	500	1829.7

t/l	h/l	s/l	ϵ	Re_l	Pr_f	k_s/k_f	Nu_{unit}	
1361	0.02	0.2	0.24	0.83916	1	7	500	597.75
1362	0.02	0.2	0.24	0.83916	10	7	500	613.01
1363	0.02	0.2	0.24	0.83916	15	7	500	636.81
1364	0.02	0.2	0.24	0.83916	25	7	500	668.55
1365	0.02	0.2	0.24	0.83916	35	7	500	704.47
1366	0.02	0.2	0.24	0.83916	50	7	500	752.6
1367	0.02	0.2	0.24	0.83916	75	7	500	787.54
1368	0.02	0.2	0.24	0.83916	100	7	500	823.2
1369	0.02	0.2	0.24	0.83916	150	7	500	923.77
1370	0.02	0.2	0.24	0.83916	200	7	500	1009
1371	0.02	0.2	0.24	0.83916	300	7	500	1116.2
1372	0.02	0.2	0.24	0.83916	400	7	500	1254.8
1373	0.02	0.2	0.24	0.83916	600	7	500	1521.2
1374	0.02	0.2	0.28	0.84848	1	7	500	506.4
1375	0.02	0.2	0.28	0.84848	10	7	500	529.47
1376	0.02	0.2	0.28	0.84848	15	7	500	547.02
1377	0.02	0.2	0.28	0.84848	25	7	500	585.06
1378	0.02	0.2	0.28	0.84848	35	7	500	615.41
1379	0.02	0.2	0.28	0.84848	50	7	500	646.1
1380	0.02	0.2	0.28	0.84848	75	7	500	685.94
1381	0.02	0.2	0.28	0.84848	100	7	500	717.93
1382	0.02	0.2	0.28	0.84848	150	7	500	766.91
1383	0.02	0.2	0.28	0.84848	200	7	500	830.36
1384	0.02	0.2	0.28	0.84848	300	7	500	958.3
1385	0.02	0.2	0.28	0.84848	400	7	500	1149.3
1386	0.02	0.2	0.28	0.84848	600	7	500	1320.2
1387	0.02	0.2	0.32	0.85561	100	7	500	633.13
1388	0.02	0.2	0.4	0.8658	100	7	500	522.9
1389	0.02	0.2	0.48	0.87273	10	7	500	360.19
1390	0.02	0.2	0.48	0.87273	100	7	500	451.52
1391	0.02	0.24	0.12	0.79121	1	7	500	1436.7
1392	0.02	0.24	0.12	0.79121	10	7	500	1435.4
1393	0.02	0.24	0.12	0.79121	15	7	500	1456
1394	0.02	0.24	0.12	0.79121	25	7	500	1499.4
1395	0.02	0.24	0.12	0.79121	35	7	500	1534.2
1396	0.02	0.24	0.12	0.79121	50	7	500	1600.6
1397	0.02	0.24	0.12	0.79121	75	7	500	1720.9
1398	0.02	0.24	0.12	0.79121	100	7	500	1851.2
1399	0.02	0.24	0.12	0.79121	150	7	500	2004.9
1400	0.02	0.24	0.12	0.79121	200	7	500	2163.3
1401	0.02	0.24	0.12	0.79121	300	7	500	2467.8
1402	0.02	0.24	0.12	0.79121	400	7	500	2888.2
1403	0.02	0.24	0.16	0.82051	1	7	500	922.53
1404	0.02	0.24	0.16	0.82051	10	7	500	922.77
1405	0.02	0.24	0.16	0.82051	15	7	500	943.37
1406	0.02	0.24	0.16	0.82051	25	7	500	971.9
1407	0.02	0.24	0.16	0.82051	35	7</td		

	t/l	h/l	s/l	ϵ	Re_l	Pr_f	k_s/k_f	Nu_{unit}
1441	0.02	0.24	0.24	0.85207	600	7	500	1303.9
1442	0.02	0.24	0.28	0.86154	1	7	500	437.66
1443	0.02	0.24	0.28	0.86154	10	7	500	453.56
1444	0.02	0.24	0.28	0.86154	15	7	500	470.22
1445	0.02	0.24	0.28	0.86154	25	7	500	508.18
1446	0.02	0.24	0.28	0.86154	35	7	500	535.05
1447	0.02	0.24	0.28	0.86154	50	7	500	550.56
1448	0.02	0.24	0.28	0.86154	75	7	500	590.94
1449	0.02	0.24	0.28	0.86154	100	7	500	618.63
1450	0.02	0.24	0.28	0.86154	150	7	500	680.11
1451	0.02	0.24	0.28	0.86154	200	7	500	732.6
1452	0.02	0.24	0.28	0.86154	300	7	500	840.14
1453	0.02	0.24	0.28	0.86154	400	7	500	979.4
1454	0.02	0.24	0.28	0.86154	600	7	500	1100.7
1455	0.02	0.24	0.32	0.86878	10	7	500	397.69
1456	0.02	0.24	0.32	0.86878	100	7	500	551.53
1457	0.02	0.24	0.4	0.87912	10	7	500	330.48
1458	0.02	0.24	0.48	0.88615	10	7	500	290.39
1459	0.02	0.24	0.48	0.88615	100	7	500	375
1460	0.02	0.28	0.12	0.8	1	7	500	1388
1461	0.02	0.28	0.12	0.8	10	7	500	1379.9
1462	0.02	0.28	0.12	0.8	15	7	500	1396.8
1463	0.02	0.28	0.12	0.8	25	7	500	1436.8
1464	0.02	0.28	0.12	0.8	35	7	500	1463.8
1465	0.02	0.28	0.12	0.8	50	7	500	1530.5
1466	0.02	0.28	0.12	0.8	75	7	500	1657.9
1467	0.02	0.28	0.12	0.8	100	7	500	1739
1468	0.02	0.28	0.12	0.8	150	7	500	1917.2
1469	0.02	0.28	0.12	0.8	200	7	500	2077.7
1470	0.02	0.28	0.12	0.8	300	7	500	2349.1
1471	0.02	0.28	0.12	0.8	400	7	500	2725.1
1472	0.02	0.28	0.16	0.82963	1	7	500	872.15
1473	0.02	0.28	0.16	0.82963	10	7	500	870.53
1474	0.02	0.28	0.16	0.82963	15	7	500	887.89
1475	0.02	0.28	0.16	0.82963	25	7	500	915.8
1476	0.02	0.28	0.16	0.82963	35	7	500	956.3
1477	0.02	0.28	0.16	0.82963	50	7	500	1015.8
1478	0.02	0.28	0.16	0.82963	75	7	500	1116
1479	0.02	0.28	0.16	0.82963	100	7	500	1150.9
1480	0.02	0.28	0.16	0.82963	150	7	500	1265
1481	0.02	0.28	0.16	0.82963	200	7	500	1363.2
1482	0.02	0.28	0.16	0.82963	300	7	500	1524.9
1483	0.02	0.28	0.16	0.82963	400	7	500	1942.4
1484	0.02	0.28	0.16	0.82963	600	7	500	2227.6
1485	0.02	0.28	0.2	0.84848	1	7	500	623.78
1486	0.02	0.28	0.2	0.84848	10	7	500	629.68
1487	0.02	0.28	0.2	0.84848	15	7	500	638.4
1488	0.02	0.28	0.2	0.84848	25	7	500	672.73
1489	0.02	0.28	0.2	0.84848	35	7	500	707.63
1490	0.02	0.28	0.2	0.84848	50	7	500	751.07
1491	0.02	0.28	0.2	0.84848	75	7	500	800.86
1492	0.02	0.28	0.2	0.84848	100	7	500	852.64
1493	0.02	0.28	0.2	0.84848	150	7	500	945.02
1494	0.02	0.28	0.2	0.84848	200	7	500	1014.1
1495	0.02	0.28	0.2	0.84848	300	7	500	1120.6
1496	0.02	0.28	0.2	0.84848	400	7	500	1238.2
1497	0.02	0.28	0.24	0.86154	1	7	500	481.99
1498	0.02	0.28	0.24	0.86154	10	7	500	491.54
1499	0.02	0.28	0.24	0.86154	15	7	500	505.33
1500	0.02	0.28	0.24	0.86154	25	7	500	541.88
1501	0.02	0.28	0.24	0.86154	35	7	500	575.35
1502	0.02	0.28	0.24	0.86154	50	7	500	591.6
1503	0.02	0.28	0.24	0.86154	75	7	500	640.32
1504	0.02	0.28	0.24	0.86154	100	7	500	674.32
1505	0.02	0.28	0.24	0.86154	150	7	500	763.92
1506	0.02	0.28	0.24	0.86154	200	7	500	792.98
1507	0.02	0.28	0.24	0.86154	300	7	500	894.77
1508	0.02	0.28	0.24	0.86154	400	7	500	988.49
1509	0.02	0.28	0.24	0.86154	600	7	500	1202.7
1510	0.02	0.28	0.28	0.87111	1	7	500	393.29
1511	0.02	0.28	0.28	0.87111	10	7	500	409.48
1512	0.02	0.28	0.28	0.87111	15	7	500	426.14
1513	0.02	0.28	0.28	0.87111	25	7	500	460.6
1514	0.02	0.28	0.28	0.87111	35	7	500	487.72
1515	0.02	0.28	0.28	0.87111	50	7	500	515.01
1516	0.02	0.28	0.28	0.87111	75	7	500	536.05
1517	0.02	0.28	0.28	0.87111	100	7	500	568.3
1518	0.02	0.28	0.28	0.87111	150	7	500	610.84
1519	0.02	0.28	0.28	0.87111	200	7	500	669.67
1520	0.02	0.28	0.28	0.87111	300	7	500	761.84

	t/l	h/l	s/l	ϵ	Re_l	Pr_f	k_s/k_f	Nu_{unit}
1521	0.02	0.28	0.28	0.87111	400	7	500	916.63
1522	0.02	0.28	0.32	0.87843	1	7	500	333.54
1523	0.02	0.28	0.32	0.87843	10	7	500	355.11
1524	0.02	0.28	0.32	0.87843	15	7	500	369.22
1525	0.02	0.28	0.32	0.87843	35	7	500	421.21
1526	0.02	0.28	0.32	0.87843	50	7	500	437.5
1527	0.02	0.28	0.32	0.87843	75	7	500	464.78
1528	0.02	0.28	0.32	0.87843	100	7	500	494.58
1529	0.02	0.28	0.32	0.87843	200	7	500	570.37
1530	0.02	0.28	0.32	0.87843	300	7	500	657.81
1531	0.02	0.28	0.32	0.87843	400	7	500	757.41
1532	0.02	0.28	0.4	0.88889	1	7	500	261.05
1533	0.02	0.28	0.4	0.88889	10	7	500	285.59
1534	0.02	0.28	0.4	0.88889	15	7	500	302.87
1535	0.02	0.28	0.4	0.88889	35	7	500	336.2
1536	0.02	0.28	0.4	0.88889	50	7	500	350.7
1537	0.02	0.28	0.4	0.88889	100	7	500	392.17
1538	0.02	0.28	0.4	0.88889	150	7	500	419.62
1539	0.02	0.28	0.4	0.88889	200	7	500	453.95
1540	0.02	0.28	0.4	0.88889	400	7	500	558.33
1541	0.02	0.28	0.48	0.896	1	7	500	220.22
1542	0.02	0.28	0.48	0.896	10	7	500	247.71
1543	0.02	0.28	0.48	0.896	50	7	500	297.94
1544	0.02	0.32	0.12	0.80672	10	7	500	1336.1
1545	0.02	0.32	0.12	0.80672	100	7	500	1745.1
1546	0.02	0.32	0.16	0.8366	10	7	500	827.02
1547	0.02	0.32	0.16	0.8366	100	7	500	1147.2
1548	0.02	0.32	0.2	0.85561	10	7	500	586.42
1549	0.02	0.32	0.24	0.86878	10	7	500	460.8
1550	0.02	0.32	0.24	0.86878	100	7	500	626.5
1551	0.02	0.32	0.28	0.87843	1	7	500	363.21
1552	0.02	0.32	0.28	0.87843	10	7	500	374.19
1553	0.02	0.32	0.28	0.87843	25	7	500	425.28
1554	0.02	0.32	0.28	0.87843	35	7	500	451.17
1555	0.02	0.32	0.28	0.87843	75	7	500	488.6
1556	0.02	0.32	0.28	0.87843	100	7	500	532.63
1557	0.02	0.32	0.28	0.87843	150	7	500	569.67
1558	0.02	0.32	0.28	0.87843	200	7	500	620.51
1559	0.02	0.32	0.28	0.87843	400	7	500	752.52
1560	0.02	0.32	0.32	0.88581	1	7	500	305.76
1561	0.02	0.32	0.32	0.88581	15	7	500	335.78
1562	0.02	0.32	0.32	0.88581	25	7	500	362.73
1563	0.02	0.32	0.32	0.88581	35	7	500	386.8
1564	0.02	0.32	0.32	0.88581	75	7	500	428.45
1565	0.02	0.32	0.32	0.88581	100	7	500	463.1
1566	0.02	0.32	0.32	0.88581	150	7	500	480.51
1567	0.02	0.32	0.32	0.8858				

t/l	h/l	s/l	ϵ	Re_l	Pr_f	k_s/k_f	Nu_{unit}	
1601	0.02	0.48	0.28	0.896	200	7	500	492.65
1602	0.02	0.48	0.28	0.896	400	7	500	593.67
1603	0.02	0.48	0.32	0.90353	25	7	500	299.69
1604	0.02	0.48	0.32	0.90353	150	7	500	383.72
1605	0.02	0.48	0.32	0.90353	200	7	500	411.52
1606	0.02	0.48	0.32	0.90353	300	7	500	454.07
1607	0.02	0.48	0.4	0.91429	1	7	500	178.04
1608	0.02	0.48	0.4	0.91429	10	7	500	194.42
1609	0.02	0.48	0.4	0.91429	50	7	500	241.67
1610	0.02	0.48	0.4	0.91429	100	7	500	265.85
1611	0.02	0.48	0.48	0.9216	1	7	500	139.34
1612	0.02	0.48	0.48	0.9216	10	7	500	159.74
1613	0.02	0.48	0.48	0.9216	15	7	500	163.18
1614	0.02	0.48	0.48	0.9216	25	7	500	174.14
1615	0.02	0.48	0.48	0.9216	35	7	500	181.93
1616	0.02	0.48	0.48	0.9216	50	7	500	193.12
1617	0.02	0.48	0.48	0.9216	75	7	500	205.73
1618	0.02	0.48	0.48	0.9216	100	7	500	214.34
1619	0.02	0.48	0.48	0.9216	150	7	500	231.69
1620	0.02	0.56	0.12	0.82759	10	7	500	1199.7
1621	0.02	0.56	0.12	0.82759	300	7	500	1980.4
1622	0.02	0.56	0.16	0.85824	10	7	500	725.88
1623	0.02	0.56	0.2	0.87774	10	7	500	488.78
1624	0.02	0.56	0.2	0.87774	100	7	500	660.07
1625	0.02	0.56	0.24	0.89125	10	7	500	366.6
1626	0.02	0.56	0.28	0.90115	1	7	500	280.68
1627	0.02	0.56	0.28	0.90115	10	7	500	288.12
1628	0.02	0.56	0.28	0.90115	25	7	500	334.35
1629	0.02	0.56	0.28	0.90115	50	7	500	356.38
1630	0.02	0.56	0.28	0.90115	100	7	500	400.49
1631	0.02	0.56	0.28	0.90115	300	7	500	515.9
1632	0.02	0.56	0.32	0.90872	10	7	500	237.71
1633	0.02	0.56	0.32	0.90872	25	7	500	265.49
1634	0.02	0.56	0.32	0.90872	100	7	500	332.13
1635	0.02	0.56	0.32	0.90872	150	7	500	373.11
1636	0.02	0.56	0.32	0.90872	300	7	500	430.96
1637	0.02	0.56	0.4	0.91954	10	7	500	178.78
1638	0.02	0.56	0.4	0.91954	25	7	500	198.57
1639	0.02	0.56	0.4	0.91954	35	7	500	208.93
1640	0.02	0.56	0.4	0.91954	75	7	500	233.82
1641	0.02	0.56	0.4	0.91954	100	7	500	246.16
1642	0.02	0.56	0.4	0.91954	150	7	500	268.94
1643	0.02	0.56	0.48	0.9269	10	7	500	143.93
1644	0.02	0.56	0.48	0.9269	15	7	500	150.55
1645	0.02	0.56	0.48	0.9269	25	7	500	158.9
1646	0.02	0.56	0.48	0.9269	35	7	500	167.53
1647	0.02	0.56	0.48	0.9269	50	7	500	174.44
1648	0.02	0.56	0.48	0.9269	75	7	500	185.03
1649	0.02	0.56	0.48	0.9269	100	7	500	193.79
1650	0.02	0.56	0.48	0.9269	150	7	500	209.6
1651	0.02	0.68	0.12	0.83265	10	7	500	1176.3
1652	0.02	0.68	0.16	0.86349	10	7	500	691.21
1653	0.02	0.68	0.16	0.86349	100	7	500	890.18
1654	0.02	0.68	0.2	0.88312	10	7	500	471.14
1655	0.02	0.68	0.24	0.8967	10	7	500	344.19
1656	0.02	0.68	0.24	0.8967	100	7	500	473.81
1657	0.02	0.68	0.28	0.90667	10	7	500	270.2
1658	0.02	0.68	0.28	0.90667	75	7	500	358.42
1659	0.02	0.68	0.28	0.90667	100	7	500	374.15
1660	0.02	0.68	0.28	0.90667	150	7	500	401.73
1661	0.02	0.68	0.28	0.90667	200	7	500	426.25
1662	0.02	0.68	0.28	0.90667	300	7	500	469.75
1663	0.02	0.68	0.32	0.91429	1	7	500	218.92
1664	0.02	0.68	0.32	0.91429	10	7	500	221.55
1665	0.02	0.68	0.32	0.91429	25	7	500	247.19
1666	0.02	0.68	0.32	0.91429	35	7	500	259.41
1667	0.02	0.68	0.32	0.91429	50	7	500	276.27
1668	0.02	0.68	0.32	0.91429	75	7	500	290.52
1669	0.02	0.68	0.32	0.91429	100	7	500	306.24
1670	0.02	0.68	0.32	0.91429	300	7	500	385.29
1671	0.02	0.68	0.4	0.92517	1	7	500	150.89
1672	0.02	0.68	0.4	0.92517	10	7	500	158.66
1673	0.02	0.68	0.4	0.92517	150	7	500	239.27
1674	0.02	0.68	0.4	0.92517	200	7	500	249.4
1675	0.02	0.68	0.48	0.93257	1	7	500	114.93
1676	0.02	0.68	0.48	0.93257	10	7	500	126
1677	0.02	0.68	0.48	0.93257	100	7	500	172.67
1678	0.02	1.0	0.12	0.84034	10	7	500	1127.5
1679	0.02	1.0	0.12	0.84034	300	7	500	1786
1680	0.02	1.0	0.16	0.87146	100	7	500	838.4

t/l	h/l	s/l	ϵ	Re_l	Pr_f	k_s/k_f	Nu_{unit}	
1681	0.02	1.0	0.2	0.89127	10	7	500	431.6
1682	0.02	1.0	0.2	0.89127	100	7	500	571.85
1683	0.02	1.0	0.24	0.90498	10	7	500	310.25
1684	0.02	1.0	0.28	0.91503	1	7	500	245.9
1685	0.02	1.0	0.28	0.91503	10	7	500	238.38
1686	0.02	1.0	0.28	0.91503	15	7	500	245.75
1687	0.02	1.0	0.28	0.91503	35	7	500	275.98
1688	0.02	1.0	0.28	0.91503	50	7	500	294.41
1689	0.02	1.0	0.28	0.91503	100	7	500	330.6
1690	0.02	1.0	0.28	0.91503	300	7	500	405.9
1691	0.02	1.0	0.32	0.92272	1	7	500	195.56
1692	0.02	1.0	0.32	0.92272	10	7	500	191.14
1693	0.02	1.0	0.32	0.92272	25	7	500	214.91
1694	0.02	1.0	0.32	0.92272	100	7	500	264.99
1695	0.02	1.0	0.32	0.92272	200	7	500	302.61
1696	0.02	1.0	0.4	0.93371	10	7	500	135.7
1697	0.02	1.0	0.4	0.93371	25	7	500	155.09
1698	0.02	1.0	0.4	0.93371	35	7	500	163.3
1699	0.02	1.0	0.4	0.93371	50	7	500	170.97
1700	0.02	1.0	0.4	0.93371	200	7	500	212.73
1701	0.02	1.0	0.48	0.94118	10	7	500	105.7
1702	0.02	1.0	0.48	0.94118	15	7	500	111.96
1703	0.02	1.0	0.48	0.94118	25	7	500	119.9
1704	0.02	1.0	0.48	0.94118	35	7	500	124.36
1705	0.02	1.0	0.48	0.94118	50	7	500	130.33
1706	0.02	1.0	0.48	0.94118	75	7	500	138.02
1707	0.02	1.0	0.48	0.94118	100	7	500	143.86
1708	0.04	0.12	0.12	0.5625	1	7	500	1746
1709	0.04	0.12	0.12	0.5625	10	7	500	1837.1
1710	0.04	0.12	0.12	0.5625	15	7	500	1885.9
1711	0.04	0.12	0.12	0.5625	25	7	500	1975.9
1712	0.04	0.12	0.12	0.5625	35	7	500	2056.6
1713	0.04	0.12	0.12	0.5625	50	7	500	2172.2
1714	0.04	0.12	0.12	0.5625	75	7	500	2390.6
1715	0.04	0.12	0.12	0.5625	100	7	500	2591.8
1716	0.04	0.12	0.12	0.5625	150	7	500	3009.6
1717	0.04	0.12	0.12	0.5625	200	7	500	3602.3
1718	0.04	0.12	0.12	0.5625	300	7	500	4895.5
1719	0.04	0.12	0.12	0.5625	400	7	500	6960.2
1720	0.04	0.12	0.16	0.6	1	7	500	1271.5
1721	0.04	0.12	0.16	0.6	10	7	500	1332
1722	0.04	0.12	0.16	0.6	15	7	500	1361.9
1723	0.04	0.12	0.16	0.6	25	7	500	1434.1
1724	0.04	0.12	0.16	0.6	35	7	500	1498.9
1725	0.04	0.12	0.16	0.6	50	7	500	1595.9
1726	0.04	0.12	0.16	0.6	75	7	500	1748.7
1727	0.04	0.12	0.16	0.6	100	7	500	1886.6
1728	0.04							

t/l	h/l	s/l	ϵ	Re_l	Pr_f	k_s/k_f	Nu_{unit}	
1761	0.04	0.12	0.28	0.65625	50	7	500	1041.8
1762	0.04	0.12	0.28	0.65625	75	7	500	1104.7
1763	0.04	0.12	0.28	0.65625	100	7	500	1164.3
1764	0.04	0.12	0.28	0.65625	150	7	500	1307.6
1765	0.04	0.12	0.28	0.65625	200	7	500	1485.5
1766	0.04	0.12	0.28	0.65625	300	7	500	1904
1767	0.04	0.12	0.28	0.65625	400	7	500	2353.1
1768	0.04	0.12	0.32	0.66667	10	7	500	821.02
1769	0.04	0.12	0.32	0.66667	100	7	500	1060.8
1770	0.04	0.12	0.32	0.66667	300	7	500	1692.2
1771	0.04	0.12	0.4	0.68182	10	7	500	759.67
1772	0.04	0.12	0.4	0.68182	100	7	500	930.36
1773	0.04	0.12	0.4	0.68182	300	7	500	1350.7
1774	0.04	0.12	0.48	0.69231	10	7	500	728.59
1775	0.04	0.12	0.48	0.69231	100	7	500	858.03
1776	0.04	0.12	0.48	0.69231	300	7	500	1149.6
1777	0.04	0.16	0.12	0.6	1	7	500	1522.9
1778	0.04	0.16	0.12	0.6	10	7	500	1603.9
1779	0.04	0.16	0.12	0.6	15	7	500	1653.5
1780	0.04	0.16	0.12	0.6	25	7	500	1733.3
1781	0.04	0.16	0.12	0.6	35	7	500	1813.8
1782	0.04	0.16	0.12	0.6	50	7	500	1918.5
1783	0.04	0.16	0.12	0.6	75	7	500	2112.4
1784	0.04	0.16	0.12	0.6	100	7	500	2283
1785	0.04	0.16	0.12	0.6	150	7	500	2702.8
1786	0.04	0.16	0.12	0.6	200	7	500	3172
1787	0.04	0.16	0.12	0.6	300	7	500	4233.4
1788	0.04	0.16	0.12	0.6	400	7	500	5746.5
1789	0.04	0.16	0.16	0.64	1	7	500	1049
1790	0.04	0.16	0.16	0.64	10	7	500	1102.3
1791	0.04	0.16	0.16	0.64	15	7	500	1135
1792	0.04	0.16	0.16	0.64	25	7	500	1194.1
1793	0.04	0.16	0.16	0.64	35	7	500	1240.2
1794	0.04	0.16	0.16	0.64	50	7	500	1328.4
1795	0.04	0.16	0.16	0.64	75	7	500	1475.3
1796	0.04	0.16	0.16	0.64	100	7	500	1583.3
1797	0.04	0.16	0.16	0.64	150	7	500	1846.9
1798	0.04	0.16	0.16	0.64	200	7	500	2137.1
1799	0.04	0.16	0.16	0.64	300	7	500	2888
1800	0.04	0.16	0.16	0.64	400	7	500	3670.5
1801	0.04	0.16	0.2	0.66667	1	7	500	813.57
1802	0.04	0.16	0.2	0.66667	10	7	500	858.62
1803	0.04	0.16	0.2	0.66667	15	7	500	885.47
1804	0.04	0.16	0.2	0.66667	25	7	500	940.66
1805	0.04	0.16	0.2	0.66667	35	7	500	988.23
1806	0.04	0.16	0.2	0.66667	50	7	500	1057
1807	0.04	0.16	0.2	0.66667	75	7	500	1148.4
1808	0.04	0.16	0.2	0.66667	100	7	500	1232.7
1809	0.04	0.16	0.2	0.66667	150	7	500	1448.5
1810	0.04	0.16	0.2	0.66667	200	7	500	1687
1811	0.04	0.16	0.2	0.66667	300	7	500	2067.3
1812	0.04	0.16	0.2	0.66667	400	7	500	2929
1813	0.04	0.16	0.24	0.68571	1	7	500	682.39
1814	0.04	0.16	0.24	0.68571	10	7	500	721.78
1815	0.04	0.16	0.24	0.68571	15	7	500	749.89
1816	0.04	0.16	0.24	0.68571	25	7	500	796.33
1817	0.04	0.16	0.24	0.68571	35	7	500	838.51
1818	0.04	0.16	0.24	0.68571	50	7	500	896.55
1819	0.04	0.16	0.24	0.68571	75	7	500	961.7
1820	0.04	0.16	0.24	0.68571	100	7	500	1036.8
1821	0.04	0.16	0.24	0.68571	150	7	500	1211.2
1822	0.04	0.16	0.24	0.68571	200	7	500	1393.5
1823	0.04	0.16	0.24	0.68571	300	7	500	1726.1
1824	0.04	0.16	0.24	0.68571	400	7	500	2434.6
1825	0.04	0.16	0.28	0.7	1	7	500	596.84
1826	0.04	0.16	0.28	0.7	10	7	500	637.05
1827	0.04	0.16	0.28	0.7	15	7	500	661.32
1828	0.04	0.16	0.28	0.7	25	7	500	706.04
1829	0.04	0.16	0.28	0.7	35	7	500	743.08
1830	0.04	0.16	0.28	0.7	50	7	500	781.91
1831	0.04	0.16	0.28	0.7	75	7	500	838.62
1832	0.04	0.16	0.28	0.7	100	7	500	903.04
1833	0.04	0.16	0.28	0.7	150	7	500	1034.3
1834	0.04	0.16	0.28	0.7	200	7	500	1204.5
1835	0.04	0.16	0.28	0.7	300	7	500	1491.9
1836	0.04	0.16	0.28	0.7	400	7	500	2007.3
1837	0.04	0.16	0.28	0.7	600	7	500	2895.9
1838	0.04	0.16	0.32	0.71111	10	7	500	578.89
1839	0.04	0.16	0.32	0.71111	100	7	500	807.08
1840	0.04	0.16	0.32	0.71111	400	7	500	1729.4

t/l	h/l	s/l	ϵ	Re_l	Pr_f	k_s/k_f	Nu_{unit}	
1841	0.04	0.16	0.4	0.72727	10	7	500	511.26
1842	0.04	0.16	0.4	0.72727	300	7	500	1094.5
1843	0.04	0.16	0.48	0.73846	10	7	500	475.31
1844	0.04	0.16	0.48	0.73846	100	7	500	592.43
1845	0.04	0.2	0.12	0.625	1	7	500	1410.3
1846	0.04	0.2	0.12	0.625	10	7	500	1481.5
1847	0.04	0.2	0.12	0.625	15	7	500	1528.6
1848	0.04	0.2	0.12	0.625	25	7	500	1603.9
1849	0.04	0.2	0.12	0.625	35	7	500	1684.2
1850	0.04	0.2	0.12	0.625	50	7	500	1781.1
1851	0.04	0.2	0.12	0.625	75	7	500	1948.4
1852	0.04	0.2	0.12	0.625	100	7	500	2118.8
1853	0.04	0.2	0.12	0.625	150	7	500	2445.7
1854	0.04	0.2	0.12	0.625	200	7	500	2796
1855	0.04	0.2	0.12	0.625	300	7	500	3914.8
1856	0.04	0.2	0.12	0.625	400	7	500	5173.2
1857	0.04	0.2	0.16	0.66667	1	7	500	938.19
1858	0.04	0.2	0.16	0.66667	10	7	500	981.47
1859	0.04	0.2	0.16	0.66667	15	7	500	1008.1
1860	0.04	0.2	0.16	0.66667	25	7	500	1063.3
1861	0.04	0.2	0.16	0.66667	35	7	500	1118.3
1862	0.04	0.2	0.16	0.66667	50	7	500	1201
1863	0.04	0.2	0.16	0.66667	75	7	500	1317.6
1864	0.04	0.2	0.16	0.66667	100	7	500	1427.5
1865	0.04	0.2	0.16	0.66667	150	7	500	1663.9
1866	0.04	0.2	0.16	0.66667	200	7	500	1860.1
1867	0.04	0.2	0.16	0.66667	300	7	500	2568.6
1868	0.04	0.2	0.16	0.66667	400	7	500	3275.5
1869	0.04	0.2	0.2	0.69444	1	7	500	702.78
1870	0.04	0.2	0.2	0.69444	10	7	500	740.69
1871	0.04	0.2	0.2	0.69444	15	7	500	766.15
1872	0.04	0.2	0.2	0.69444	25	7	500	806.31
1873	0.04	0.2	0.2	0.69444	35	7	500	854.69
1874	0.04	0.2	0.2	0.69444	50	7	500	920.17
1875	0.04	0.2	0.2	0.69444	75	7	500	1005.2
1876	0.04	0.2	0.2	0.69444	100	7	500	1084.4
1877	0.04	0.2	0.2	0.69444	150	7	500	1279.2
1878	0.04	0.2	0.2	0.69444	200	7	500	1492.5
1879	0.04	0.2	0.2	0.69444	300	7	500	1974.8
1880	0.04	0.2	0.2	0.69444	400	7	500	2233.5
1881	0.04	0.2	0.2	0.69444	600	7	500	3826.7
1882	0.04	0.2	0.24	0.71429	1	7	500	571.32
1883	0.04	0.2	0.24	0.71429	10	7	500	603.95
1884	0.04	0.2	0.24	0.71429	15	7	500	629.6
1885	0.04	0.2	0.24	0.71429	25	7	500	668.47
1886	0.04	0.2	0.24	0.71429	35	7	500	710.51
1887	0.04	0.2	0.24	0.71429	50	7	500	760.65
1888	0.04	0.2	0.24	0.71429	75	7	500	828.01
1889	0.04	0.2	0.24					

t/l	h/l	s/l	ϵ	Re_l	Pr_f	k_s/k_f	Nu_{unit}	
1921	0.04	0.24	0.12	0.64286	100	7	500	2014.3
1922	0.04	0.24	0.12	0.64286	150	7	500	2380.1
1923	0.04	0.24	0.12	0.64286	200	7	500	2676.5
1924	0.04	0.24	0.12	0.64286	300	7	500	3714.9
1925	0.04	0.24	0.12	0.64286	400	7	500	4798
1926	0.04	0.24	0.16	0.68571	1	7	500	875.5
1927	0.04	0.24	0.16	0.68571	10	7	500	916.11
1928	0.04	0.24	0.16	0.68571	15	7	500	940.58
1929	0.04	0.24	0.16	0.68571	25	7	500	980.64
1930	0.04	0.24	0.16	0.68571	35	7	500	1037.1
1931	0.04	0.24	0.16	0.68571	50	7	500	1116.1
1932	0.04	0.24	0.16	0.68571	75	7	500	1250
1933	0.04	0.24	0.16	0.68571	100	7	500	1328.1
1934	0.04	0.24	0.16	0.68571	150	7	500	1541.9
1935	0.04	0.24	0.16	0.68571	200	7	500	1697.2
1936	0.04	0.24	0.16	0.68571	300	7	500	2361.5
1937	0.04	0.24	0.16	0.68571	400	7	500	3056.9
1938	0.04	0.24	0.16	0.68571	600	7	500	3402.2
1939	0.04	0.24	0.2	0.71429	1	7	500	641.59
1940	0.04	0.24	0.2	0.71429	10	7	500	671.92
1941	0.04	0.24	0.2	0.71429	15	7	500	691.34
1942	0.04	0.24	0.2	0.71429	25	7	500	738.61
1943	0.04	0.24	0.2	0.71429	35	7	500	784.86
1944	0.04	0.24	0.2	0.71429	50	7	500	847.18
1945	0.04	0.24	0.2	0.71429	75	7	500	909.65
1946	0.04	0.24	0.2	0.71429	100	7	500	993.68
1947	0.04	0.24	0.2	0.71429	150	7	500	1169.5
1948	0.04	0.24	0.2	0.71429	200	7	500	1270.3
1949	0.04	0.24	0.2	0.71429	300	7	500	1727.5
1950	0.04	0.24	0.2	0.71429	400	7	500	2129.2
1951	0.04	0.24	0.2	0.71429	600	7	500	3118.2
1952	0.04	0.24	0.24	0.73469	1	7	500	506.16
1953	0.04	0.24	0.24	0.73469	10	7	500	536.27
1954	0.04	0.24	0.24	0.73469	15	7	500	552.13
1955	0.04	0.24	0.24	0.73469	25	7	500	595.72
1956	0.04	0.24	0.24	0.73469	35	7	500	637.32
1957	0.04	0.24	0.24	0.73469	50	7	500	684.13
1958	0.04	0.24	0.24	0.73469	75	7	500	744.03
1959	0.04	0.24	0.24	0.73469	100	7	500	798.26
1960	0.04	0.24	0.24	0.73469	150	7	500	897.39
1961	0.04	0.24	0.24	0.73469	200	7	500	1024.1
1962	0.04	0.24	0.24	0.73469	300	7	500	1319
1963	0.04	0.24	0.24	0.73469	400	7	500	1592.9
1964	0.04	0.24	0.24	0.73469	600	7	500	2076.1
1965	0.04	0.24	0.28	0.73469	1	7	500	421.57
1966	0.04	0.24	0.28	0.73469	10	7	500	452.69
1967	0.04	0.24	0.28	0.73469	15	7	500	473.02
1968	0.04	0.24	0.28	0.73469	25	7	500	511.14
1969	0.04	0.24	0.28	0.73469	35	7	500	540.19
1970	0.04	0.24	0.28	0.73469	50	7	500	574.74
1971	0.04	0.24	0.28	0.73469	75	7	500	619.77
1972	0.04	0.24	0.28	0.73469	100	7	500	677.63
1973	0.04	0.24	0.28	0.73469	150	7	500	789.57
1974	0.04	0.24	0.28	0.73469	200	7	500	880.46
1975	0.04	0.24	0.28	0.73469	300	7	500	1113
1976	0.04	0.24	0.28	0.73469	400	7	500	1379.1
1977	0.04	0.24	0.28	0.73469	600	7	500	1684.1
1978	0.04	0.24	0.32	0.7619	10	7	500	397.89
1979	0.04	0.24	0.32	0.7619	100	7	500	595.97
1980	0.04	0.24	0.4	0.77922	10	7	500	327.39
1981	0.04	0.24	0.4	0.77922	100	7	500	476.08
1982	0.04	0.24	0.48	0.79121	10	7	500	290.96
1983	0.04	0.28	0.12	0.65625	1	7	500	1313.8
1984	0.04	0.28	0.12	0.65625	10	7	500	1362.5
1985	0.04	0.28	0.12	0.65625	15	7	500	1408.8
1986	0.04	0.28	0.12	0.65625	25	7	500	1475.9
1987	0.04	0.28	0.12	0.65625	35	7	500	1544.6
1988	0.04	0.28	0.12	0.65625	50	7	500	1644.5
1989	0.04	0.28	0.12	0.65625	75	7	500	1754.9
1990	0.04	0.28	0.12	0.65625	100	7	500	1943.6
1991	0.04	0.28	0.12	0.65625	150	7	500	2312.6
1992	0.04	0.28	0.12	0.65625	200	7	500	2576.9
1993	0.04	0.28	0.12	0.65625	300	7	500	3504.6
1994	0.04	0.28	0.16	0.7	1	7	500	833.85
1995	0.04	0.28	0.16	0.7	10	7	500	865.87
1996	0.04	0.28	0.16	0.7	15	7	500	888.45
1997	0.04	0.28	0.16	0.7	25	7	500	941.33
1998	0.04	0.28	0.16	0.7	35	7	500	992.57
1999	0.04	0.28	0.16	0.7	50	7	500	1070.9
2000	0.04	0.28	0.16	0.7	75	7	500	1166.7

t/l	h/l	s/l	ϵ	Re_l	Pr_f	k_s/k_f	Nu_{unit}	
2001	0.04	0.28	0.16	0.7	100	7	500	1260.1
2002	0.04	0.28	0.16	0.7	150	7	500	1484.6
2003	0.04	0.28	0.16	0.7	200	7	500	1623.9
2004	0.04	0.28	0.16	0.7	300	7	500	2210
2005	0.04	0.28	0.16	0.7	400	7	500	2602.6
2006	0.04	0.28	0.16	0.7	600	7	500	4157.9
2007	0.04	0.28	0.2	0.72917	1	7	500	599.53
2008	0.04	0.28	0.2	0.72917	10	7	500	627.97
2009	0.04	0.28	0.2	0.72917	15	7	500	646.77
2010	0.04	0.28	0.2	0.72917	25	7	500	688.42
2011	0.04	0.28	0.2	0.72917	35	7	500	727.64
2012	0.04	0.28	0.2	0.72917	50	7	500	790.77
2013	0.04	0.28	0.2	0.72917	75	7	500	856.36
2014	0.04	0.28	0.2	0.72917	100	7	500	933.4
2015	0.04	0.28	0.2	0.72917	150	7	500	1085.8
2016	0.04	0.28	0.2	0.72917	200	7	500	1253.2
2017	0.04	0.28	0.2	0.72917	300	7	500	1541.3
2018	0.04	0.28	0.2	0.72917	400	7	500	1913.9
2019	0.04	0.28	0.2	0.72917	600	7	500	2831.2
2020	0.04	0.28	0.24	0.75	1	7	500	465.66
2021	0.04	0.28	0.24	0.75	10	7	500	493.45
2022	0.04	0.28	0.24	0.75	15	7	500	512.35
2023	0.04	0.28	0.24	0.75	25	7	500	552.65
2024	0.04	0.28	0.24	0.75	35	7	500	586.53
2025	0.04	0.28	0.24	0.75	50	7	500	616.1
2026	0.04	0.28	0.24	0.75	75	7	500	677.84
2027	0.04	0.28	0.24	0.75	100	7	500	741.33
2028	0.04	0.28	0.24	0.75	150	7	500	826.9
2029	0.04	0.28	0.24	0.75	200	7	500	936.19
2030	0.04	0.28	0.24	0.75	300	7	500	1164.6
2031	0.04	0.28	0.24	0.75	400	7	500	1431.9
2032	0.04	0.28	0.24	0.75	600	7	500	1884.3
2033	0.04	0.28	0.28	0.76563	1	7	500	381.62
2034	0.04	0.28	0.28	0.76563	10	7	500	411.39
2035	0.04	0.28	0.28	0.76563	15	7	500	425.45
2036	0.04	0.28	0.28	0.76563	35	7	500	494.38
2037	0.04	0.28	0.28	0.76563	75	7	500	573.5
2038	0.04	0.28	0.28	0.76563	100	7	500	621.78
2039	0.04	0.28	0.28	0.76563	150	7	500	688.75
2040	0.04	0.28	0.28	0.76563	200	7	500	799.14
2041	0.04	0.28	0.28	0.76563	300	7	500	987.78
2042	0.04	0.28	0.28	0.76563	400	7	500	1243.9
2043	0.04	0.28	0.32	0.77778	1	7	500	324.54
2044	0.04	0.28	0.32	0.77778	10	7	500	356
2045	0.04	0.28	0.32	0.77778	15	7	500	372.2
2046	0.04	0.28	0.32	0.77778	25	7	500	405.48
2047	0.04	0.28	0.32	0.77778	35	7	500	428.4
2								

t/l	h/l	s/l	ϵ	Re_l	Pr_f	k_s/k_f	Nu_{unit}	
2081	0.04	0.32	0.32	0.79012	150	7	500	551.87
2082	0.04	0.32	0.32	0.79012	200	7	500	634.56
2083	0.04	0.32	0.32	0.79012	300	7	500	795.59
2084	0.04	0.32	0.4	0.80808	1	7	500	228.95
2085	0.04	0.32	0.4	0.80808	10	7	500	257.35
2086	0.04	0.32	0.4	0.80808	15	7	500	274.67
2087	0.04	0.32	0.4	0.80808	25	7	500	289.98
2088	0.04	0.32	0.4	0.80808	75	7	500	360.99
2089	0.04	0.32	0.4	0.80808	100	7	500	379.4
2090	0.04	0.32	0.48	0.82051	1	7	500	189.63
2091	0.04	0.32	0.48	0.82051	10	7	500	219.65
2092	0.04	0.32	0.48	0.82051	100	7	500	320.21
2093	0.04	0.32	0.48	0.82051	150	7	500	375.16
2094	0.04	0.4	0.12	0.68182	100	7	500	1847
2095	0.04	0.4	0.16	0.72727	10	7	500	790.97
2096	0.04	0.4	0.2	0.75758	10	7	500	553.33
2097	0.04	0.4	0.24	0.77922	10	7	500	424.43
2098	0.04	0.4	0.24	0.77922	100	7	500	645.56
2099	0.04	0.4	0.28	0.79545	10	7	500	340.27
2100	0.04	0.4	0.32	0.80808	10	7	500	287.71
2101	0.04	0.4	0.32	0.80808	100	7	500	422.49
2102	0.04	0.4	0.48	0.83916	10	7	500	184.98
2103	0.04	0.4	0.48	0.83916	100	7	500	271.37
2104	0.04	0.48	0.12	0.69231	10	7	500	1255.1
2105	0.04	0.48	0.12	0.69231	100	7	500	1820
2106	0.04	0.48	0.16	0.73846	10	7	500	767.52
2107	0.04	0.48	0.16	0.73846	100	7	500	1196.2
2108	0.04	0.48	0.2	0.76923	10	7	500	530.49
2109	0.04	0.48	0.2	0.76923	100	7	500	797.54
2110	0.04	0.48	0.24	0.79121	10	7	500	399.28
2111	0.04	0.48	0.28	0.80769	1	7	500	299.15
2112	0.04	0.48	0.28	0.80769	100	7	500	490.23
2113	0.04	0.48	0.28	0.80769	200	7	500	600.66
2114	0.04	0.48	0.32	0.82051	10	7	500	263.86
2115	0.04	0.48	0.32	0.82051	15	7	500	282.84
2116	0.04	0.48	0.32	0.82051	25	7	500	312.99
2117	0.04	0.48	0.32	0.82051	100	7	500	413.87
2118	0.04	0.48	0.32	0.82051	150	7	500	440.11
2119	0.04	0.48	0.32	0.82051	300	7	500	579.2
2120	0.04	0.48	0.4	0.83916	1	7	500	176.28
2121	0.04	0.48	0.4	0.83916	10	7	500	201.75
2122	0.04	0.48	0.4	0.83916	25	7	500	233.19
2123	0.04	0.48	0.4	0.83916	50	7	500	256.96
2124	0.04	0.48	0.4	0.83916	100	7	500	302.23
2125	0.04	0.48	0.4	0.83916	400	7	500	531.78
2126	0.04	0.48	0.48	0.85207	1	7	500	138.59
2127	0.04	0.48	0.48	0.85207	10	7	500	164.63
2128	0.04	0.48	0.48	0.85207	15	7	500	174.25
2129	0.04	0.48	0.48	0.85207	25	7	500	187.34
2130	0.04	0.48	0.48	0.85207	35	7	500	193.96
2131	0.04	0.48	0.48	0.85207	50	7	500	209.77
2132	0.04	0.48	0.48	0.85207	75	7	500	226.87
2133	0.04	0.48	0.48	0.85207	100	7	500	238.15
2134	0.04	0.48	0.48	0.85207	150	7	500	274.79
2135	0.04	0.48	0.48	0.85207	300	7	500	362.21
2136	0.04	0.56	0.12	0.7	300	7	500	3099.3
2137	0.04	0.56	0.16	0.74667	10	7	500	744.39
2138	0.04	0.56	0.2	0.77778	100	7	500	813.26
2139	0.04	0.56	0.24	0.8	10	7	500	382.14
2140	0.04	0.56	0.24	0.8	100	7	500	595.61
2141	0.04	0.56	0.28	0.81667	10	7	500	300.94
2142	0.04	0.56	0.28	0.81667	75	7	500	425.79
2143	0.04	0.56	0.28	0.81667	100	7	500	468.11
2144	0.04	0.56	0.28	0.81667	300	7	500	641.56
2145	0.04	0.56	0.28	0.81667	400	7	500	831.24
2146	0.04	0.56	0.28	0.81667	600	7	500	975.85
2147	0.04	0.56	0.32	0.82963	10	7	500	249.11
2148	0.04	0.56	0.32	0.82963	15	7	500	267.05
2149	0.04	0.56	0.32	0.82963	50	7	500	332.93
2150	0.04	0.56	0.32	0.82963	200	7	500	453.04
2151	0.04	0.56	0.32	0.82963	300	7	500	538.31
2152	0.04	0.56	0.4	0.84848	1	7	500	164.98
2153	0.04	0.56	0.4	0.84848	10	7	500	187.46
2154	0.04	0.56	0.4	0.84848	25	7	500	211.66
2155	0.04	0.56	0.4	0.84848	75	7	500	251.97
2156	0.04	0.56	0.4	0.84848	100	7	500	270.29
2157	0.04	0.56	0.4	0.84848	150	7	500	305.64
2158	0.04	0.56	0.4	0.84848	200	7	500	339.84
2159	0.04	0.56	0.48	0.86154	1	7	500	126.26
2160	0.04	0.56	0.48	0.86154	10	7	500	151.64

t/l	h/l	s/l	ϵ	Re_l	Pr_f	k_s/k_f	Nu_{unit}	
2161	0.04	0.56	0.48	0.86154	35	7	500	179.1
2162	0.04	0.56	0.48	0.86154	100	7	500	216.5
2163	0.04	0.56	0.48	0.86154	200	7	500	269.94
2164	0.04	0.68	0.12	0.70833	10	7	500	1209.6
2165	0.04	0.68	0.12	0.70833	100	7	500	1747.2
2166	0.04	0.68	0.2	0.78704	10	7	500	500.34
2167	0.04	0.68	0.2	0.78704	100	7	500	782.47
2168	0.04	0.68	0.24	0.80952	100	7	500	567.26
2169	0.04	0.68	0.28	0.82639	10	7	500	287.59
2170	0.04	0.68	0.28	0.82639	15	7	500	303.59
2171	0.04	0.68	0.28	0.82639	75	7	500	416.93
2172	0.04	0.68	0.28	0.82639	150	7	500	466.41
2173	0.04	0.68	0.28	0.82639	200	7	500	507.58
2174	0.04	0.68	0.32	0.83951	1	7	500	219.94
2175	0.04	0.68	0.32	0.83951	10	7	500	235.73
2176	0.04	0.68	0.32	0.83951	50	7	500	305.68
2177	0.04	0.68	0.32	0.83951	100	7	500	343.19
2178	0.04	0.68	0.32	0.83951	200	7	500	412.85
2179	0.04	0.68	0.4	0.85859	10	7	500	174.39
2180	0.04	0.68	0.4	0.85859	15	7	500	188.01
2181	0.04	0.68	0.4	0.85859	75	7	500	243.06
2182	0.04	0.68	0.4	0.85859	100	7	500	247.61
2183	0.04	0.68	0.4	0.85859	200	7	500	312.01
2184	0.04	0.68	0.48	0.87179	1	7	500	115.25
2185	0.04	0.68	0.48	0.87179	10	7	500	138.75
2186	0.04	0.68	0.48	0.87179	25	7	500	150.69
2187	0.04	0.68	0.48	0.87179	50	7	500	177.43
2188	0.04	0.68	0.48	0.87179	75	7	500	189.47
2189	0.04	0.68	0.48	0.87179	100	7	500	194.59
2190	0.04	0.68	0.48	0.87179	150	7	500	215.2
2191	0.04	1.0	0.12	0.72115	300	7	500	3074.8
2192	0.04	1.0	0.16	0.76923	10	7	500	692.18
2193	0.04	1.0	0.16	0.76923	100	7	500	1023.4
2194	0.04	1.0	0.24	0.82418	10	7	500	339.73
2195	0.04	1.0	0.24	0.82418	100	7	500	547.98
2196	0.04	1.0	0.28	0.84135	10	7	500	266.12
2197	0.04	1.0	0.28	0.84135	35	7	500	336.21
2198	0.04	1.0	0.28	0.84135	300	7	500	508.48
2199	0.04	1.0	0.32	0.8547	1	7	500	201.5
2200	0.04	1.0	0.32	0.8547	15	7	500	231.95
2201	0.04	1.0	0.32	0.8547	25	7	500	259.68
2202	0.04	1.0	0.32	0.8547	75	7	500	287.39
2203	0.04	1.0	0.32	0.8547	100	7	500	304.32
2204	0.04	1.0	0.32	0.8547	100	7	500	335.68
2205	0.04	1.0	0.32	0.8547	200	7	500	359.87
2206	0.04	1.0	0.32	0.8547	300	7	500	357.01
2207	0.04	1.0	0.4					

	t/l	h/l	s/l	ϵ	Re_l	Pr_f	k_s/k_f	Nu_{unit}
2241	0.06	0.12	0.24	0.53333	150	7	500	1717
2242	0.06	0.12	0.24	0.53333	200	7	500	2138.8
2243	0.06	0.12	0.24	0.53333	300	7	500	3290.9
2244	0.06	0.12	0.48	0.59259	100	7	500	827.96
2245	0.06	0.12	0.48	0.59259	300	7	500	1427.7
2246	0.06	0.12	0.48	0.59259	600	7	500	2055.2
2247	0.06	0.24	0.12	0.53333	1	7	500	1276.7
2248	0.06	0.24	0.12	0.53333	10	7	500	1379.7
2249	0.06	0.24	0.12	0.53333	15	7	500	1522.4
2250	0.06	0.24	0.12	0.53333	25	7	500	1662.1
2251	0.06	0.24	0.12	0.53333	35	7	500	1583
2252	0.06	0.24	0.12	0.53333	50	7	500	1676.8
2253	0.06	0.24	0.12	0.53333	75	7	500	2135.1
2254	0.06	0.24	0.12	0.53333	100	7	500	2418.6
2255	0.06	0.24	0.12	0.53333	150	7	500	3046.4
2256	0.06	0.24	0.12	0.53333	200	7	500	3795.7
2257	0.06	0.24	0.24	0.64	1	7	500	486.82
2258	0.06	0.24	0.24	0.64	10	7	500	534.24
2259	0.06	0.24	0.24	0.64	15	7	500	557.02
2260	0.06	0.24	0.24	0.64	25	7	500	607.35
2261	0.06	0.24	0.24	0.64	35	7	500	647.88
2262	0.06	0.24	0.24	0.64	50	7	500	688.72
2263	0.06	0.24	0.24	0.64	75	7	500	774.22
2264	0.06	0.24	0.24	0.64	100	7	500	864.3
2265	0.06	0.24	0.24	0.64	150	7	500	1077.4
2266	0.06	0.24	0.24	0.64	200	7	500	1299.1
2267	0.06	0.24	0.24	0.64	300	7	500	1798.6
2268	0.06	0.24	0.24	0.64	400	7	500	2063.6
2269	0.06	0.24	0.24	0.64	600	7	500	3089.5
2270	0.06	0.24	0.48	0.71111	100	7	500	442.42
2271	0.06	0.48	0.12	0.59259	10	7	500	1242.6
2272	0.06	0.48	0.48	0.79012	1	7	500	138.55
2273	0.06	0.48	0.48	0.79012	10	7	500	168.03
2274	0.06	0.48	0.48	0.79012	15	7	500	176.06
2275	0.06	0.48	0.48	0.79012	25	7	500	189.46
2276	0.06	0.48	0.48	0.79012	35	7	500	202.91
2277	0.06	0.48	0.48	0.79012	50	7	500	218.2
2278	0.06	0.48	0.48	0.79012	75	7	500	236.85
2279	0.06	0.48	0.48	0.79012	100	7	500	263.63
2280	0.06	0.48	0.48	0.79012	150	7	500	314.89
2281	0.06	0.48	0.48	0.79012	200	7	500	372.92
2282	0.06	0.48	0.48	0.79012	300	7	500	439.36

Appendix D: Additional periodically developed Nusselt number data for the study on the influence Pr_f and k_s/k_f

	t/l	h/l	s/l	ϵ	Re_l	Pr_f	k_s/k_f	Nu_{unit}
1	0.02	0.24	0.24	0.85207	10	0.7	10	395.01
2	0.02	0.24	0.24	0.85207	10	0.7	20	432.79
3	0.02	0.24	0.24	0.85207	10	0.7	50	477.61
4	0.02	0.24	0.24	0.85207	10	0.7	100	501.79
5	0.02	0.24	0.24	0.85207	10	0.7	200	516.74
6	0.02	0.24	0.24	0.85207	10	0.7	500	527.29
7	0.02	0.24	0.24	0.85207	10	0.7	1000	531.01
8	0.02	0.24	0.24	0.85207	10	0.7	5000	535.4
9	0.02	0.24	0.24	0.85207	10	0.7	10000	535.73
10	0.02	0.24	0.24	0.85207	10	1	500	527.05
11	0.02	0.24	0.24	0.85207	10	1	10000	533.78
12	0.02	0.24	0.24	0.85207	10	2	500	525.26
13	0.02	0.24	0.24	0.85207	10	2	10000	535.15
14	0.02	0.24	0.24	0.85207	10	4	500	529.13
15	0.02	0.24	0.24	0.85207	10	4	10000	536.94
16	0.02	0.24	0.24	0.85207	10	7	10	399.01
17	0.02	0.24	0.24	0.85207	10	7	20	437.12
18	0.02	0.24	0.24	0.85207	10	7	50	481.67
19	0.02	0.24	0.24	0.85207	10	7	100	504.73
20	0.02	0.24	0.24	0.85207	10	7	200	527.42
21	0.02	0.24	0.24	0.85207	10	7	500	536.27
22	0.02	0.24	0.24	0.85207	10	7	1000	552.52
23	0.02	0.24	0.24	0.85207	10	7	5000	555.66
24	0.02	0.24	0.24	0.85207	10	7	10000	553.82
25	0.02	0.24	0.24	0.85207	10	10	500	551.38
26	0.02	0.24	0.24	0.85207	10	10	10000	570.51
27	0.02	0.24	0.24	0.85207	10	20	500	607.25
28	0.02	0.24	0.24	0.85207	10	20	10000	616.46
29	0.02	0.24	0.24	0.85207	10	50	500	670.28
30	0.02	0.24	0.24	0.85207	10	50	10000	701.32
31	0.02	0.24	0.24	0.85207	10	100	500	741.56
32	0.02	0.24	0.24	0.85207	10	100	10000	778.91
33	0.02	0.24	0.24	0.85207	100	0.7	10	403.41
34	0.02	0.24	0.24	0.85207	100	0.7	20	443.45
35	0.02	0.24	0.24	0.85207	100	0.7	50	490.43
36	0.02	0.24	0.24	0.85207	100	0.7	100	515.55
37	0.02	0.24	0.24	0.85207	100	0.7	200	533.84
38	0.02	0.24	0.24	0.85207	100	0.7	500	550.98
39	0.02	0.24	0.24	0.85207	100	0.7	1000	563.75
40	0.02	0.24	0.24	0.85207	100	0.7	5000	562.17
41	0.02	0.24	0.24	0.85207	100	0.7	10000	558.96
42	0.02	0.24	0.24	0.85207	100	1	500	563.22
43	0.02	0.24	0.24	0.85207	100	1	10000	585.11
44	0.02	0.24	0.24	0.85207	100	2	500	621.81
45	0.02	0.24	0.24	0.85207	100	2	10000	640.79
46	0.02	0.24	0.24	0.85207	100	4	500	703.46
47	0.02	0.24	0.24	0.85207	100	4	10000	711.65
48	0.02	0.24	0.24	0.85207	100	7	10	469.1
49	0.02	0.24	0.24	0.85207	100	7	20	533.59
50	0.02	0.24	0.24	0.85207	100	7	50	612.82
51	0.02	0.24	0.24	0.85207	100	7	100	663.69
52	0.02	0.24	0.24	0.85207	100	7	200	699.8
53	0.02	0.24	0.24	0.85207	100	7	500	752.66
54	0.02	0.24	0.24	0.85207	100	7	1000	771.38
55	0.02	0.24	0.24	0.85207	100	7	5000	779.05
56	0.02	0.24	0.24	0.85207	100	7	10000	785.42
57	0.02	0.24	0.24	0.85207	100	10	500	798.82
58	0.02	0.24	0.24	0.85207	100	10	10000	829.19
59	0.02	0.24	0.24	0.85207	100	20	500	904.13
60	0.02	0.24	0.24	0.85207	100	20	10000	968.58
61	0.02	0.24	0.24	0.85207	100	50	500	1154.4
62	0.02	0.24	0.24	0.85207	100	50	10000	1316.5

REFERENCES

- ¹S. Kandlikar, S. Garimella, D. Li, S. Colin, and M. R. King, *Heat transfer and fluid flow in minichannels and microchannels* (Elsevier, 2005).
- ²W. A. Khan, J. Culham, and M. Yovanovich, “The role of fin geometry in heat sink performance,” *Journal of Electronic Packaging* **128**, 324–330 (2006).
- ³T. İzci, M. Koz, and A. Koşar, “The effect of micro pin-fin shape on thermal and hydraulic performance of micro pin-fin heat sinks,” *Heat Transfer Engineering* **36**, 1447–1457 (2015).
- ⁴D. Yang, Z. Jin, Y. Wang, G. Ding, and G. Wang, “Heat removal capacity of laminar coolant flow in a micro channel heat sink with different pin fins,” *International Journal of Heat and Mass Transfer* **113**, 366–372 (2017).
- ⁵A. V. Bapat and S. G. Kandlikar, “Thermohydraulic performance analysis of offset strip fin microchannel heat exchangers,” in *International Conference on Nanochannels, Microchannels, and Minichannels*, Vol. 47608 (2006) pp. 347–353.
- ⁶C.-Y. Yang, C.-T. Yeh, W.-C. Liu, and B.-C. Yang, “Advanced micro-heat exchangers for high heat flux,” *Heat transfer engineering* **28**, 788–794 (2007).
- ⁷F. Hong and P. Cheng, “Three dimensional numerical analyses and optimization of offset strip-fin microchannel heat sinks,” *International Communications in Heat and Mass Transfer* **36**, 651–656 (2009).
- ⁸K. H. Do, B.-I. Choi, Y.-S. Han, and T. Kim, “Experimental investigation on the pressure drop and heat transfer characteristics of a recuperator with offset strip fins for a micro gas turbine,” *International Journal of Heat and Mass Transfer* **103**, 457–467 (2016).
- ⁹T. Nagasaki, R. Tokue, S. Kashima, and Y. Ito, “Conceptual design of recuperator for ultramicro gas turbine,” in *Proceedings of the International Gas Turbine Congress* (Citeseer, 2003) pp. 2–7.
- ¹⁰Y. Yang, Y. Li, B. Si, and J. Zheng, “Heat transfer performances of cryogenic fluids in offset strip fin-channels considering the effect of fin efficiency,” *International Journal of Heat and Mass Transfer* **114**, 1114–1125 (2017).
- ¹¹Q. Jiang, M. Zhuang, Z. Zhu, and J. Shen, “Thermal hydraulic characteristics of cryogenic offset-strip fin heat exchangers,” *Applied Thermal Engineering* **150**, 88–98 (2019).
- ¹²M. Yang, X. Yang, X. Li, Z. Wang, and P. Wang, “Design and optimization of a solar air heater with offset strip fin absorber plate,” *Applied Energy* **113**, 1349–1362 (2014).

- ¹³K. Pottler, C. M. Sippel, A. Beck, and J. Fricke, “Optimized finned absorber geometries for solar air heating collectors,” *Solar Energy* **67**, 35–52 (1999).
- ¹⁴D. B. Tuckerman and R. F. W. Pease, “High-performance heat sinking for vlsi,” *IEEE Electron device letters* **2**, 126–129 (1981).
- ¹⁵A. Bartolini, M. Cacciari, A. Tilli, and L. Benini, “Thermal and energy management of high-performance multicores: Distributed and self-calibrating model-predictive controller,” *IEEE Transactions on Parallel and Distributed Systems* **24**, 170–183 (2012).
- ¹⁶A. Vangeffelen, G. Buckinx, M. R. Vetrano, and M. Baelmans, “Friction factor for steady periodically developed flow in micro-and mini-channels with arrays of offset strip fins,” *Physics of Fluids* **33**, 103610 (2021).
- ¹⁷R. Shah and A. London, *Laminar Flow Forced Convection in Ducts*, Vol. 1 (Elsevier, 1978).
- ¹⁸A. Renfer, M. K. Tiwari, R. Tiwari, F. Alfieri, T. Brunschwiler, B. Michel, and D. Poulikakos, “Microvortex-enhanced heat transfer in 3d-integrated liquid cooling of electronic chip stacks,” *International Journal of Heat and Mass Transfer* **65**, 33–43 (2013).
- ¹⁹G. Xia, Z. Chen, L. Cheng, D. Ma, Y. Zhai, and Y. Yang, “Micro-piv visualization and numerical simulation of flow and heat transfer in three micro pin-fin heat sinks,” *International Journal of Thermal Sciences* **119**, 9–23 (2017).
- ²⁰L.-z. Zhang and Z.-y. Chen, “Convective heat transfer in cross-corrugated triangular ducts under uniform heat flux boundary conditions,” *International Journal of Heat and Mass Transfer* **54**, 597–605 (2011).
- ²¹J. Gong, J. Onishi, A. He, Y. Kametani, Y. Hasegawa, and N. Shikazono, “Heat transfer enhancement and pressure loss in a plate-fin heat exchanger with v-shaped oblique wavy surface,” *International Journal of Heat and Mass Transfer* **161**, 120263 (2020).
- ²²A. Priyam and P. Chand, “Thermal and thermohydraulic performance of wavy finned absorber solar air heater,” *Solar Energy* **130**, 250–259 (2016).
- ²³S. Manson, “Correlations of heat transfer data and of friction data for interrupted plate fins staggered in successive rows, naca tech,” Tech. Rep. (Note 2237, National Advisory Committee for Aeronautics, Washington, DC, 1950).
- ²⁴A. R. Wieting, “Empirical correlations for heat transfer and flow friction characteristics of rectangular offset-fin plate-fin heat exchangers,” *Journal of Heat Transfer* **79**, 488–490 (1975).
- ²⁵W. M. Kays and A. L. London, *Compact heat exchangers* (McGraw-Hill, New York, NY, 1984).

- ²⁶H. M. Joshi and R. L. Webb, “Heat transfer and friction in the offset stripfin heat exchanger,” International Journal of Heat and Mass Transfer **30**, 69–84 (1987).
- ²⁷R. M. Manglik and A. E. Bergles, “Heat transfer and pressure drop correlations for the rectangular offset strip fin compact heat exchanger,” Experimental Thermal and Fluid Science **10**, 171–180 (1995).
- ²⁸J. Dong, J. Chen, Z. Chen, and Y. Zhou, “Air-side thermal hydraulic performance of offset strip fin aluminum heat exchangers,” Applied Thermal Engineering **27**, 306–313 (2007).
- ²⁹M.-S. Kim, J. Lee, S.-J. Yook, and K.-S. Lee, “Correlations and optimization of a heat exchanger with offset-strip fins,” International Journal of Heat and Mass Transfer **54**, 2073–2079 (2011).
- ³⁰B. Cukurel and T. Arts, “Local heat transfer dependency on thermal boundary condition in ribbed cooling channel geometries,” Journal of heat transfer **135** (2013).
- ³¹W. Li, L. Yang, J. Ren, and H. Jiang, “Effect of thermal boundary conditions and thermal conductivity on conjugate heat transfer performance in pin fin arrays,” International Journal of Heat and Mass Transfer **95**, 579–592 (2016).
- ³²S. Hu and K. E. Herold, “Prandtl number effect on offset fin heat exchanger performance: predictive model for heat transfer and pressure drop,” International Journal of Heat and Mass Transfer **38**, 1043–1051 (1995).
- ³³C.-C. Wang, R. L. Webb, and K.-Y. Chi, “Data reduction for air-side performance of fin-and-tube heat exchangers,” Experimental Thermal and Fluid Science **21**, 218–226 (2000).
- ³⁴S. D. Jadhav, L. R. Goossens, Y. Kinds, B. Van Hooreweder, and K. Vanmeensel, “Laser-based powder bed fusion additive manufacturing of pure copper,” Additive Manufacturing **42**, 101990 (2021).
- ³⁵R. K. Shah and A. L. London, “Offset rectangular plate-fin surfaces—heat transfer and flow friction characteristics.” Tech. Rep. (Stanford University, California, Department of Mechanical Engineering, 1967).
- ³⁶F. Walters, “Hypersonic research engine project-phase iia, category i test report on fin heat transfer and pressure drop testing, data item no. 63.02, airesearch manufacturing co. doc,” AiResearch Manufacturing Co., Torrance, CA, USA, Doc. AP-69-5348 (1969).
- ³⁷L. Guo, F. Qin, J. Chen, and Z. Chen, “Lubricant side thermal–hydraulic characteristics of steel offset strip fins with different flow angles,” Applied thermal engineering **28**, 907–914 (2008).
- ³⁸H. Bhowmik and K.-S. Lee, “Analysis of heat transfer and pressure drop characteristics in an offset strip fin heat exchanger,” International Communications in Heat and Mass Transfer **36**,

259–263 (2009).

³⁹F. Tinaut, A. Melgar, and A. R. Ali, “Correlations for heat transfer and flow friction characteristics of compact plate-type heat exchangers,” International journal of heat and mass transfer **35**, 1659–1665 (1992).

⁴⁰G. Buckinx and M. Baelmans, “Macro-scale heat transfer in periodically developed flow through isothermal solids,” Journal of Fluid Mechanics **780**, 274–298 (2015).

⁴¹G. Buckinx and M. Baelmans, “Macro-scale conjugate heat transfer in periodically developed flow through solid structures,” Journal of Fluid Mechanics **804**, 298–322 (2016).

⁴²M. Quintard, M. Kaviany, and S. Whitaker, “Two-medium treatment of heat transfer in porous media: numerical results for effective properties,” Advances in water resources **20**, 77–94 (1997).

⁴³C. T. DeGroot and A. G. Straatman, “Closure of non-equilibrium volume-averaged energy equations in high-conductivity porous media,” International journal of heat and mass transfer **54**, 5039–5048 (2011).

⁴⁴D. L. Penha, S. Stolz, J. G. Kuerten, M. Nordlund, A. K. Kuczaj, and B. J. Geurts, “Fully-developed conjugate heat transfer in porous media with uniform heating,” International journal of heat and fluid flow **38**, 94–106 (2012).

⁴⁵P.-S. Lee, S. V. Garimella, and D. Liu, “Investigation of heat transfer in rectangular microchannels,” International journal of heat and mass transfer **48**, 1688–1704 (2005).

⁴⁶P.-S. Lee and S. V. Garimella, “Thermally developing flow and heat transfer in rectangular microchannels of different aspect ratios,” International journal of heat and mass transfer **49**, 3060–3067 (2006).

⁴⁷S. Patankar, C. Liu, and E. Sparrow, “Fully developed flow and heat transfer in ducts having streamwise-periodic variations of cross-sectional area,” Journal of Heat Transfer—Transactions of the ASME **99**, 180–186 (1977).

⁴⁸M. S. Alnæs, J. Blechta, J. Hake, A. Johansson, B. Kehlet, A. Logg, C. Richardson, J. Ring, M. E. Rognes, and G. N. Wells, “The fenics project version 1.5,” Archive of Numerical Software **3** (2015), 10.11588/ans.2015.100.20553.

⁴⁹L. F. Richardson, “Ix. the approximate arithmetical solution by finite differences of physical problems involving differential equations, with an application to the stresses in a masonry dam,” Philosophical Transactions of the Royal Society of London. Series A, Containing Papers of a Mathematical or Physical Character **210**, 307–357 (1911).

- ⁵⁰P. J. Roache, “Perspective: a method for uniform reporting of grid refinement studies,” *Journal of Fluids Engineering* **116**, 405–413 (1994).
- ⁵¹R. K. Shah and D. P. Sekulic, *Fundamentals of heat exchanger design* (John Wiley & Sons, 2003).
- ⁵²N. Wakao and T. Funazkri, “Effect of fluid dispersion coefficients on particle-to-fluid mass transfer coefficients in packed beds: correlation of sherwood numbers,” *Chemical Engineering Science* **33**, 1375–1384 (1978).
- ⁵³G. Hwang and C. Chao, “Heat transfer measurement and analysis for sintered porous channels,” *Journal of Heat Transfer* **116**, 456–464 (1994).
- ⁵⁴A. R. Martin, C. Saltiel, and W. Shyy, “Frictional losses and convective heat transfer in sparse, periodic cylinder arrays in cross flow,” *International journal of heat and mass transfer* **41**, 2383–2397 (1998).
- ⁵⁵F. Kuwahara, M. Shirota, and A. Nakayama, “A numerical study of interfacial convective heat transfer coefficient in two-energy equation model for convection in porous media,” *International journal of heat and mass transfer* **44**, 1153–1159 (2001).
- ⁵⁶V. Mandhani, R. Chhabra, and V. Eswaran, “Forced convection heat transfer in tube banks in cross flow,” *Chemical Engineering Science* **57**, 379–391 (2002).
- ⁵⁷M. B. Saito and M. J. De Lemos, “A correlation for interfacial heat transfer coefficient for turbulent flow over an array of square rods,” *Journal of Heat Transfer* , 444–452 (2006).
- ⁵⁸G. Gamrat, M. Favre-Marinet, and S. Le Person, “Numerical study of heat transfer over banks of rods in small reynolds number cross-flow,” *International Journal of Heat and Mass Transfer* **51**, 853–864 (2008).
- ⁵⁹A. Alshare, P. J. Strykowski, and T. W. Simon, “Modeling of unsteady and steady fluid flow, heat transfer and dispersion in porous media using unit cell scale,” *International Journal of Heat and Mass Transfer* **53**, 2294–2310 (2010).
- ⁶⁰X. Lu and Y. Zhao, “Effect of flow regime on convective heat transfer in porous copper manufactured by lost carbonate sintering,” *International Journal of Heat and Fluid Flow* **80**, 108482 (2019).
- ⁶¹D. Lasseux, A. A. Abbasian Arani, and A. Ahmadi, “On the stationary macroscopic inertial effects for one phase flow in ordered and disordered porous media,” *Physics of fluids* **23**, 073103 (2011).

⁶²J. Yih and H. Wang, “Experimental characterization of thermal-hydraulic performance of a microchannel heat exchanger for waste heat recovery,” *Energy Conversion and Management* **204**, 112309 (2020).

⁶³P. Virtanen, R. Gommers, T. E. Oliphant, M. Haberland, T. Reddy, D. Cournapeau, E. Burovski, P. Peterson, W. Weckesser, J. Bright, S. J. van der Walt, M. Brett, J. Wilson, K. J. Millman, N. Mayorov, A. R. J. Nelson, E. Jones, R. Kern, E. Larson, C. J. Carey, İ. Polat, Y. Feng, E. W. Moore, J. VanderPlas, D. Laxalde, J. Perktold, R. Cimrman, I. Henriksen, E. A. Quintero, C. R. Harris, A. M. Archibald, A. H. Ribeiro, F. Pedregosa, P. van Mulbregt, and SciPy 1.0 Contributors, “SciPy 1.0: Fundamental Algorithms for Scientific Computing in Python,” *Nature Methods* **17**, 261–272 (2020).

⁶⁴D. Sivia, W. David, K. Knight, and S. Gull, “An introduction to bayesian model selection,” *Physica D: Nonlinear Phenomena* **66**, 234–242 (1993).